CNWRA A center of excellence in earth sciences and engineering

A Division of Southwest Research Institute™
6220 Culebra Road • San Antonio, Texas, U.S.A. 78228-5166
(210) 522-5160 • Fax (210) 522-5155

April 18, 2002
Contract NRC–02–97–009
Account No. 20.01402.861

U.S. Nuclear Regulatory Commission
ATTN: Mr. Neil M. Coleman
Two White Flint North
11545 Rockville Pike
Mail Stop 7 C6
Washington, DC 20555

Subject: Intermediate Milestone 20.01402.861.200, Flow Paths in the Unsaturated Zone—Letter Report

Dear Mr. Coleman:

This letter transmits Intermediate Milestone 20.01402.861.200, Flow Paths in the Unsaturated Zone-Letter Report. The final title for this deliverable is Unsaturated Zone Flow at Yucca Mountain, Nevada: Effects of Fracture Heterogeneity and Flow in the Paintbrush Nonwelded Tuff Unit.

As you know, unsaturated zone flow is important to the performance of the high-level waste repository proposed for Yucca Mountain, Nevada. Significant uncertainties in flow models for the unsaturated zone include the potential for focused or preferential flow and the possibility for lateral diversion of infiltrating water away from the repository horizon. This report provides analysis of recent U.S. Department of Energy (DOE) numerical models for unsaturated zone flow in light of independent modeling and field studies. This work directly supports ongoing issue resolution activities and evaluation of U.S. Nuclear Regulatory Commission (NRC)/DOE agreement item responses.

The DOE has concluded, based on numerical modeling, that lateral diversion within the Paintbrush unit can divert substantial amounts of flow away from the repository area. This modeling relies on idealized and unrealistic geometries and rock property distributions. Conversely, field and laboratory evidence strongly suggests that lateral flow is likely to be limited. Thus, any DOE reliance on significant lateral diversion as part of their performance assessments does not appear to be appropriate.

If you have any questions about this deliverable, please contact me (210.522.5540) or Mr. Randall Fedors (210.522.6818).

Sincerely,

for English C. Pearcy
Manager, Geohydrology and Geochemistry

ECP/ph
enclosure

cc:	J. Linehan	W. Reamer	W. Ford	W.C. Patrick	T. Nagy (SwRI Contracts)
	B. Meehan	D. Brooks	H. Arlt	B. Sagar	Letter only:
	D. DeMarco	B. Leslie	J. Bradbury	R. Fedors	CNWRA Directors
	E. Whitt	J. Schlueter	A. Campbell	J. Winterle	CNWRA Element Managers
	J. Greeves	L. Hamden	W. Dam	C. Dinwiddie	P. Maldonado

Washington Office • Twinbrook Metro Plaza #210
12300 Twinbrook Parkway • Rockville, Maryland 20852-1606

PREDECISIONAL

UNSATURATED ZONE FLOW AT YUCCA MOUNTAIN, NEVADA: EFFECTS OF FRACTURE HETEROGENEITY AND FLOW IN THE NONWELDED PAINTBRUSH TUFF UNIT

Prepared for

U.S. Nuclear Regulatory Commission
Contract NRC–02–97–009

Prepared by

R.W. Fedors
J.R. Winterle
W.A. Illman
C.L. Dinwiddie
D.L. Hughson

Center for Nuclear Waste Regulatory Analyses
San Antonio, Texas

April 2002

ABSTRACT

Unsaturated zone flow is an important natural-system component of the multiple-barrier strategy for the proposed nuclear waste repository at Yucca Mountain, Nevada. Important uncertainties in the unsaturated zone flow model include the potential for development of focused or preferential flow paths as a result of flow-system heterogeneity and the potential for lateral diversion of infiltrating water at stratigraphic layer interfaces that may form capillary or permeability barriers. The U.S. Department of Energy (DOE) recently conducted numerical flow modeling of both fracture network heterogeneity and the formation of capillary barriers to demonstrate that its approach is conservative for evaluating unsaturated zone flow to support the total system performance assessment for site recommendation. In this report, these recent DOE models are reviewed, and results of independent modeling analyses and field studies are reported.

DOE modeling of heterogenous flow suggests the ranges of flow-focusing factors used for the total system performance assessment for site recommendation are reasonably conservative for the assumed correlation scale of fracture heterogeneity. Improved knowledge of the correlation scale for flow-system heterogeneity is a recommended objective for ongoing and planned field studies at Yucca Mountain. This report presents independent stochastic simulations that show areas of focused flow in the Paintbrush unit matrix are correlated to the areas where focused fracture flow arrives from the base of the Tiva Canyon unit and that flow exiting the base of the Paintbrush unit is quickly redistributed according to the degree of heterogeneity in the fracture continuum of the underlying Topopah Spring welded unit. Additional modeling is recommended to evaluate whether matrix heterogeneity in the Paintbrush unit could result in widely spaced zones of focused flow. Independent stochastic continuum modeling results also suggest the possibility that active-fracture spacing used in the DOE radionuclide transport abstraction could result in overly optimistic radionuclide transport simulations. DOE researchers concluded, based on numerical modeling, that significant lateral diversion along capillary barriers within the nonwelded Paintbrush unit can divert substantial amounts of flow laterally toward faults and away from significant portions of the proposed repository area. This conclusion, however, is largely based on a layer-cake-type model that assumes homogenous layers with sharp, smooth layer interfaces. Conversely, field and laboratory evidence strongly suggest that lateral flow is limited. Thus, credit for significant lateral diversion of flow would not be appropriate for any total system performance assessment to support a potential license application for a proposed repository at Yucca Mountain.

CONTENTS

FIGURES

FIGURES (continued)

TABLES

ACKNOWLEDGMENTS

This report was prepared to document work performed by the Center for Nuclear Waste Regulatory Analyses (CNWRA) for the U.S. Nuclear Regulatory Commission (NRC) under Contract No. NRC–02–97–009. The activities reported here were performed on behalf of the NRC Office of Nuclear Material Safety and Safeguards, Division of Waste Management. The report is an independent product of the CNWRA and does not necessarily reflect the views or regulatory position of the NRC.

The authors wish to thank Ron Green for thorough technical review and useful insights, Barbara Long and Cathy Cudd for editorial expertise, and Pat Mackin for programmatic review. The administrative and format support provided by Paulette Houston is greatly appreciated.

QUALITY OF DATA, ANALYSES, AND CODE DEVELOPMENT

DATA: Original data presented in Section 3.4 of this report were collected at the Bishop Tuff field site in Inyo County, California, and are documented in CNWRA Scientific Notebooks 354, 428, and 432E.

ANALYSES AND CODES: The METRA Code Version 1.2.3 was used for analysis contained in Section 2.2 of this report. The METRA code is controlled under the CNWRA Software Configuration Procedures. The METRA model runs and results presented in Section 2.2 are documented in CNWRA Scientific Notebook 509E; model input and output files are stored on CD-ROM and kept with that notebook, and can be obtained on request. The HYDRUS2D Code Version 2.02 was used in Section 3.4 to model field observations. The HYDRUS2D code is controlled under the CNWRA Software Configuration Procedures.

1 INTRODUCTION

The unsaturated zone is an important natural-system component of the multiple-barrier strategy for the proposed nuclear waste repository at Yucca Mountain, Nevada. The U.S. Department of Energy (DOE) model for unsaturated zone flow [Civilian Radioactive Waste Management System Management and Operating Contractor (CRWMS M&O), 2000a] conceptualizes the Paintbrush Tuff as a hydrostratigraphic unit having hydrologic properties that act to dampen the highly episodic nature of surface infiltration and to laterally redistribute focused flow from above. Based on this conceptualization, the unsaturated zone flow model makes use of a simplifying assumption of steady-state flow and, to improve computational efficiency, a grid-block scale larger than that of the infiltration model.

Steady-state, laterally distributed flow results in slower flow velocities, reduced possibility of focused flow that could lead to seepage or dripping into drift openings, and a contact of percolating water with a greater amount of fracture-matrix surface area. All these factors bode well for performance predictions for the proposed repository. Thus, it is important to evaluate unsaturated zone features and processes that may affect the current conceptualization of flow in the Paintbrush Tuff unit To this end, DOE recently conducted numerical flow modeling of both fracture network heterogeneity (Bechtel SAIC Company, LLC, 2001, Section 4.3.2) and the effects of capillary barriers in the Paintbrush unit (Wu, et al., 2000) to demonstrate that the abstraction for unsaturated zone flow is conservatively applied in the Total System Performance Assessment Model for Site Recommendation (CRWMS M&O, 2000b).

In this report, these recent DOE models are reviewed, and results of independent modeling from Center for Nuclear Waste Regulatory Analyses (CNWRA) staff analyses and field studies are reported. The report is topically divided into two sections. The first topical section (Chapter 2) addresses the effects of heterogeneity within individual hydrostratigraphic layers on the potential for development of preferential flow paths. This section begins with a review of the DOE process model for flow focusing and discrete flow paths in the Topopah Spring hydrogeologic unit (Bechtel SAIC Company, LLC, 2001, Section 4.3.2). Results are then presented for an independent model, developed at CNWRA, to evaluate effects of fracture network heterogeneity in a multilayered flow system.

The second topical section of this report (Chapter 3) deals with effects of interlayer heterogeneity (i.e., change in hydrologic properties across layer interfaces) on the formation of permeability or capillary barriers—especially within and at the boundaries of the Paintbrush unit—that might affect lateral flow of downward-percolating waters. This section includes a review of the DOE process models of lateral flow within the Paintbrush nonwelded tuff unit (Bechtel SAIC Company, LLC, 2001, Section 3.2.3; Wu, et al., 2000). Results of a CNWRA independent field study of the effects of fractures on the lateral spreading of flow in a nonwelded volcanic tuff are presented for comparison.

2 EFFECTS OF INTRALAYER HETEROGENEITY ON UNSATURATED ZONE FLOW

Intralayer heterogeneity of hydrologic properties can lead to the development of preferential flow along higher permeability pathways. Developing preferential flow paths within hydrostratigraphic layers cannot be evaluated in the DOE site-scale unsaturated zone model because of the large grid blocks used and the assumption of homogenous layer properties. This deficiency is not necessarily problematic because the DOE performance assessment abstraction accounts for smaller scale effects in other ways. For example, preferential or focused flow paths are accounted for in the drift seepage abstraction through the use of a flow-focusing factor to increase the modeled seepage flux (CRWMS M&O, 2000c). This report chapter evaluates the potential effects of intralayer heterogeneity and assesses whether these potential effects are adequately included in DOE performance assessments.

2.1 DOE Process Model of Discrete Flow Paths in the Topopah Spring Unit

The DOE performance assessment abstraction for drift seepage uses a flow-focusing factor to account for the potential focusing of flow caused by heterogeneity of fracture hydrologic properties. DOE investigators developed statistical distributions from which the value of the flow-focusing factors are sampled for performance assessment modeling (CRWMS M&O, 2000c, Section 6.3.3). Three different distributions for the flow-focusing factor were developed, corresponding to total system performance assessment analyses for the low-, medium-, and high-infiltration scenarios. All three distributions are log-uniform with a lower bound of 1.0. The upper bound values for the flow-focusing factor distributions are 47, 22, and 9.7 for the low, medium (basecase), and high infiltration scenarios, respectively. The fact that the flow-focusing factors decrease with higher infiltration rates suggests a conceptual model wherein the distance between focused flow paths decreases as the deep percolation rate increases.

One concern with this DOE approach is that the flow-focusing factor distributions are based on theoretical considerations, and no consideration is given to how flow focusing may be affected by fracture patterns in the proposed repository host horizon. DOE researchers have begun to address this concern by conducting a series of modeling exercises to provide support for the range of flow-focusing factors used in the seepage abstraction for performance assessments (Bechtel SAIC Company, LLC, 2001, Section 4.3.2). This two-dimensional, single-continuum model of flow focusing and discrete flow paths in the Topopah Spring welded unit comprised a grid 100 m [330 ft] wide by 150 m [490 ft] high. The grid was finely discretized into 0.25 × 0.5-m [1.6 × 0.8-ft] grid blocks, and heterogenous fracture properties for five different hydrogeologic layers (tsw31–tsw35) were assigned. Only heterogeneity in fracture permeability was considered. All other properties were assigned constant values within each hydrostratigraphic layer. The mean fracture permeability for each layer was based on the DOE Calibrated Properties Model (CRWMS M&O, 2000d), and the range of assigned permeabilities in the stochastic continuum model was varied by nearly three orders of magnitude. The reference-case model used an isotropic correlation length of 1.0 m [3.3 ft] for heterogeneity and a mean top boundary infiltration rate of 5 mm/yr [0.2 in/yr]. The model was then used to evaluate the sensitivity of unsaturated fracture flow paths to (i) a different realization of random permeability, (ii) different spatial distributions of top boundary infiltration flux (uniform versus focused), (iii) different infiltration rates, and (iv) the correlation scale of heterogeneity.

Results of the basecase model showed that the spacing between focused flow paths, or weeps, with fluxes greater than the applied flux was approximately 3–5 m [10–16 ft] (Bechtel SAIC Company, LLC, 2001, Figure 4.3.2-2). Flow paths with fluxes more than double the applied flux were typically spaced approximately 5–10 m [16–33 ft] apart. The DOE researchers also simulated conservative tracer transport with the basecase stochastic model. Tracer transport results showed that the tracer fronts in the more closely spaced weeps tended to coalesce into a few major focused transport paths, spaced approximately 10 m [33 ft] apart with leading edges associated with areas where focused flow rates were three to five times as great as the applied flux (Bechtel SAIC Company, LLC, 2001, Figure 4.3.2-5).

Perhaps the most important conclusion reached by the DOE modelers for the reference-case heterogenous model are that a value of 6.0 is an appropriate upper bound for the flow-focusing factor in the seepage abstraction for performance assessment (Bechtel SAIC Company, LLC, 2001, Section 4.3.2.5.1). DOE asserts that "This flow focusing factor is considerably lower than what is currently used in the TSPA–SR models, in which local fluxes were increased by up to a factor of 47 over prevailing percolation flux. The wide spread of flow focusing factors used in TSPA–SR yields a wider, albeit conservative, distribution of drift seepage."

Sensitivity studies performed using this different realization of random heterogeneity yielded results consistent with the reference-case model. This suggests the scale of the model is sufficiently large that a single realization can produce a representative range of stochastic variability. A similar conclusion is reached in Section 2.2 of this report based on the results of the independent CNWRA modeling study of heterogeneity effects on flow.

The sensitivity analysis of a nonuniform spatial distribution of top-boundary infiltration led the DOE modelers to conclude that "if a spatially variable infiltration is used, flow patterns behave as if the flux condition at the upper boundary were uniform" (Bechtel SAIC Company, LLC, 2001, Section 4.3.2.5.2). This conclusion is potentially important because the process model for the seepage abstraction is a heterogenous fracture-continuum model that assigns uniform infiltration at the top model boundary. Unfortunately, the results of the nonuniform infiltration analysis are not shown in the model documentation, and no details are given regarding how the infiltration was distributed in the nonuniform case. Some additional insight into the spatial redistribution of focused flow in heterogenous fracture continua is provided in the independent modeling by CNWRA staff presented in Section 2.2. Basically, areas of focused flow at the top boundary of a hydrostratigraphic layer are redistributed according to the degree of heterogeneity in that layer after traveling a distance equivalent to several correlation length scales. This conclusion may not hold true, however, if the horizontal distance between focused flow paths is much greater that the correlation scale for heterogeneity.

The analysis of sensitivity to the applied infiltration rate showed that the number of focused flow paths did not increase with infiltration rate. Results for infiltration rates of 1, 5, 25, 100, and 500 mm/yr [0.04, 0.2, 1, 4, and 20 in/yr] were presented, and the distribution of focused flow paths was similar for all cases. This result is counter to the present DOE approach of using differing flow focusing factors for the different infiltration rate cases in its performance assessment analyses. Results of these DOE simulations indicate that the same uncertainty distribution for the flow-focusing factor could be used for all three of the infiltration cases evaluated in performance assessment.

The final sensitivity analysis showed that the number of focused flow paths is affected by the correlation scale of heterogeneity. For the case with a stochastically generated permeability field, DOE researchers also tested a model based on a correlation length of 3 m [10 ft] and, although they do not show the results for this case, they report that the greater correlation length resulted in fewer but slightly larger weeps. This result indicates that values used for the flow-focusing factor in performance assessment calculations need to be consistent with the correlation scale of fracture network heterogeneity in the unsaturated zone at Yucca Mountain. A larger correlation scale would result in a greater value for the flow-focusing factor. An analysis cited by the DOE modelers (CRWMS M&O, 2001, Sections 6.3.2 and 6.4.2) concludes that fracture permeability near the proposed repository is essentially random at the drift scale, with no significant spatial correlation. If this conclusion is true, a flow-focusing factor estimated using the reference-case model with a correlation scale larger than the grid-block size should provide a reasonably conservative estimate of the flow-focusing factor.

In summary, modeling of heterogenous flow in the Topopah Spring unit suggests the ranges of flow-focusing factors used by DOE for its total system performance assessment model for the site recommendation (CRWMS M&O, 2000b) are reasonably conservative. These results provide justification for DOE to rely on a single uncertainty distribution for the flow-focusing factor in future performance assessment analyses. Ongoing DOE field studies may provide additional validation for the range of flow-focusing factors that might be used in a potential license application. Knowledge of the correlation scale for flow-system heterogeneity is an important input for establishing appropriate values for the focusing factor.

2.2 Independent Random Field Simulations of Flow in Layered, Fractured Rocks

The DOE unsaturated zone flow model used for performance assessment analyses of Yucca Mountain (CRWMS M&O, 2000a) relies on a simplifying assumption of homogenous rock properties within each of the model hydrostratigraphic layers. To investigate the consequences of simplifying the site hydrogeology, simulations of flow in a three-layer, unsaturated, fractured rock system were conducted at CNWRA. Results from a simulation of flow in the three-layer system with homogenous fracture and matrix properties are compared to results of a model that treats spatial variability in the fracture permeability of each layer.

2.2.1 Model Development

The two-phase, dual-continuum, nonisothermal flow model simulations were generated using the METRA numerical code Version 1.2.3 (Lichtner, et al., 2000). The computational domain consists of 1.0-m^3 [35.3-ft^3] elements representing overlapping matrix and fracture continua in a 99 × 99 grid. The size of the cubic grid blocks is commensurate with the support volume of fractured rock properties estimated from single-hole, pneumatic injection tests.

The top 36 m [118 ft] of the model domain represent the highly fractured, moderately to densely welded Tiva Canyon Tuff. The next 33 m [108 ft] represent the nonwelded Paintbrush Tuff, which is less fractured relative to the welded units and has a much higher matrix porosity and permeability. The bottom 30 m [98 ft] of the model domain represent the highly fractured, moderately to densely welded Topopah Spring welded tuff. It is assumed the modeled region is deep enough in the unsaturated zone that evapotranspiration and near-surface thermal processes can be neglected.

Infiltration rates of 12.5, 22.5, and 42.5 mm/yr [0.49, 0.89, and 1.67 in/yr] are considered in this study to evaluate effects of fracture-continuum heterogeneity for a range of flow rates representative of the projected spatial variability of infiltration projected for present and future climate conditions. These rates are within the range predicted by the DOE infiltration model for Yucca Mountain (CRWMS M&O, 2000e), which predicts spatial variability of mean annual infiltration to range from 0–20 mm/yr [0–0.8 in/yr] for modern-day climate conditions and from 1–50 mm/yr [0.04–2.0 in/yr] for projected future climate conditions.

Constant gas saturation, temperature, and liquid flux are specified for the top model boundary. Total water flux at the top boundary was varied, as described in the preceding paragraph. For all cases, 2.5 mm/yr [0.1 in/yr] of the total top boundary flux was uniformly applied to the matrix continuum and the remainder was specified for the fracture continuum. The left and right boundaries are specified as no-flow boundaries. Constant field variables were specified at the bottom boundary for all cases. Isothermal conditions were maintained by fixing the temperature at the top and bottom boundaries at 20 °C [68 °F].

The numerical experiments begin with a model simulation that uses uniform fracture and matrix properties assigned to each layer. The purpose of this simulation is to obtain results from a model with homogenous layer properties that can be compared to subsequent probabilistic simulations. Parameters used for the homogenous layer analyses were adapted from the unsaturated zone hydrology model developed for the Total System Performance Assessment–Viability Assessment (CRWMS M&O, 1998). Table 2-1 lists the parameter values used for the fracture and matrix continua. The values listed in Table 2-1 for the Tiva Canyon, Paintbrush, and Topopah Spring layers are mean values estimated from the hydrogeologic subunits used by DOE for the viability assessment (DOE, 1998). Harmonic means were computed from matrix and fracture permeabilities of the subunits to obtain composite permeability (k) values for the Tiva Canyon welded, Paintbrush nonwelded, and Topopah Spring welded units. Arithmetic means were used to estimate composite values for matrix and fracture porosities (φ), van Genuchten parameters (α, m, S_r), fracture frequency (f), and fracture-matrix connection area (X_{fm}). The subscripts m and f in Table 2-1 designate matrix and fracture.

Table 2-1. METRA Model Parameter Input Values

Parameter	Symbol	Units	Model Layer: Tiva Canyon	Model Layer: Paintbrush	Model Layer: Topopah Spring
Matrix permeability	k_m	m^2	9.68×10^{-18}	1.29×10^{-14}	8.32×10^{-17}
Matrix porosity	φ_m	m^3/m^3	0.10	0.38	0.09
Matrix moisture-retention parameters	α_m	Pa^{-1}	9.83×10^{-7}	6.60×10^{-5}	1.65×10^{-5}
	m_m	—	0.33	0.33	0.26
	S_m	—	0.23	0.12	0.08

Table 2-1. METRA Model Parameter Input Values (continued)

Parameter	Symbol	Units	Model Layer		
			Tiva Canyon	Paintbrush	Topopah Spring
Fracture permeability	k_f	m^2	1.58×10^{-12}	1.26×10^{-13}	3.16×10^{-12}
Fracture porosity	φ_f	m^3/m^3	1.85×10^{-4}	6.69×10^{-5}	1.09×10^{-4}
Fracture moisture-retention parameters	α_f	Pa^{-1}	1.93×10^{-4}	1.49×10^{-3}	6.66×10^{-5}
	m_f	—	0.49	0.45	0.49
	S_{rf}	—	0.01	0.01	0.01
Fracture frequency	f	m^{-1}	1.55	0.55	1.06
Fracture-matrix connection area	X_{fm}	m^2/m^2	4.90×10^{-4}	3.10×10^{-1}	5.76×10^{-5}

For the stochastic simulations, random fracture-permeability fields were generated independently for each layer using a direct Fourier Transform Method (Robin, et al., 1993). A 2.0-m [6.6-ft] isotropic correlation length was used. This correlation length, although somewhat arbitrary, was used because available site data are not sufficient to reliably determine correlation structure of fracture permeability. Random field simulations were based on the mean value of fracture permeability provided in Table 2-1. To simulate varying degrees of heterogeneity, four values for variance of $\log_{10}$ fracture permeability—0.5, 1.0, 1.5, and 2.0—were used. Ten realizations of random fields were generated for each value of variance for a total of forty random fields. Figures 2-1a through d illustrate the effect of changing the permeability variance on one of the random fields. The range of variance considered for $\log_{10}$ fracture permeability is based on studies at Yucca Mountain (Wang, et al., 1998) and at Apache Leap Research Site in central Arizona (Vesselinov, et al., 2001).

Only fracture permeability was treated as a random variable; other parameters were assumed constant for each layer. Geostatistical analysis of data on the interstitial, pneumatic, hydraulic, and thermal properties of the unsaturated fractured tuffs at the Apache Leap Research Site (Illman, et al., 1998, 2002; Chen, et al., 2000) indicate high spatial variability in fracture permeability compared to parameters that can be estimated *in situ*. A potentially important parameter that cannot be reliably determined *in situ* is the α parameter of the van Genuchten (1980) moisture retention function. The α parameter represents how strongly a porous medium will retain water with capillary tension. Because the value of α is related to pore-size or fracture-aperture distribution, it may be correlated to the permeability, which can also be affected by pore size or fracture aperture. Possible correlations between permeability and the α parameter are not tested in the present CNWRA modeling study, but may be evaluated in future efforts.

Matrix permeability was treated as homogenous because spatially distributed matrix permeability data from Yucca Mountain are not available at the same scale as the permeability estimates derived by means of single-hole, pneumatic injection tests. This is not problematic

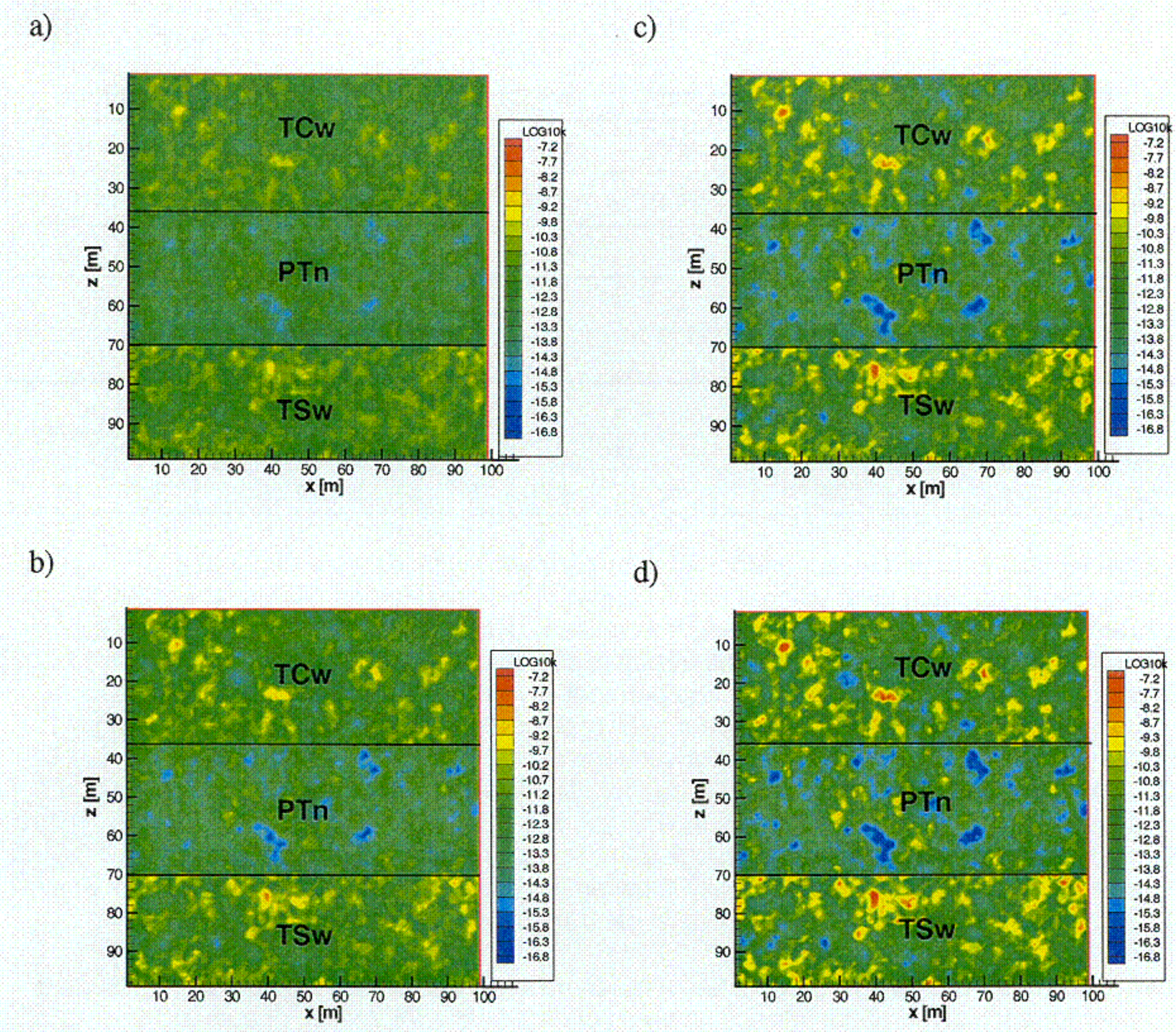

Figure 2-1. Random Fields with $\log_{10}$ Fracture Permeability Variance Values of a) $\sigma^2 = 0.5$; b) $\sigma^2 = 1.0$; c) $\sigma^2 = 1.5$; and d) $\sigma^2 = 2.0$ (Note: 1 m = 3.2808 ft)

C01

for the Tiva Canyon and Topopah Spring geologic units because matrix permeability is several orders of magnitude lower than fracture permeability, and fracture flow dominates at ambient percolation rates. In the Paintbrush unit, however, matrix flow dominates at ambient deep percolation rates. Thus, spatial heterogeneity of the Paintbrush Tuff matrix may cause a higher degree of flow focusing than is indicated by the results of this modeling study. A future modeling study is being planned by CNWRA to evaluate matrix heterogeneity within the Paintbrush unit.

2.2.2 Model Results

Model results were obtained for 123 simulations representing 3 different water flow rates at the top boundary for each of 40 random heterogeneous permeability fields and 1 uniform permeability field. Results of many of the simulations were qualitatively similar and are not discussed individually.

Uniform-Layer Model Results

Results of the model with uniform layer properties and a steady-state boundary flux of 42.5 mm/yr [1.67 in/yr] are shown in Figures 2-2a through d. Figures 2-2a and 2-2b show that water saturation is uniform in the fracture and matrix continua for the welded units. Saturation is generally low in the fracture continua of both welded and nonwelded units and in the matrix continuum of the nonwelded Paintbrush unit. Fracture saturation decreases with depth in the nonwelded Paintbrush unit as water is imbibed into the matrix.

A thin zone of increased saturation forms in the fracture continuum at the base of the Tiva Canyon unit because of the decrease in fracture permeability in the underlying Paintbrush unit. A saturation buildup also forms in the matrix continuum at the base of the Paintbrush unit above the permeability barrier of the Topopah Spring matrix and the capillary barrier of the Topopah Spring fracture continuum.

Figures 2-2c and 2-2d show that water flux in the fracture continuum is highest in the welded Tiva Canyon and Topopah Spring units, with the highest values occurring just above the Tiva Canyon–Paintbrush contact. The white stream lines in Figures 2-2c and 2-2d indicate gravity dominated flow in both fracture and matrix continua with a straight downward pathway.

Results from the uniform-layer model cases with boundary fluxes of 12.5 and 22.5 mm/yr [0.49 and 0.89 in/yr] are not shown, but were qualitatively similar to the case with 42.5 mm/yr [1.67 in/yr]. Straight downward flow was fracture-dominated in the Tiva Canyon and Topopah Spring units and matrix-dominated in the Paintbrush unit. The only differences between these lower-infiltration cases and the results shown in Figure 2-2 were proportionately lower fluxes and slightly lower saturation. For example, matrix saturation in most of the Paintbrush unit was about 0.73 for the 42.5-m/yr [1.67-in/yr] boundary-flux case and was reduced only slightly to 0.65 for the 12.5-mm/yr [0.49-in/yr] case.

Stochastic Model Results

A total of 120 stochastic simulations was run to evaluate 4 values for variance of $\log_{10}$ permeability and 3 top boundary flux rates for each of 10 realizations of stochastic random

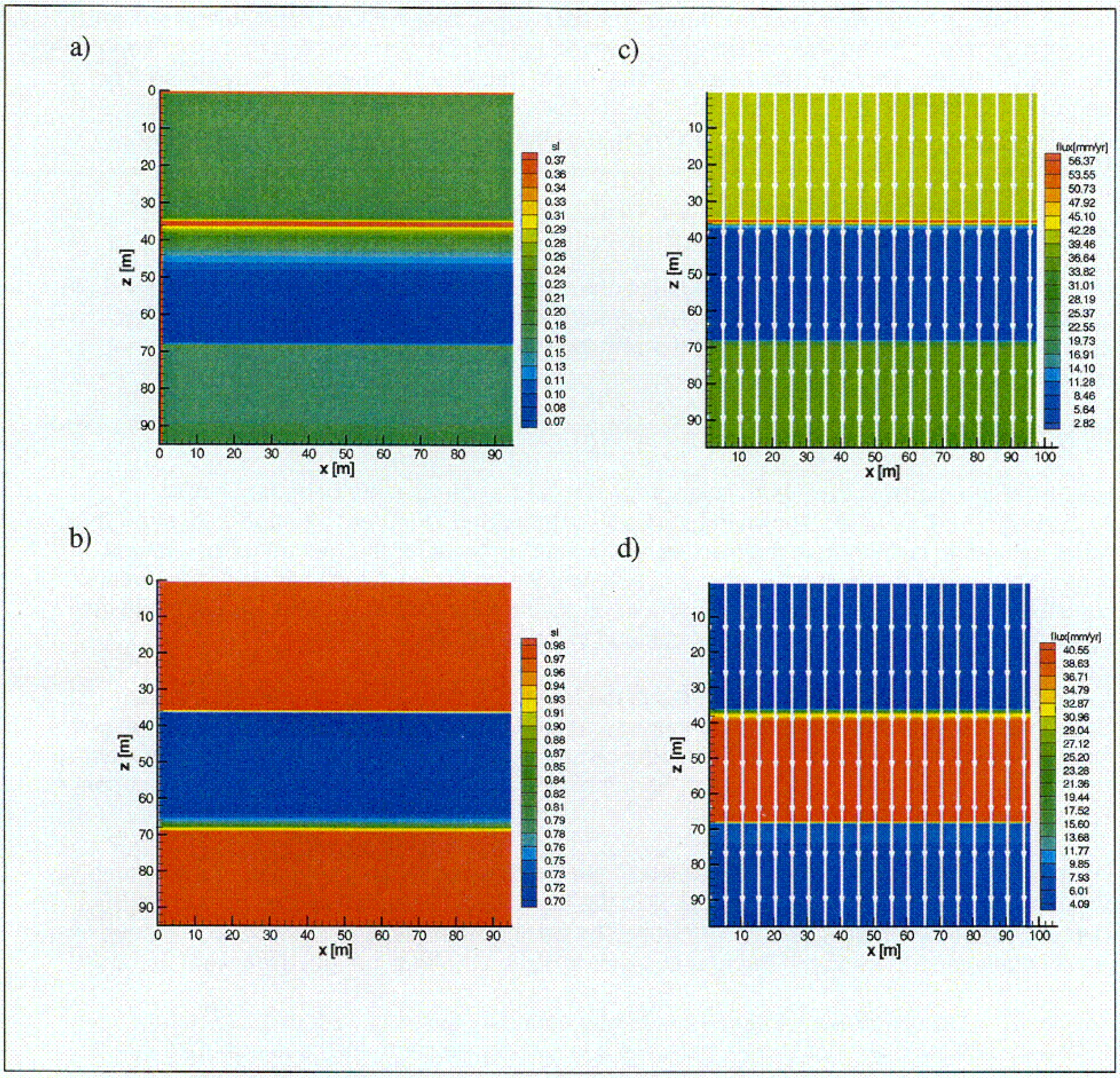

Figure 2-2. Steady-State Distribution of a) Fracture Saturation, b) Matrix Saturation, c) Fracture Water Flux, and d) Matrix Water Flux with Homogeneous Fracture Permeability for Each Layer and a Top Boundary Flux of 42.5 mm/yr [1.67 in/yr] (Note: 1 m = 3.2808 ft)

C02

permeability fields. Results for the 10 realizations of random permeability were qualitatively similar for each combination of top-boundary flux and permeability variance. Hence, results presented in the following discussion are from a single random-field realization that can be considered representative of the other random-field realizations

Results of a stochastic random-field simulation with a variance of 1.0 and a top boundary flux of 42.5 mm/yr [1.67 in/yr] are shown in Figures 2-3a through d. Figure 2-3a shows that the distribution of saturation in the fracture continuum is highly variable, particularly in the welded units, compared to the uniform-layer simulation. The fracture saturation is highest locally where permeability in the fracture continuum is low (e.g., compare Figure 2-1b to Figure 2-3a) and at the Tiva Canyon–Paintbrush boundary where the contrast in fracture permeability causes a permeability barrier. Figures 2-3a and 2-3b show that the spatial variability in fracture and matrix saturation decreases with depth within the Paintbrush unit as water progressively redistributes from the fracture continuum to the matrix continuum. The locations of highest saturations in the Paintbrush unit matrix coincide with the area beneath the highest input fluxes at the bottom of the Tiva Canyon unit fracture continuum. Figures 2-3c and 2-3d show the development of preferential flow paths in the fracture continuum of the Tiva Canyon and Topopah Spring welded units. The variability in fracture permeability causes these preferential flow paths in the welded tuff units despite the uniform application of water at the top boundary. Preferential flow paths also form in the matrix continuum of the Paintbrush unit beneath areas of highest flux at the base of the Tiva Canyon unit. As shown in Figure 2-3d, however, contrast between high- and low-flux flow paths in the Paintbrush unit diminishes substantially with depth.

Although not shown, results from the same stochastic random field simulation with top boundary fluxes of 12.5 and 22.5 mm/yr [0.49 and 0.89 in/yr] show the development of preferential flow paths identical to those shown in Figures 2-3a through d for the 42.5-mm/yr [1.67-in/yr] case with proportionately lower fluxes. Thus, within the range considered, the water flux rate does not affect the frequency of preferential flow channels in the heterogenous fracture continuum.

The effect from changes in the degree of fracture heterogeneity, expressed as the variance of the $\log_{10}$ permeability, was also evaluated. Figures 2-4a through d show model results for the same random field and 42.5-mm/yr [1.67-in/yr] boundary flux shown in Figure 2-3 after lowering the variance from 1.0 to 0.5. The reduced variance translates to reduced spatial contrast in permeability. The result is a more uniform distribution of saturation in the fracture continuum of the welded units and in the matrix of the Paintbrush unit (Figures 2-4a,b). By comparing the scale bars in Figures 2-4c and 2-3c, it can be seen that the reduced variance results in a lesser amount of the total infiltration flux flowing in focused flow paths. Figure 2-4d shows that differences in high- and low-flux areas in the matrix of the Paintbrush unit also are reduced as a result of less spatial variability of downward flux at the base of the Tiva Canyon unit. Results for the cases with input fluxes of 12.5 and 22.5 mm/yr [0.49 and 0.89 in/yr] are qualitatively similar and, hence, not shown.

Figures 2-5a through d and 2-6a through d show the results of increasing the variance of $\log_{10}$ fracture permeability to 1.5 and 2.0. The relative amount of infiltration flux flowing focused flow paths in fractures of the welded units increases with variance, leaving a larger volume of the rock drier. In fact, some of the flow paths seem to terminate as fewer flow paths carry larger amounts of water. These results show that the variance in fracture permeability correlates well with the degree of flow focusing in welded units where fracture flow dominates. Increased

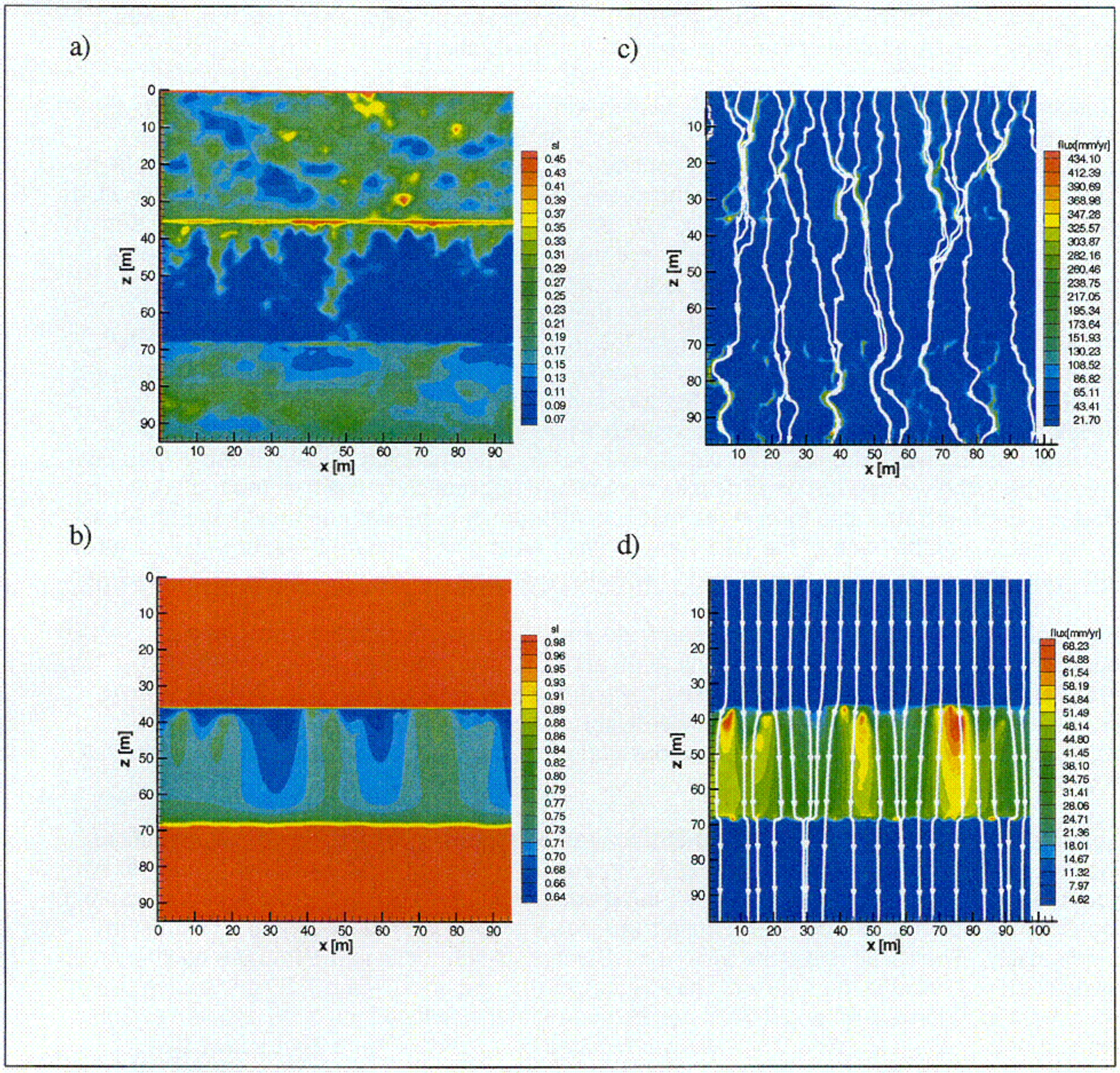

Figure 2-3. Steady-State Distribution of a) Fracture Saturation, b) Matrix Saturation, c) Fracture Water Flux, and d) Matrix Water Flux with Applied Water Flux of 42.5 mm/yr [1.67 in/yr] for a Stochastic Simulation with σ^2 = 1.0 (Note: 1 m = 3.2808 ft)

C03

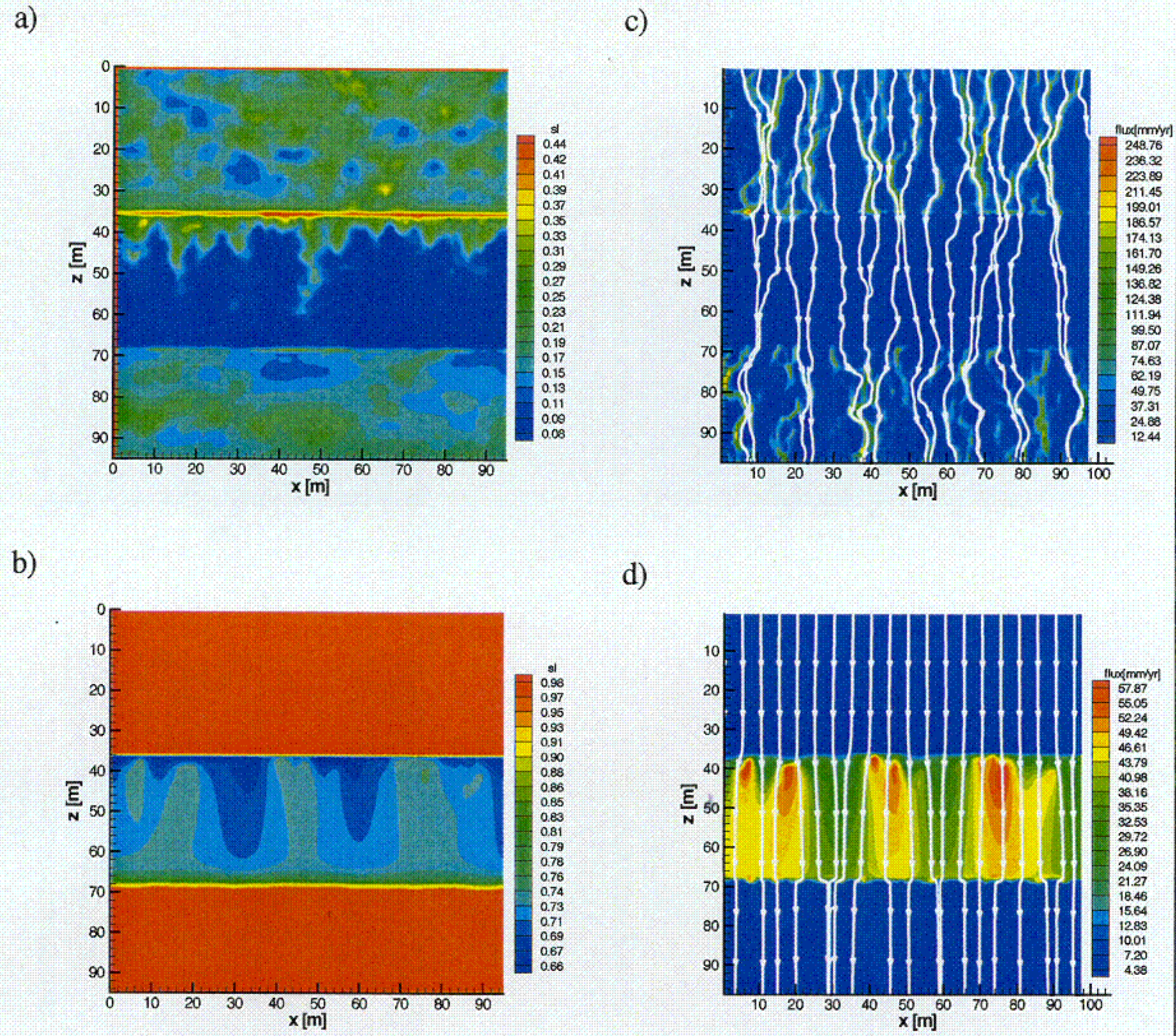

Figure 2-4. Steady-State Distribution of a) Fracture Saturation, b) Matrix Saturation, c) Fracture Water Flux, and d) Matrix Water Flux with Applied Water Flux of 42.5 mm/yr [1.67 in/yr] for a Stochastic Realization with σ^2 = 0.5 (Note: 1 m = 3.2808 ft)

C04

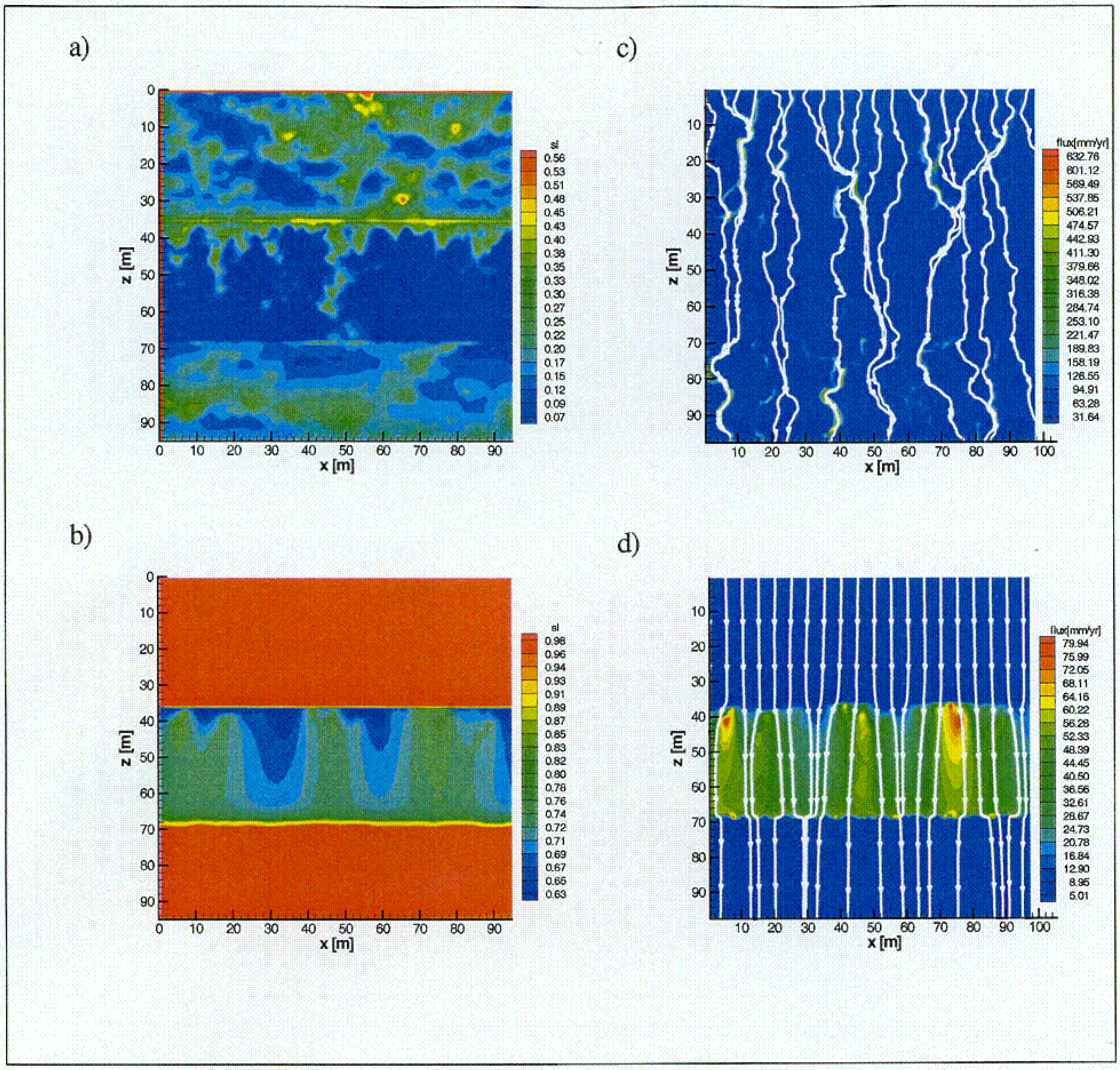

Figure 2-5. Steady State Distribution of a) Fracture Saturation, b) Matrix Saturation, c) Fracture Water Flux, and d) Matrix Water Flux with Applied Water Flux of 42.5 mm/yr [1.67 in/yr] for a Stochastic Simulation with σ^2 = 1.5 (Note: 1 m = 3.2808 ft)

C05

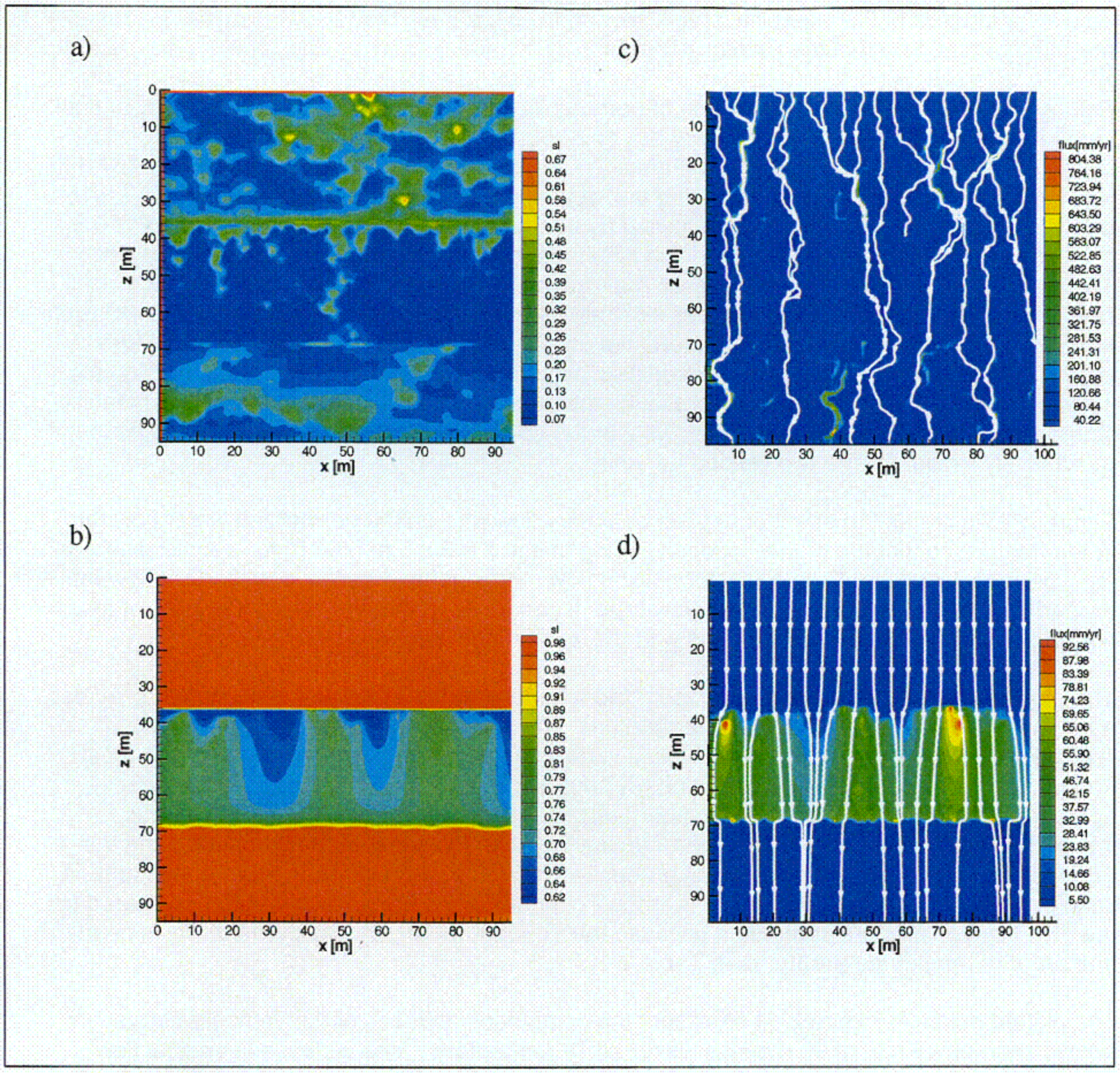

Figure 2-6. Steady-State Distribution of a) Fracture Saturation, b) Matrix Saturation, c) Fracture Water Flux, and d) Matrix Water Flux with Applied Water Flux of 42.5 mm/yr [1.67 in/yr] for a Stochastic Simulation with σ^2 = 2.0 (Note: 1 m = 3.2808 ft)

C06

variance also leads to increased flow focusing in the matrix of the Paintbrush unit; however, this result is attributed to the variability of flux arriving from the base of the Tiva Canyon unit rather than heterogeneity within the Paintbrush unit.

Figures 2-7 and 2-8 illustrate the effect of permeability variance on the spatial variability of flow in the fracture continua with a boundary flux of 22.5 mm/yr [0.89 in/yr]. The horizontal distribution of vertical flow is shown in Figure 2-7 for the Tiva Canyon unit at z = 20.5 m [67.3 ft] and in Figure 2-8 for the Topopah Spring unit at z = 80.5 m [264 ft]. The prefixes v05, v1, v15, and v2 in the legends of these and following figures represent the cases with variances of 0 5, 1.0, 1.5, and 2.0; the suffixes LF, MF, and HF stand for low-, medium-, and high-flux cases. The r9 in the legends refers to stochastic realization number nine; results from other realizations were similar. These figures illustrate, in a more quantitative manner, the conclusion that the magnitude of flow rates in preferential pathways increases with variance in fracture permeability, while the number of focused flow paths remains constant. For areas outside the preferential flow paths, water fluxes are lower than for the cases with homogenous permeability. Comparison of Figures 2-7 and 2-8 shows that the spatial variability of focused flow paths is qualitatively similar for the two welded tuff units.

Figure 2-9 illustrates the effect of applied boundary flow rate on the normalized water flow rate in the fracture continuum of the Topopah Spring unit at z = 80. 5 m [264 ft] for a realization with $\log_{10}$ permeability variance of 1.0. Normalized flow rate is defined as the local vertical flow rate divided by the total applied boundary flow rate. It can be seen that the relative amount of total flow in preferential channels increases with the applied flow rate.

The plotted points in Figure 2-10 represent the mean average of the vertical fracture flux across each row of 99 model cells for all 10 realizations. Therefore, each point on Figure 2-10 represents the mean value of 990 individual vertical flux values. It can be seen that the mean fracture flux in the Tiva Canyon unit is nearly constant with depth. The mean fracture flux approaches a small value within 15 m [49 ft] after it enters the Paintbrush unit as water is imbibed into the rock matrix. The mean fracture flux then increases abruptly on reaching the Topopah Spring contact and increases gradually to a stable value in the fracture continuum. A smaller percentage of total water flux is in the Topopah Spring fracture continuum compared to the Tiva Canyon fracture continuum because the Topopah Spring matrix permeability is nearly one order of magnitude greater (see Table 2-1).

The plotted points in Figure 2-11 represent the computed variances of the vertical fracture flux across each entire row of 99 model cells for all 10 realizations. The variance in vertical flow rate across each row of model cells provides an indication how far downward flow must go after entering a new layer before it is redistributed according to the degree of heterogeneity. Examination of the figure shows that vertical-flow variance in the Tiva Canyon and Topopah Spring welded tuff units appears to reach relatively constant values after about three to five correlation lengths, regardless of permeability variance or total applied water flux. This result is useful for future modeling of flow in the Paintbrush Tuff because it shows that effects of heterogeneity on focusing of flow from the overlying Tiva Canyon Tuff can be captured using a model with a thinner Tiva Canyon unit. For example, the results in Figure 2-11 show that the effects of heterogeneity on flow variability in the Tiva Canyon unit could have been captured using a 10-m [33-ft] thick Tiva Canyon unit (i.e , a thickness of five correlation lengths) instead of the 36-m [118-ft] section used in this modeling study.

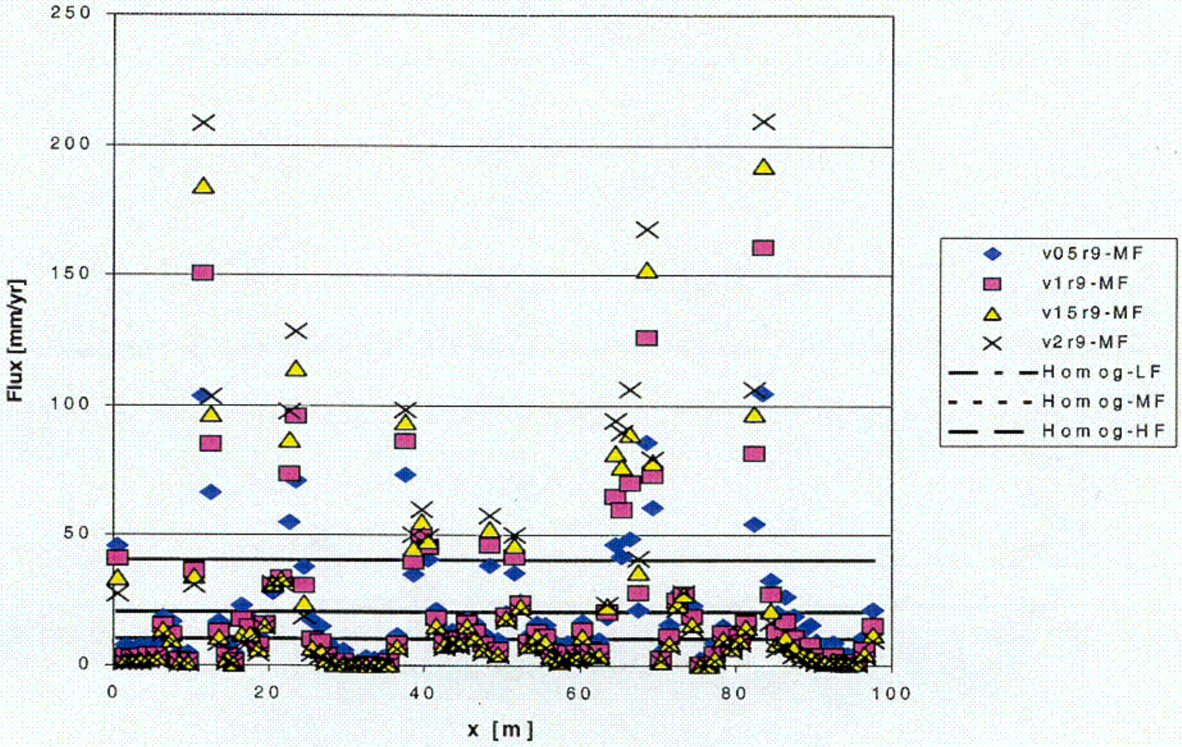

Figure 2-7. Flux of Water in the Fracture Continuum in the Tiva Canyon Unit at z = 20.5 m [67.3 ft] from Top Boundary: Stochastic Simulation Results Compared to Homogenous Simulations (Note: 1 m = 3.2808 ft; 1mm = 0.3937 in)

C07

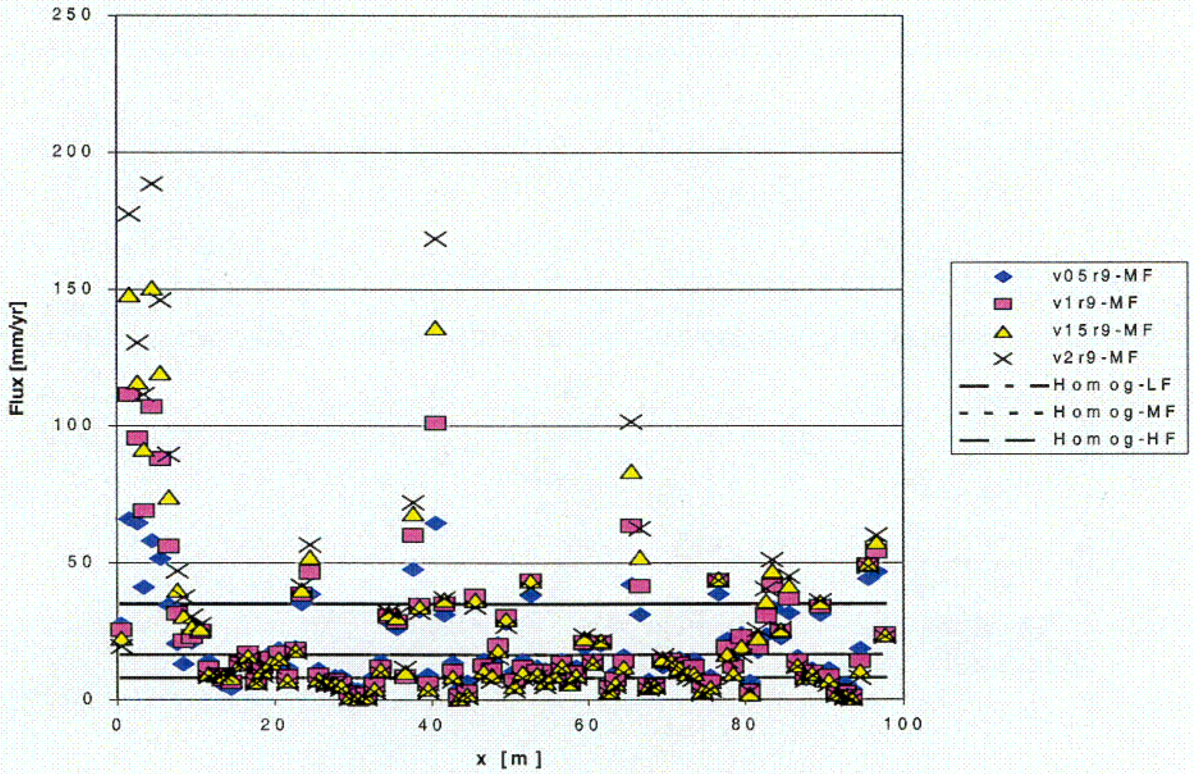

Figure 2-8. Flux of Water in the Fracture Continuum in the Topopah Spring Unit at z = 80.5 m [264 ft] from Top Boundary: Stochastic Simulation Results Compared to Homogenous Simulations (Note: 1 m = 3.2808 ft; 1mm = 0.3937 in)

C08

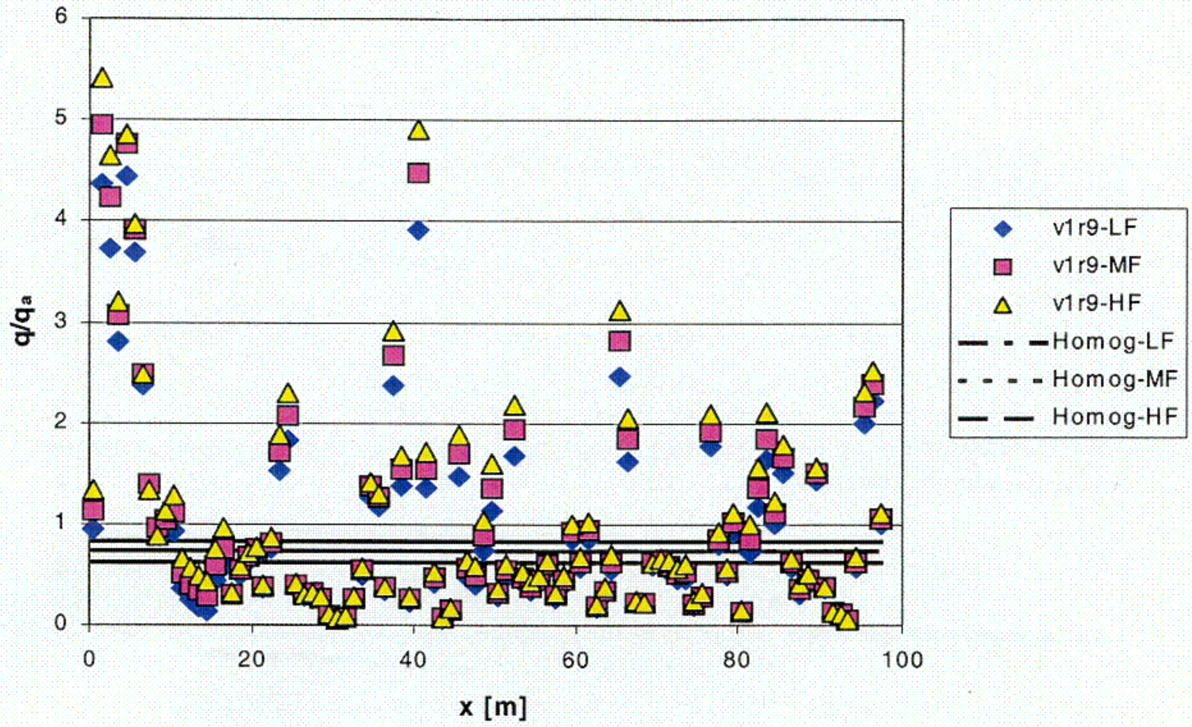

Figure 2-9. Normalized Flux of Water (q/q_a) in the Fracture Continuum in the Topopah Spring Unit at z = 80.5 m [264 ft] from Top Boundary for a Stochastic Simulation with σ^2 = 1.0 (Note: 1 m = 3.2808 ft)

C09

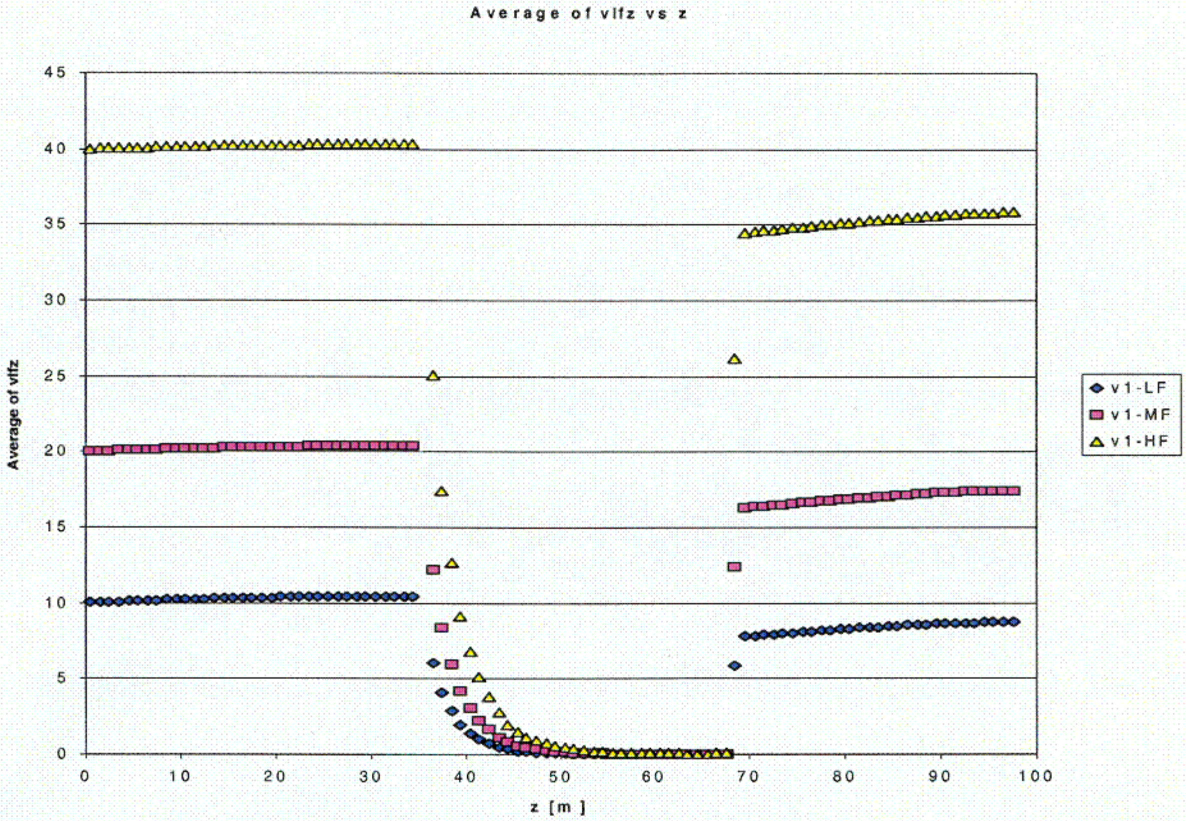

Figure 2-10. Mean Vertical Water Flux in the Fracture Continua of All 10 Stochastic Realizations with a $\log_{10}$ Permeability Variance of 1.0 (Note: 1 m = 3.2808 ft)

C10

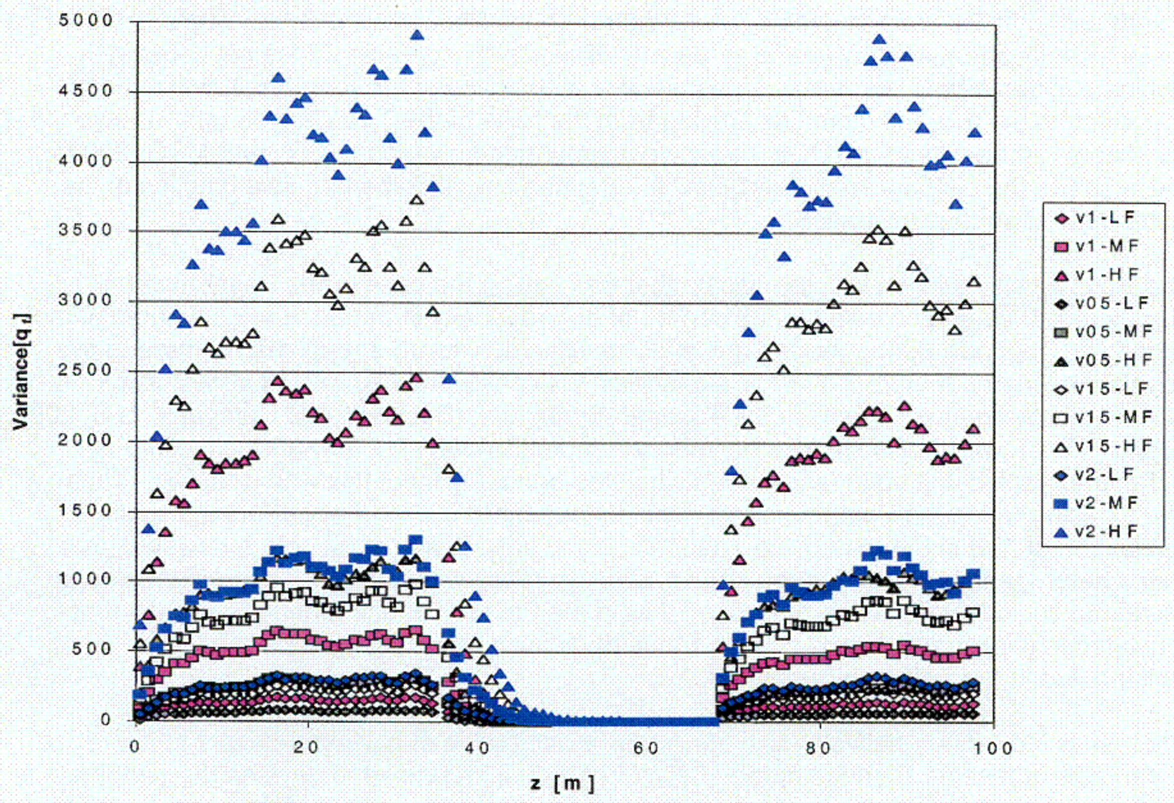

Figure 2-11. Variance of Fracture Flux Across Each Horizontal Row of the Model Grid Calculated Using Data from All 10 Stochastic Realizations (Note: 1 m = 3.2808 ft)

C11

2.2.3 Applicability of Results to the Review of DOE Models for Total System Performance Assessment

The stochastic simulations conducted in this study show that areas of focused flow in the Paintbrush unit matrix are correlated to the areas where focused fracture flow arrives from the base of the Tiva Canyon unit and are not attributable to the fracture heterogeneity within the Paintbrush unit. As water moves downward through the Paintbrush unit, the degree of focusing is significantly attenuated by lateral spreading. This lateral spreading does not completely eliminate focused flow, and areas of highest flux at the base of the Paintbrush unit remain correlated to the focused input flux arriving from the base of the Tiva Canyon unit. This result is consistent with results of the DOE site-scale unsaturated flow model (CRWMS M&O, 2000a), which shows the distribution of flow below the Paintbrush unit to be largely a function of the distribution of surface infiltration.

The stochastic simulation results indicate that flow exiting the base of the Paintbrush unit is quickly redistributed according to the degree of heterogeneity in the fracture continuum of the underlying Topopah Spring welded unit after traveling downward approximately three to five correlation lengths (Figure 2-11). This conclusion is consistent also with DOE results of modeling heterogeneity effects in the Topopah Spring unit (Bechtel SAIC Company, LLC, 2001, Section 4.3.2), which also showed rapid horizontal redistribution of flow after crossing hydrostratigraphic unit boundaries, even when the boundary input flux was localized. Thus, flow focusing within the Paintbrush unit does not appear to substantially affect the spatial distribution of flow in the underlying Topopah Spring unit. It should be noted, however, that matrix heterogeneity in the Paintbrush unit, such as zones with different degrees on mineral alteration, could lead to zones of focused flow in the Paintbrush unit farther apart than those simulated in this study. Widely spaced zones of focused flow may not be as readily redistributed in the Topopah Spring unit.

The results indicating relatively rapid horizontal redistribution of flow are relevant to the review of the DOE drift scale seepage model (CRWMS M&O, 2000f) used to develop the performance assessment abstraction for seepage into the proposed repository drifts The upper boundary surface of the heterogenous DOE seepage model is simulated by an extra grid cell with constant percolation flux connected to all the grid cells in the upper boundary, so flow is free to move into these cells according to local property parameters. A potential concern with this approach is that it was previously unclear whether seepage model results might differ with a spatially variable flux applied to the upper grid cells of the model. The stochastic simulation results suggest, however, that there is no need for concern because there are 10 m [33 ft] of model domain between the top seepage model boundary and the area of interest at the drift crown, this represents 20 correlation lengths for the assumed correlation length scale of 0.5 m [1.6 ft] used in the DOE seepage model.

The horizontal scale of the model grid used in this study is similar in magnitude to a single grid cell of the DOE site-scale model. Thus, the stochastic simulation results are useful for reviewing the assumption that hydrostratigraphic units can be treated as homogenous continua at the grid scale of the DOE site-scale model. Basically, the homogenous continuum assumption implies that each model grid block incorporates a range of heterogeneity such that the average hydraulic properties of each grid cell within a hydrostratigraphic unit are approximately the same. Simulation results for the 10 stochastic realizations of heterogeneity for each combination of permeability variance and flow rate were qualitatively similar in the resulting distribution of preferential flow paths and flow rate variability. This result suggests that grid blocks on the scale of several tens of meters, as used in the DOE site-scale model, can be treated as a homogenous continuum when the correlation length scale of fracture heterogeneity is on the order of 2 m [6.6 ft], as used in this study. There is uncertainty regarding the true correlation length scale for fracture permeability in the various hydrogeologic units at Yucca Mountain, however, available data from air-injection tests at multiple scales suggest that most of the variability in fracture permeability of the welded tuff units can be observed for scales of just a few meters (e.g., CRWMS M&O, 2000g).

Although the simulations presented in this report do not model transport pathways below the proposed repository, the results are generally applicable for review of the DOE approach to modeling radionuclide transport in fractures of the welded tuff units. The stochastic simulations show that a significant portion of the water flowing in fractures of the welded units can bypass a large volume of rock, thus reducing the available fracture-matrix interface area. The DOE radionuclide transport model used for performance assessment calculations (CRWMS M&O, 2000h) accounts for reduced interface area by incorporating the active-fracture concept of Liu, et al. (1998). The active-fracture conceptual model is a mathematical treatment of the variability of the fraction of active fractures as a power function of effective water saturation in connected fractures. Thus, in the DOE model, the matrix-fracture interface area available for diffusion of radionuclides from fractures into low-permeability rock matrix varies with fracture saturation (and, hence, deep percolation flux). At low percolation fluxes, effective fracture saturation is low and few fractures are active in the transport of water. When percolation flux increases, fracture saturation increases as does the number of active fractures. At full saturation of the fracture continuum, 100 percent of connected fractures are considered active in the DOE approach. The values of the active-fracture parameter for the DOE flow and radionuclide transport models are inferred through inverse modeling, using the site-scale unsaturated zone model and rock saturation data collected at Yucca Mountain (CRWMS M&O, 2000d).

The spacing between active fractures is an important input parameter in the radionuclide transport abstraction for DOE performance assessments. Liu, et al. (1998) estimated that approximately 18–27 percent of connected fractures in the Topopah Spring unit actively conduct water in ambient conditions. This estimate suggests that active-fracture spacing is approximately four to five times as great as the geometric fracture spacing. Liu, et al. (1998) estimated that active-fracture spacings range between 1.8 and 7.2 m [5.9 and 23.6 ft] for subunits of the Topopah Spring Tuff in the area of the proposed repository. Geometric fracture spacings used for the DOE model used for performance assessment are on the order of 0.25 m [0.82 ft] for that portion of the Topopah Spring unit below the proposed repository (CRWMS M&O, 2000h). Thus, active-fracture spacings would be on the order of 1 m [3 ft] if only about one-fourth of fractures are active in ambient conditions. This active-fracture spacing is small compared to the spacings between preferential flow paths in the welded units predicted by the stochastic simulations in this study. For example, Figures 2-7 and 2-8 show that spacings between grid cells with fluxes greater than the average applied flux are on the order of about 5 m [16 ft], albeit somewhat variable. The active-fracture spacings used in the DOE transport model are intended mainly to account for small-scale processes such as flow fingering within individual fractures and do not account for larger-scale fracture network heterogeneity. Thus, DOE performance assessments could result in overly optimistic radionuclide transport simulations because closer active-fracture spacings result in greater rates of matrix diffusion.

To address this concern, DOE agreed[1] to collect additional data from ongoing unsaturated zone field studies to either support or provide a basis for updating the active-fracture parameters used in the radionuclide transport abstraction. The model simulations conducted in this study and future modeling efforts will provide staff with technical bases for reviewing the DOE interpretation of its unsaturated zone field studies.

2.2.4 Considerations for Future Work

The stochastic simulations presented in this report do not consider possible correlations between fracture continuum permeability and moisture-retention characteristics. Such correlations may exist because fractures with narrower apertures would exhibit lower permeability but greater capillary suction of water. For conditions of correlated permeability and moisture retention, water would flow preferentially in the low-permeability, high-suction cells at lower infiltration rates. At increasing infiltration rates, as lower-permeability cells become more saturated, flow would then move into the higher-permeability cells with less capillary suction. Thus, the number of preferential flow paths in a heterogenous model may increase with the infiltration rate for a case with correlated permeability and moisture-retention properties. Future modeling work to evaluate the effects of such correlations would improve the technical basis for reviewing the DOE application of the active-fracture conceptual model to the radionuclide transport abstraction for performance assessment.

The present model does not incorporate such geologic complexities as sloping beds, large faults, and offsets in strata. Spatial variability in matrix permeability is also neglected; matrix heterogeneity is potentially important to flow in the Paintbrush unit, where flow occurs mainly in matrix rather than in fractures. Consideration of those factors and mechanisms may be attempted in future modeling to develop improved risk insights regarding the role of the Paintbrush nonwelded tuff unit in attenuating episodic and spatially variable flow that could lead to rapid or focused flow paths to the proposed repository horizon.

[1]Schlueter, J R. "U S Nuclear Regulatory Commission/U.S Department of Energy Technical Exchange and Management Meeting on Unsaturated and Saturated Flow Under Isothermal Conditions (August 16–17, 2000)." Letter (September 8) to S Brocoum, DOE Washington, DC NRC. 2000.

3 EFFECTS OF THE NONWELDED PAINTBRUSH TUFF ON THE SPATIAL AND TEMPORAL DISTRIBUTIONS OF UNSATURATED ZONE FLOW

The nonwelded Paintbrush Tuff is bounded above and below by the moderately to densely welded Tiva Canyon and Topopah Spring Tuffs. The nonwelded Paintbrush Tuff generally exhibits higher porosity and lower fracture intensity than either unit above or below it. The nonwelded hydrostratigraphic layers play an important role in controlling flow through the unsaturated zone at Yucca Mountain. Matrix-dominated flow through the nonwelded Paintbrush layers acts to dampen the episodic and spatially heterogeneous fracture flow that arrives through the Tiva Canyon moderately to densely welded units. The dampening of episodic flow by the nonwelded Paintbrush unit is the basis used to justify the steady-state infiltration boundary condition in the DOE site-scale unsaturated zone model for Yucca Mountain (CRWMS M&O, 2000a). The degree to which the flow is dampened has been questioned because of previous observations of bomb-pulse Cl-36 found below the nonwelded Paintbrush unit and the dilute chemical composition of the perched water relative to the matrix pore waters of the Paintbrush and Topopah Spring units. The dilute chemical composition of the perched water likely reflects rapid infiltration of water through fractures and faults. Both the Cl-36 observations and the dilute perched water reflect some fraction of percolation not in contact with the matrix of the Paintbrush unit for a significant length of time. A mechanism for bypassing matrix flow in the nonwelded units is the possible occurrence of lateral flow to large faults above the nonwelded Paintbrush unit.

Conditions favorable to the formation of one or more barriers to vertical flow may exist in the vicinity of the nonwelded Paintbrush Tuff of Yucca Mountain. Based on the modeling in Wu, et al. (2000), Bechtel SAIC Company, LLC (2001) suggests that large-scale lateral diversion would cause a significant amount of water to divert from the proposed repository footprint to faults located downslope away from the proposed repository drifts. If lateral diversion was to occur on a large scale, and assuming it focused flow into faulted zones, such a phenomenon could benefit performance if DOE could identify the important fault zones at depth and avoid placement of waste packages there.

Intralayer heterogeneity and gradational contacts would act to constrain the extent of lateral diversion. In addition, DOE notes that fractures, faults, and the occasional absence of the nonwelded Paintbrush Tuff (Bechtel SAIC Company, LLC, 2001) would also serve to limit lateral flow.

This chapter evaluates field evidence and the modeling of Wu, et al. (2000) to ascertain the potential for large-scale lateral flow above the proposed repository diverting water away from the proposed drifts.

3.1 Introduction and Background

During the Expert Elicitation for the Unsaturated Zone (CRWMS M&O, 1997), it was concluded there was likely lateral flow associated with the Paintbrush unit, however, it was on a scale of tens of meters. Because the lateral diversion was on a smaller scale than the size of the numerical grids used in the three-dimensional unsaturated zone flow model, lateral flow should not be reflected in the numerical model. Recently, Wu, et al. (2000) concluded that significant lateral flow can occur in the Paintbrush unit, based on a modeling exercise using refined numerical grids. They postulate that water flows laterally along capillary barriers into large faults, then vertically in the faults, thus, bypassing much of the proposed repository footprint. DOE summarized the work of Wu, et al. (2000) and incorporated the effect of enhanced lateral flow in the site-scale model by increasing the horizontal to vertical anisotropy from isotropic to ratios of 100:1 and 1000:1 (Bechtel SAIC Company, LLC, 2001). It was concluded that measured matrix pore water chloride data below the Paintbrush unit were better matched by the site-scale model with the large horizontal anisotropic permeability.

At low percolation rates, the potential exists for a capillary barrier to occur where the fine-grained matrix of the Tiva Canyon welded tuff unit overlies the coarse-grained matrix of the nonwelded Paintbrush Tuff. Alternatively, at elevated percolation rates, the potential exists for a permeability barrier to occur where large aperture open fractures of the Tiva Canyon welded tuff overlie the coarse-grained matrix of the nonwelded Paintbrush Tuff. Additionally, the potential exists for a capillary barrier to occur between the coarse-grained matrix of the nonwelded Paintbrush Tuff at its lower boundary and the fracture network of the densely welded Topopah Spring Tuff in locations where large aperture open fractures exist. Alternatively, the potential exists for a permeability barrier to occur between the coarse-grained matrix of the nonwelded Paintbrush Tuff and the densely welded Topopah Spring Tuff in locations where its once-open fractures are now filled with fine-grained alteration minerals. In this case, conditions are the reverse of those necessary for capillary barrier formation [i.e., a coarse-grained layer overlies a fine-grained layer (Flint, 1998)]. At low percolation rates, it would actually be possible to have capillarity-induced vertical flow enhancement between the coarse-grained matrix of the nonwelded Paintbrush Tuff and the underlying fine-grained matrix of the Topopah Spring welded tuff. Flint (1998) identified the crystal-rich vitrophyre of the Topopah Spring welded tuff as a potential source for flow barrier enhancement. That is, assuming that either a capillary barrier or permeability barrier exists, the resulting elevated matrix saturations may contribute toward the alteration of parent material to clays during extended periods of time, causing hydraulic property contrasts to increase and reinforcing the governing barrier phenomenon in discrete locations. Thus, such vitric zones potentially impose substantial control on the physical flow system, leading to the conclusion that detailed characterization of vitric zones is important, as is capturing the effect of its presence or absence during modeling efforts. Favorable conditions for capillary barrier and permeability barrier formation are also possible between individual hydrogeologic units within the nonwelded Paintbrush Tuff, based on the certainty of contrasting hydraulic properties (Wu, et al., 2000).

In general, the nonwelded Paintbrush Tuff exhibits a 10-degree or lower dip toward the east, while it thins from north to south. Above the proposed repository footprint, the thickness of the unit ranges between 60 m [197 ft] and 30 m [98 ft] (CRWMS M&O, 2000a). Wu, et al. (2000) based their hydrogeologic layering strategy on (i) the Geologic Framework Model 3.1 (CRWMS M&O, 2000i), (ii) analyses of rock property data (Flint, 1998), and (iii) the current mountain-scale unsaturated zone flow model (CRWMS M&O, 2000a). The lithostratigraphic unit boundaries defined by the Geologic Framework Model do not always correlate with the hydrogeologic unit boundaries defined through analyses of hydrologic matrix property data (Flint, 1998). Nomenclature of the nonwelded layers of the Paintbrush Group used by Wu, et al. (2000), and in this report, is included in Table 3-1. The Yucca Mountain hydrostratigraphy was delineated based on measurements of hydrologic properties of cores by Flint (1998), with porosity as the primary distinguishing factor. For example, the currently available hydrologic property data from lithostratigraphic layers Tpbt2, Tptrv3, and Tptrv2 do not exhibit a degree of variation sufficient to justify separate hydrogeologic layers. Thus, these three lithostratigraphic layers are represented as the unsaturated zone model layer ptn26. Conversely, analyses of the

Table 3-1. Thermal-Mechanical and Hydrostratigrahphy Associated with the Nonwelded Paintbrush Group (CRWMS M&O, 2000j)

Major Hydrostratigraphic Units	Thermal-Mechanical Stratigraphy	Description	Hydrostratigraphy Used in Site-Scale and Wu, et al. (2000) Models
Tiva Canyon Tuff	Tpcpv3	Welded basal vitric	tcw13
	Tpcpv2	Moderately welded basal vitric	
	Tpcpv1	Nonwelded basal vitric	ptn21
Nonwelded Paintbrush Tuff	Tpbt4	Bedded tuff	ptn22
	Tpy	Yucca Tuff	ptn23 ptn24
	Tpbt3	Bedded tuff	
	Tpp	Pah Canyon Tuff	ptn25
	Tpbt2	Bedded tuff	ptn26
Topopah Spring Tuff	Tptrv3	Upper nonwelded vitric	
	Tptrv2	Upper moderately welded vitric	

available hydrologic property data have suggested that the single Tpy lithostratigraphic unit is justifiably separated into three hydrogeologic units based on degree of welding. Thus, the upper and lower portions of the Tpy, which exhibit porosities greater than 30 percent, are combined with the Tpbt4 and Tpbt3 to create the ptn22 and ptn24 unsaturated zone model layers. The middle third of the lithostratigraphic unit Tpy exhibits porosities less than or equal to 30 percent and, thus, forms the unsaturated zone model layer ptn23. The ptn23 layer is not present in the Wu, et al. (2000) numerical model grid when the moderately welded horizon is less than 6 m [20 ft] thick. Wu, et al. (2000) employ the same six nonwelded Paintbrush layers and calibrated rock properties as used in the three-dimensional site-scale unsaturated flow model.

Wu, et al. (2000) modeled flow in the nonwelded Paintbrush Tuff using the TOUGH2 code (Pruess, 1991) with both a coarse and refined grid, and they relied on a highly refined grid to simulate capillary barrier-induced lateral flow diversion. They used the dual continuum/active-fracture conceptual model of the unsaturated zone, wherein fracture and matrix continua overlap and interact within the same domain. All four modeled cross sections have a top boundary coincident with the bedrock surface of Yucca Mountain, and the conditions applied thereto were those of net infiltration flux. A steady but spatially distributed net infiltration flux averaging 5 mm/yr [0.2 in/yr] was used, though focused flow was also evaluated either on the west end (updip) or the east end (downdip). Three of the four modeled cross sections have a bottom boundary located at the nonwelded Paintbrush Tuff and Topopah Spring welded tuff interface in such a manner that any potential capillary barrier in this transition zone could not be investigated. Instead, a gravitational drainage flow boundary is employed, whereby vertical capillary gradients are reduced to zero. Wu, et al. (2000) concluded that use of this boundary condition was reasonable when analyses of two alternative simulations using specified-head boundary conditions (based on matrix and fracture water potentials) led to the conclusion that the two-dimensional models were not sensitive to the type of boundary condition used at the bottom of the model. The remaining cross-sectional model has its bottom boundary at the water table and employs a Dirichlet (specified-head) boundary condition. Wu, et al. (2000) maintain that the results of this particular model are similar to their other models, none of which consider the part of the system below the nonwelded Paintbrush Tuff. Each cross-sectional model employs no-flow lateral boundary conditions, which is a reasonable assumption for many of the cross sections bounded laterally (especially downdip) by faults.

Sensitivity analyses performed with this cross-sectional model also suggest that uncertainties related to the fracture properties of the nonwelded Paintbrush Tuff are not particularly critical because a negligible effect on percolation flux at the nonwelded Paintbrush Tuff/Topopah Spring welded tuff interface is observed when simulations assume either arithmetically-averaged homogeneous fracture properties throughout the entire Paintbrush Tuff unit or an absence of fractures, as opposed to the usual assumption of homogeneous intralayer fracture properties. The effect of transient but uniform infiltration pulses was investigated with this cross-sectional model, leading Wu, et al. (2000) to conclude that the unique characteristics of the nonwelded Paintbrush Tuff effectively dampen transient pulses such that a state of dynamic equilibrium is the end result at the base of the nonwelded Paintbrush Tuff. Staff believe that this investigation would have been of greater value had infiltration pulses been representative of the elevated infiltration rates anticipated during future climate states, rather than the 5 mm/yr [0.2 in/yr] expected for current climate conditions.

Thus, the effect of heterogeneity on potential capillary barrier-induced lateral flow diversion in the vicinity of the nonwelded Paintbrush Tuff needs to be evaluated. DOE agreed[1] to evaluate spatial heterogeneity of hydrologic properties within hydrostratigraphic units and the effects this heterogeneity has on model results of unsaturated flow, seepage into drifts, and transport (agreement TSPAI.3.23). DOE acknowledged that future simulations of the nonwelded Paintbrush Tuff, which will incorporate lateral heterogeneity, are anticipated to demonstrate a lesser degree of lateral flow diversion and focus more on flow into preferential pathways than previous models (Bechtel SAIC Company, LLC, 2001). Wu, et al. (2000) conclude by stating that future investigation of flow behavior within the nonwelded Paintbrush Tuff should focus on characterization of the two hydrogeologic units (ptn21 and ptn23) most responsible for capillary barrier effects, including quantification of the detailed spatial variation of hydrologic properties. CNWRA staff are performing independent modeling of heterogeneity in hydrostratigraphic units with particular emphasis on the ability of the nonwelded Paintbrush Tuff unit to attenuate transient and spatially variable flow.

---

[1]Reamer, C.W. "U.S Nuclear Regulatory Commission/U S. Department of Energy Technical Exchange and Management Meeting on Total System Performance Assessment and Integration (August 6–10, 2001)." Letter (August 23) to S Brocoum, DOE. Washington, DC: NRC. 2001

3.2 Indications of Lateral Flow from Field Observations

Saturated horizons (perching or elevated saturations), sharp linear contacts, and spring deposits where the Paintbrush unit crops out would all indicate the possibility of extended lateral flow in layers associated with the Paintbrush unit. CRWMS M&O (1997), Flint (1998), and Flint, et al. (2001) point out the lack of supporting evidence for extended lateral diversion associated with the Paintbrush unit. This section describes field observations and measurements that appear to support only localized lateral diversion in the Paintbrush unit.

The transition at the base of the Tiva Canyon Tuff into the top of the nonwelded Paintbrush group proceeds from moderately welded, vapor-phase corroded to nonwelded (CRWMS M&O, 2000j). The transition in the basal Tiva Canyon unit also corresponds to a change from devitrified to vitric, with a concurrent increase in mineral alteration. One interpretation for the increasing mineral alteration is longterm presence of elevated water saturations. Underlying the altered zone is the sharp contact of the nonwelded bedded tuffs of the Paintbrush unit. At the North Ramp, the saturation profile reflects a nearly saturated basal Tiva Canyon markedly dropping off to 50-percent saturation in the upper bedded unit of the Paintbrush Tuff.

A possible location for a permeability barrier is the lower bedded Paintbrush Tuff horizon overlying welded rock of the Topopah Spring unit (CRWMS M&O, 2000j). The matrix of the bedded tuff has much larger permeability than the welded matrix of the Topopah Spring. Flint (1998) suggests that vapor-phase alteration may significantly reduce fracture permeability locally in the upper Topopah Spring rock, thus causing a barrier to downward flow. Because the alteration is not widespread, however, flow would generally proceed vertically through the fractures of welded tuff.

A survey of vertical saturation profiles measured or estimated for boreholes crossing the Paintbrush unit was undertaken to identify possible horizons where lateral flow may be occurring. Saturation profiles with sharp increases, possibly up to full saturation, overlying sharp decreases in saturation may be indicative of lateral flow caused by capillary barriers. The degree of welding must be factored into the analysis because saturation of welded rocks is generally more than 90 percent, while those of nonwelded rocks is 40–60 percent.

There are no consistent horizons of elevated saturations that would be associated with large-scale lateral flow due to a capillary or permeability barrier. Some zones of elevated saturations are associated with zones of mineral alteration. The alteration to clays in these zones caused saturations to be elevated, with or without lateral diversion. Mineral alteration is not laterally extensive across the proposed repository footprint.

Observations from profiles of saturation are

- Vertical profiles of saturation in boreholes in the North Ramp of the Exploratory Studies Facility suggest the elevated saturations are associated with zones of mineral alteration. Mineralogy, texture, and hydraulic properties were determined from 21 boreholes vertically crossing the section (CRWMS M&O, 2000j). The mineral alteration zones includes the formation of clays, leading to a low permeability, in the lower Tiva Canyon (Tpcpv1) and the lower bedded unit of the Paintbrush Tuff (Tbpt2). Both mineral alteration zones were associated with elevated saturation. It appears that the upper zone (Tpcpv1) could be a permeability barrier that causes flow to occur in the overlying fractured, moderately welded rocks. In the other high saturation zone, the Tpbt2 horizon, saturation could build up above a possible capillary barrier between the bedded tuff (Tpbt2) and fractures of the underlying vitric unit of the Topopah Spring Tuff.

- Flint (1998) presents saturation profiles for boreholes SD–7, SD–9, N54, N55, and N31. Important features for the saturation profiles in the Tpcpv1 unit are (i) borehole N31 shows that the basal nonwelded tuff of the Tiva Canyon (Tpcpv1) is near full saturation; (ii) boreholes SD–7, SD–9, and N55 show there is a downward change from nearly 100 percent to approximately 50 percent in the Tpcpv1 unit; and (iii) borehole N54 shows that Tpcpv1 remains less than 50 percent saturated. For the remaining portion of the Paintbrush Tuff (below Tpcpv1), the saturation remains between 30 and 60 percent for all these boreholes: N31, N54, N55, SD–7, and SD–9.

- Wu, et al. (2000) plot saturations for UZ–14, but they do not subdivide the hydrostratigraphy of the Paintbrush Tuff. It appears that saturations are elevated in the lower portion of the Paintbrush Tuff and that there is a sharp reduction in the saturations from 60 to 30 percent in the middle of the Paintbrush Tuff. The latter zone may coincide with the capillary barrier at the ptn23/ptn24 contact reported by Wu, et al. (2000).

- Measurement of core saturations from SD–6 (Figure 3-1a) exhibit an increase to full saturation in a zone above the Tpcpv1 horizon and a gradational decrease down to approximately 30 percent saturation in the Tpcpv1 (uppermost ptn21 hydrostratigraphic layer). The shape of the profile is not consistent with a capillary barrier, but is consistent with a zone of mineral alteration where the alteration may be decreasing in the ptn21 layer. The high saturations in tcw13 could also be a reflection of the fine pore sizes associated with quenching of the vitric tuff. Lateral diversion may occur in the tcw13, though the presence of any fractures in the moderately welded tcw13 layer would promote vertical flow. The isolated high saturation at the top of ptn26 does not, in itself, support the presence of a barrier causing lateral flow.

- Interpretations of geophysical measurements supported by local core measurements of saturations are plotted for SD–12 in Figure 3-1b. There is one prominent feature of the saturation profile of SD–12. The sharp increase in saturation at the base of the ptn21 hydrostratigraphic layer appears to correspond with the thermal mechanical layer boundary between the basal nonwelded vitric of the Tiva Canyon Tuff (Tpcpv1) and the bedded tuff (Tpbt4). The slight decrease in the porosity corresponding with the sharp increase in saturation may reflect mineral alteration. The Yucca Tuff is not present at SD–12.

- Figure 3-2 is a generalized saturation profile of the Paintbrush Tuff layers developed from the hundreds of saturation measurements from cores reported in Flint (1998). The average saturation for each hydrostratigraphic layer is plotted in the middle of the layer. In an average sense, there do not appear to be any prominent features of the saturation profile that might reflect lateral diversion by capillary or permeability barriers.

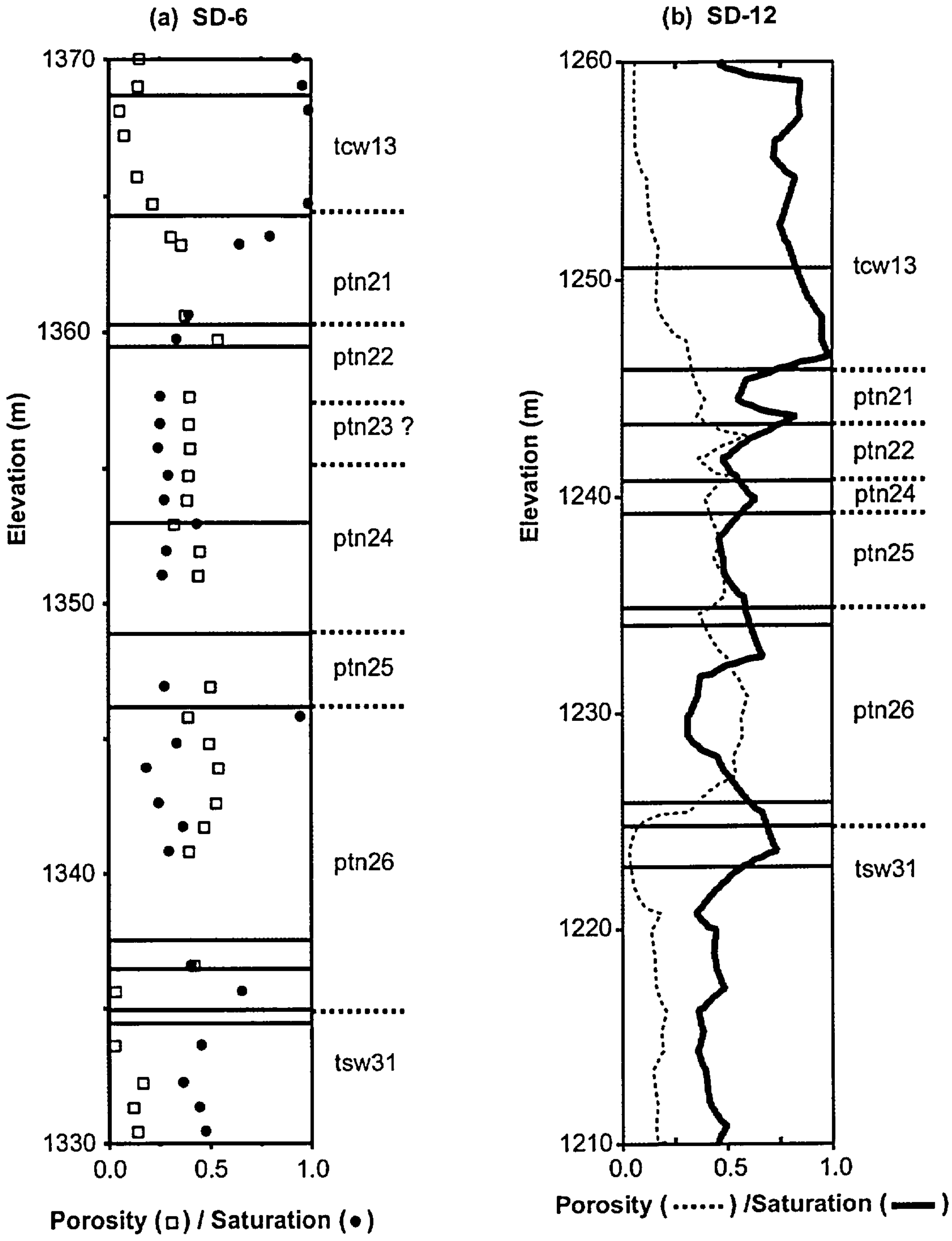

Figure 3-1. Saturation and Porosity Profiles from (a) Measured Core Data for SD–6 and (b) Interpreted Geophysical Data for SD–12. Lines Within Plot Area Mark the Thermal Mechanical Stratigraphy. Hydrostratigraphy Is on Right Axis. (Note: 1m = 3.2808 ft)

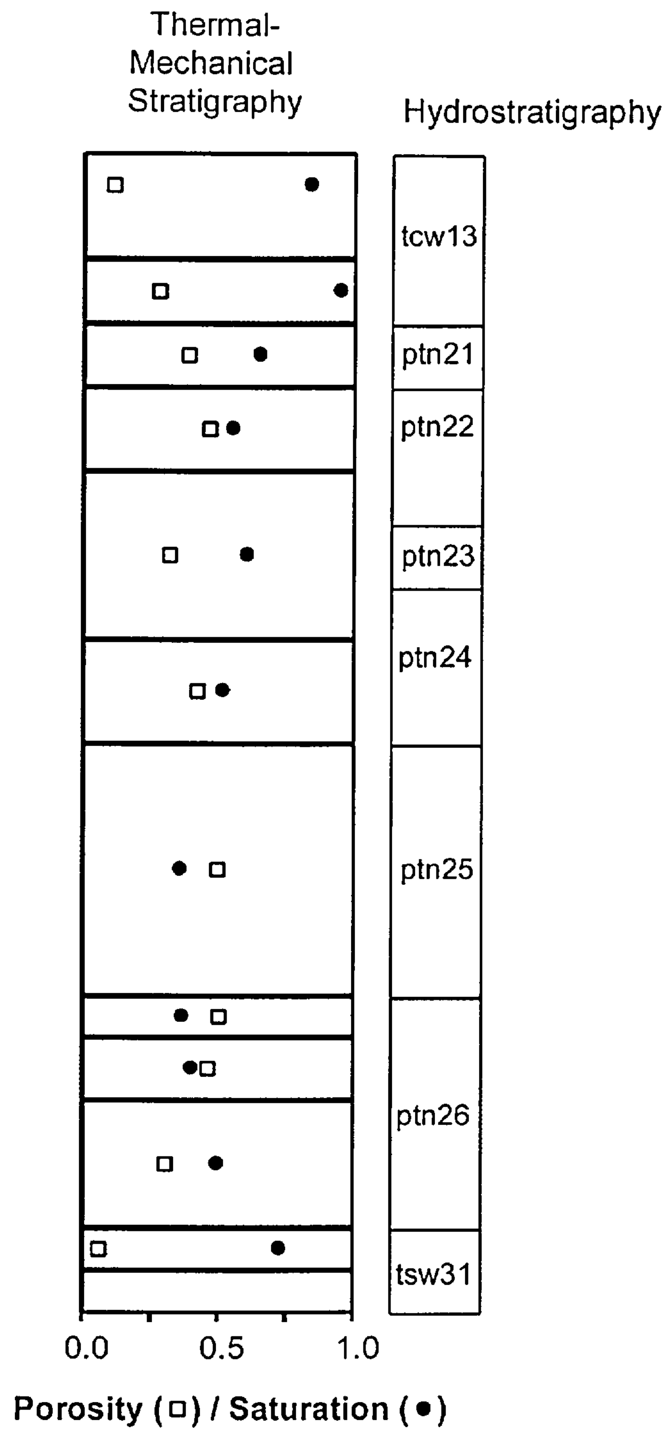

Figure 3-2. Generalized Saturation and Porosity Profile Developed from Flint (1998) Data

- Episodic flow through the Tiva Canyon, as supported by pneumatic and matric potential data monitored in Pageny Wash during an El Niño event (LeCain, et al., 2000) can saturate the fracture network. Saturation of the overlying layer in an otherwise capillary barrier scenario, completely disables the barrier. Saturated flow in the fracture network of the Tiva Canyon likely would only affect breakthrough for the uppermost capillary barrier. The episodic pulse would likely be dampened and shift to unsaturated4 flow as it migrates through nonwelded layers. It is not clear if saturation of the fracture network occurs with every percolation event, hence, episodic flow may not always lead to the breakdown of a capillary barrier in the upper portion of the nonwelded Paintbrush unit.

Based on the saturation profiles, lateral diversion could be occurring locally where there is mineral alteration near the top of the Paintbrush Tuff and in the lower layer of the Paintbrush Tuff. If these are zones of lateral diversion, lateral flow would be occurring in or above the tcw13 layer and in the ptn26 layer. Lateral flow in the tcw13 layer, related to the alteration, would be classified as a permeability barrier. In the ptn26 layer, mineral alteration was noted only in the North Ramp study (CRWMS M&O, 2000j). Neither of these locations for lateral flow, in or about tcw13 and in ptn26, are consistent with the locations (ptn21 and ptn23) predicted by Wu, et al. (2000) for extensive lateral diversion.

3.3 Analysis of Capillary Barrier Potential Associated with the Paintbrush Tuff

Capillary barriers can occur where a fine-grained layer overlies a coarse-grained layer. In this application, the grain size distribution is used as a surrogate for the pore size distribution. At low-flow conditions, capillarity dictates that water preferentially remains in the small pores rather than in the large pores. Hence, for a sloped interface, water preferentially flows downslope in the overlying fine-grained porous media. At some point downslope, the matric potential in the fine layer will have risen to levels needed for flow to breakthrough into the coarse underlying layer. Beyond the breakthrough point, there is a downslope zone where breakthrough is some fraction of percolation flux. At some point further downslope, the capillary barrier will self-regulate and the flux crossing the interface will equal the percolation flux entering the system, hence, there will be no net increase in lateral flow. The downslope length for breakthrough is a function of the unsaturated zone properties of each layer, the slope angle of the interface, and the percolation rate.

Idealized numerical modeling of homogeneous layers with smooth linear surfaces (Wu, et al., 2000) indicates that lateral diversion in the Paintbrush Tuff is a prominent feature above the proposed repository at Yucca Mountain. Their modeling suggests 40 percent of the percolation above the Paintbrush unit for the entire model domain is diverted to faults; the percentage for the proposed repository footprint would be higher. Morphology of the layer boundary surfaces, saturation data from boreholes, and heterogeneity of matrix properties all indicate a limited amount of lateral flow likely occurs within the nonwelded Paintbrush hydrostratigraphic units.

There are three important aspects for modeling capillary barriers when a dual continuum representation is used: (i) adequate representation of the geologic structures and changes in textures; (ii) grid size in relation to retention properties, particularly the bubbling pressure head; and (iii) adequacy of the dual-continuum representation to represent the capillary barrier process.

DOE uses uniform properties within each hydrostratigraphic layer, which have been referred to as a layer-cake-type model. Sharp changes in properties occur at the boundary of each layer in such a model. Often, this approximation is acceptable, given the objectives of the modeling exercise. For modeling exercises that intend to demonstrate the presence of capillary barriers (e.g., Wu, et al., 2000), however, treating all layer boundaries as sharp contrasts in properties is not reasonable, because the type of transition of hydrologic properties at lithologic and hydrostratigraphic boundaries can control such processes. Lithologic and hydrostratigraphic boundaries in the Paintbrush Tuff are described in Section 3.3.1.

3.3.1 Layer Boundaries

Topology and type of hydrostratigraphic contacts determine the likelihood and magnitude of capillary and permeability barriers. Sharp, smooth layer boundaries promote lateral diversions. Uneven boundaries or gradational contacts significantly reduce the potential for lateral diversion.

The term uneven boundaries refers to the smoothness of the planar surface defining the contact between hydrostratigraphic layers. Considering the processes of ashfall and ignimbrite deposition on an existing uneven land surface, uneven boundaries would be expected as the norm. Any amount of unevenness of the hydrostratigraphic contact planes would reduce the extent of lateral diversion.

Gradational contacts also significantly reduce the capillary barrier potential. Table 3-2 contains the thermal-mechanical stratigraphy, the hydrostratigraphy used in the three-dimensional site-scale unsaturated flow model (CRWMS M&O, 2000a), and the types of contacts between the different units. The bedded tuffs (Tpbt4,3,2) exhibit fine to coarse layering and have sharp contacts with overlying and underlying layers, consistent with episodic ash and pumice air-fall deposition. On the other hand, the Yucca Tuff (Tpy) and Pah Canyon Tuff (Tpp) are massive nonwelded ignimbrites with little internal distinct layering. Portions of each tuff may grade to moderately welded rock type. In the vicinity of Yucca Mountain, only the Yucca Tuff exhibits moderate welding, albeit ill-defined spatially. The basal vitric Tiva Canyon and upper Topopah Spring units grade from welded to nonwelded for vertical distances on the scale of meters to tens of meters.

Table 3-2. Stratigraphy and Type of Contacts for the Paintbrush Tuff Layers. The Lower Contact Refers to the Thermal-Mechanical Horizons Except for the Yucca Tuff (Tpy), Which Wu, et al. (2000) Break Out Because of the Local Presence of a Moderately Welded Zone.

Thermal-Mechanical Stratigraphy	Hydrostratigraphy	Lower Contact
Tpcpv3	tcw13	gradational
Tpcpv2		gradational
Tpcpv1	ptn21	sharp
Tpbt4	ptn22	sharp

Table 3-2. Stratigraphy and Type of Contacts for the Paintbrush Tuff Layers. The Lower Contact Refers to the Thermal-Mechanical Horizons Except for the Yucca Tuff (Tpy), Which Wu, et al. (2000) Break Out Because of the Local Presence of a Moderately Welded Zone. (continued)

Thermal-Mechanical Stratigraphy	Hydrostratigraphy	Lower Contact
Tpy		gradational
	ptn23	gradational
	ptn24	sharp
Tpbt3		sharp
Tpp	ptn25	sharp
Tpbt2	ptn26	sharp
Tptrv3		gradational
Tptrv2		gradational

Sharp contacts or disconformities promote lateral diversion because there is a sharp contrast in hydrologic properties at the contact. Gradational contacts are counter to the development of lateral flow, but are difficult to implement in numerical models. Wu, et al. (2000) use homogeneous properties for each hydrostratigraphic layer, which forces a sharp contact in the numerical model even when gradational contacts occur in the field. Indications of lateral flow derived from barriers in numerical models where gradational contacts occur should be considered suspect.

Wu, et al. (2000) indicate that lateral flow occurs in the ptn23 unit. However, ptn23 is defined as the portion of the Yucca Tuff that exhibits a moderate degree of welding (Flint, 1998; Wu, et al., 2000), which would necessarily have gradational contacts with the less welded or nonwelded portions of the Yucca Tuff above and below ptn23. Wu, et al. (2000) also concluded that a lesser extent of lateral flow occurred in the ptn21 layer. As a bedded tuff, the lower contact of the ptn21 layer is sharp; that is, the contact is readily identified in the field or borehole cores. In conclusion, Wu, et al. (2000) predict less lateral flow at a contact where sharp changes in properties actually occur and more lateral flow at an artificially imposed sharp contact.

3.3.2 Analysis of Unsaturated Zone Properties of the Paintbrush Tuff

Analysis of matrix and fracture constitutive relations gives an indication of the potential for a capillary barrier to form. Conceptually, the constitutive relations for retention and relative permeability reflect the pore size distribution. The relationships of the effective permeability curves for a capillary barrier scenario are distinctive. The curves cross; the lower coarse layer is more conductive at small (less negative) matric potentials and less conductive at large (more negative) matric potentials than indicated by the curve for the upper fine layer. Effective permeability curves for the two layers associated with each horizon noted by Wu, et al. (2000) as being capillary barriers with lateral flow in the upper layers are plotted in Figure 3-3. The case of ptn21 overlying ptn22 (Figure 3-3a) clearly indicates that a capillary barrier condition should occur. For the most prominent layer with lateral flow, noted by Wu, et al. (2000) as being a capillary barrier for both matrix and fractures, the ptn23 overlying ptn24 system is actually a permeability barrier. Figure 3-3b shows that the effective permeability of ptn24 is less than that of ptn23 for all matric potential conditions.

The results of a similar analysis for each pair of layers, both matrix and fracture continuum (treated separately), are presented in Table 3-3. It can be seen here that the Wu, et al. (2000) modeling results for lateral flow in the ptn21 layer reflect a capillary barrier, whereas the lateral flow in ptn23 reflects the combined effect of a permeability barrier in the matrix continuum and a weak capillary barrier condition in the fracture continuum.

Permeability barriers occur where high-permeability porous media overlies low-permeability media, and furthermore, the value of the applicable effective permeability in the lower unit is less than the percolation rate. If the interface was horizontal, the low-permeability layer would constrain the rate of vertical percolation. Ponding would occur, with the increase in ponding height causing the percolation rate through the lower horizon to increase slightly. For an inclined interface between the high- and low-permeability layers, the portion of percolation that moves along the stratigraphic boundary in the upper layer is a function of the slope angle (which affects the component of the gravity vector) and the contrast in effective permeability (function of the matric potentials). The profile of saturations for a permeability barrier differs from that of a capillary barrier. The top of the lower layer in a permeability scenario should saturate, with the depth of saturation dependent on the permeability in the upper layer and the slope angle. The lower layer drains in a capillary barrier scenario; the top of the lower layer shows a sharp jump in saturation starting at the boundary of the two layers.

Table 3-3. Analysis of Constitutive Relations for Layers of Paintbrush Tuff to Determine Likely Capillary and Permeability Barriers Using the Values of the Calibrated Property Set Presented in CRWMS M&O (2000d) and Wu, et al. (2000)

Upper/Lower Layers	Matrix Continuum	Fracture Continuum	Contact Type
tcw13/ptn21	—	permeability barrier	gradational
ptn21/ptn22	strong capillary barrier	—	sharp
ptn22/ptn23	—	permeability barrier	gradational
ptn23/ptn24	permeability barrier	weak capillary barrier	gradational
ptn24/ptn25	—	—	sharp
ptn25/ptn26	weak capillary barrier	—	sharp

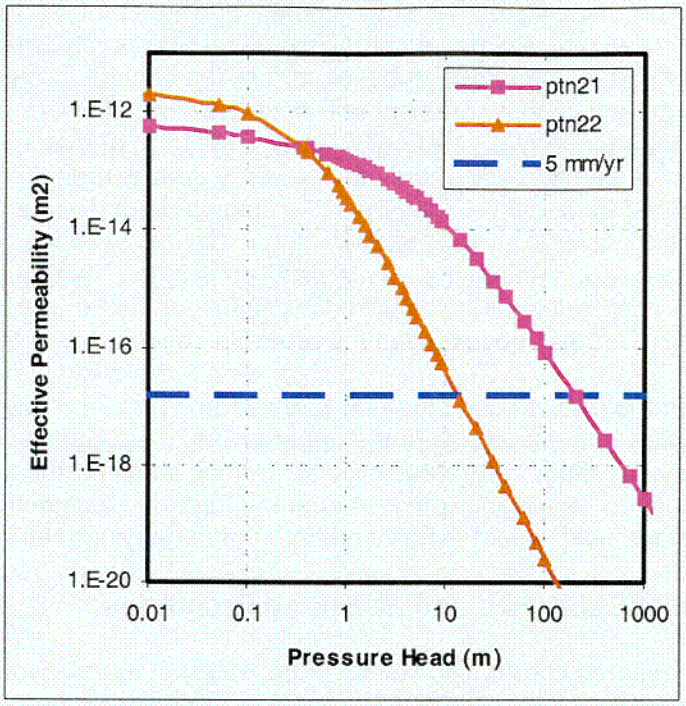

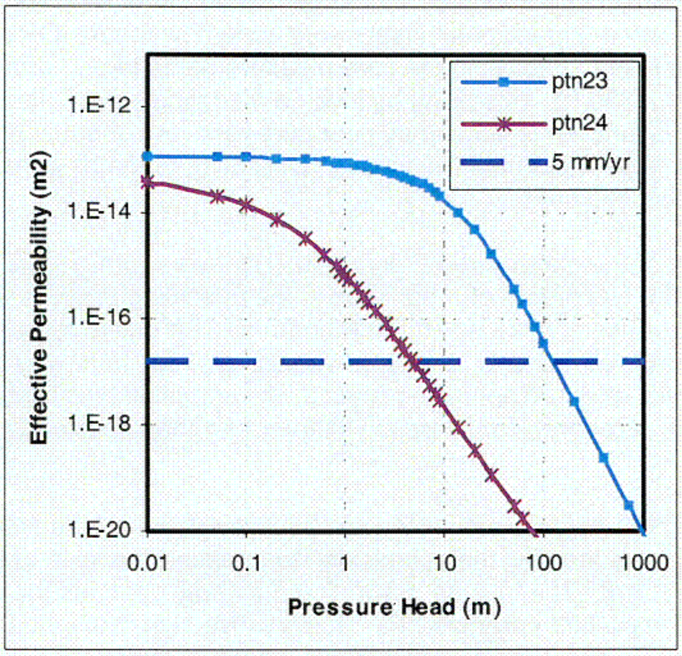

Figure 3-3. Effective Permeability as a Function of Matric Potential Is Plotted for Hydrostratigraphic Layers: (a) ptn21 Overlying ptn22 Is a Capillary Barrier and (b) ptn23 Overlying ptn24 Is a Permeability Barrier. A Percolation Rate of 5 mm/yr [0.2 in/yr] Is Plotted for Reference (Horizontal Line). (Note: 1m = 3.2808)

C12

It is difficult to assess the permeability barrier at the contact between ptn23 and ptn24 by analyzing the constitutive relations. Rough estimates used in this approach may not reflect the more precise estimates of matric potential distribution across the contact calculated by the numerical model. Matric potentials measured in the Paintbrush Tuff, however, are generally measured at less than 0.5 bars (CRWMS M&O, 2000j), or 5 m [16 ft] of matric head. At this matric potential, the effective permeability of the ptn24 layer is greater than the magnitude of the average percolation flux {~5 mm/yr [~0.2 in/yr]}. The magnitude of diversion predicted by Wu, et al. (2000) in the ptn23 layer likely reflects two things. One, downslope lateral flow is initiated in areas where percolation above the Paintbrush Tuff is large. Two, upgradient contributions of lateral flow propagate lateral flow in downslope segments where percolation rates above the Paintbrush Tuff may be less than the effective conductivity of the ptn24 layer.

The permeability barrier in the fracture continua (tcw13/ptn21 and ptn22/ptn23) does not likely create a barrier because flow in the fractures of the upper layers in each case could readily be distributed into the underlying matrix. The weak capillary barrier noted for the ptn23/ptn24 contact is not strong enough to be a significant barrier in the fracture continuum. Flow in the upper fracture network, in the field, would readily sorb into the underlying matrix

3.3.3 Comparison of Calibrated and Measured Properties

A direct comparison of measured core-based values (Flint, 1998) of matrix hydrologic properties and the calibrated set of values (CRWMS M&O, 2000a) should be performed with caution Upscaling and biased core recovery should be factored into the comparison. Inverse modeling to calibrate the three-dimensional unsaturated zone flow model (CRWMS M&O, 2000a) accomplishes the task of upscaling the core measurements to grid size greater than a length dimension of 100 m [330 ft] Upscaling by inverse modeling should also remove the biasing of core-based measurements caused by poor core recovery of horizons that generally would have the largest permeability values Upscaling of matrix permeability and van Genuchten α are discussed next.

The matrix permeabilities of the upper three Paintbrush Tuff layers (ptn21, ptn22, and ptn23) are increased by more than two orders of magnitude in the upscaling process (inverse calibration). The permeabilities of the lower three Paintbrush Tuff layers remain about the same as the geometric mean of the core measured values. It is not clear why the upscaling would cause this differential effect There is no reason why sampling bias for core measurements (poor core recovery) should be any different for the upper and lower Paintbrush Tuff layers.

Upscaling the van Genuchten parameters for the constitutive relations for unsaturated flow is complex. In dual-permeability models, the complexity is increased because of the effect of the matrix/fracture interaction term The inverse calibration markedly changes the relative values of the van Genuchten α, an important parameter for capillary diversion, from those measured on cores. Values for layer ptn21 decrease by a factor of seven and values for ptn22, ptn24, and ptn26 all increase significantly as a result of the upscaling.

Although it is understood that inverse calibration of the site-scale unsaturated zone flow model accomplishes an upscaling of core values to grid scale values and removes the bias of poor core recovery, it is not clear why marked relative changes between layers should occur It is also not clear that a refined grid as used by Wu, et al. (2000) should use the parameter values upscaled to >100 m [330 ft] grid-block length scale.

3.3.4 Effect of Heterogeneity on Lateral Flow Above a Capillary Barrier

Random heterogeneity of the unsaturated zone properties degrades the performance and effectiveness of a capillary barrier (e.g., Ho and Webb, 1998). The intralayer heterogeneity of the Paintbrush Tuff layers decreases the effectiveness of a capillary barrier predicted on homogeneous properties.

An analysis of heterogeneity of permeability is presented in Figure 3-4, which contains mean values and ranges of core measurements made at Yucca Mountain. The calibrated permeabilities from the site-scale three-dimensional unsaturated zone flow model are also plotted for reference. Deep borehole core values of permeability represent vertical heterogeneity at numerous isolated locations across Yucca Mountain. Surface-based cores were collected along transects and represent, to some extent, local lateral variability of units. Multiple transects across Yucca Mountain are reflected in Figure 3-4, so large-scale variability is also represented. It is clear from Figure 3-4 that each layer of the Paintbrush Tuff is highly variable. No appropriate geospatial analysis has been completed, possibly because the data are mostly from sparse, isolated locations.

Ho and Webb (1998) reported on a numerical study of the effect of heterogeneity of granular porous media on a capillary barrier. They found that a purely random heterogeneity led to the earliest downslope breakthrough in a sloped capillary barrier. They also found that a finely layered upper horizon, heterogeneous but with horizontal correlation, led to a more effective capillary barrier than the randomly heterogeneous media.

No geospatial analysis has been performed to determine if the Paintbrush Tuff layers would have completely random heterogeneity in the horizontal direction, or if a correlation length might be determined. It is not clear if the existing data can support a geospatial analysis. Based on the analysis of Ho and Webb (1998), this distinction is important for determining the effectiveness of a capillary barrier. Without any geospatial analysis of Paintbrush Tuff properties, purely random heterogeneous realizations should be used for each hydrostratigraphic layer. Based on the results of Ho and Webb (1998), the extent of lateral diversion in the Paintbrush Tuff at Yucca Mountain would be much less using the randomly heterogeneous data for each layer relative to the homogeneous assumption used by Wu, et al. (2000).

Caveats on using core data to represent heterogeneity are in order here. The site-scale unsaturated zone flow model upscales the matrix values from the core scale to the grid scale {>100m [330 ft] horizontal grid size}. The refined grid Wu, et al. (2000) uses, however, includes the scale of 4 m [13 ft] horizontal dimension and 1 m [3 ft] vertical. It is not clear that the upscaled data should be used for the highly refined models of Wu, et al. (2000). The caveat for the deep borehole data is that the samples are biased to indurated (lower permeability)

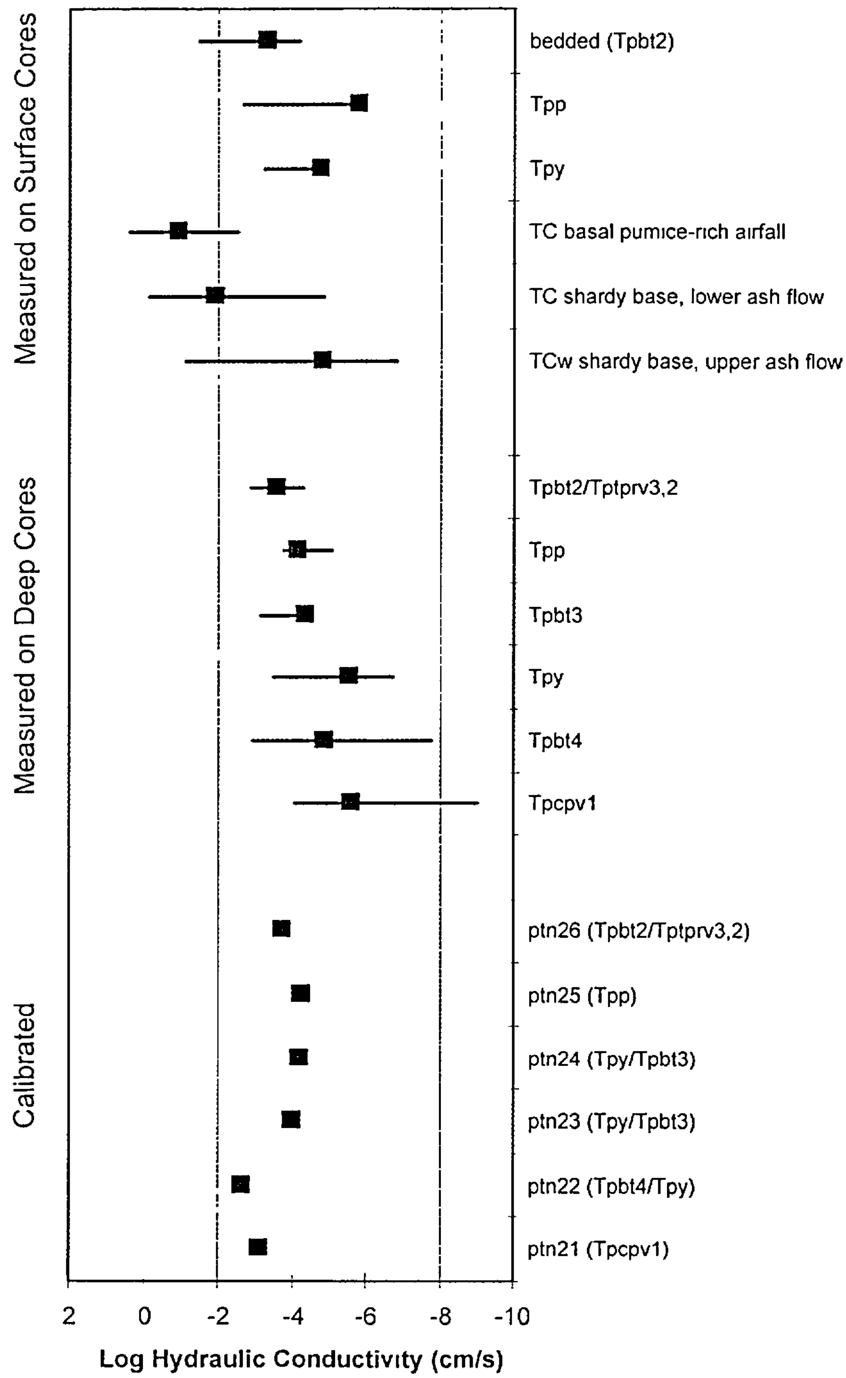

Figure 3-4. Saturated Hydraulic Conductivity from Calibrated Data Set (Wu, et al., 2000), Deep Borehole Cores (Flint, 1998), and Surface-Based Cores (Rautman, et al., 1995; Flint, et al., 1996). Symbols Represent the Calibrated Values or the Geometric Means. Vertical Line Represents the Ranges. (Conversion Factor for cm/s to ft/s Is 3.28E-2)

horizons. Poor recovery of the less indurated, and higher permeability, horizons is a common problem. The caveat for the surface-based boreholes is that the effect of the overprint of surficial processes on the permeability values is unknown. There is a smaller chance of sample bias caused by less indurated samples because alternative methods for obtaining unconsolidated samples can be employed for sampling surface exposures.

3.3.5 Modeling Barriers in Fractured Tuffs

3.3.5.1 Numerical Model Representations of Capillary Barriers

Conceptually, capillary barriers occur where fine pore-size media overlie coarse pore-size porous media. In the dual-permeability representation of flow through fractured tuffs, capillary barriers could occur where matrix overlies matrix, fracture overlies fracture, or matrix overlies fracture. Also, both matrix and fracture continua could contribute to the capillary barrier. As in Wu, et al. (2000), the lack of connections between a matrix block and an underlying fracture block prohibits adequate modeling of a capillary barrier of matrix overlying fracture. In the active-fracture model, the interaction area term is a function of the water content (Liu, et al., 1998). The linkage between matrix and fracture continua does not allow for a capillary pore-size based constitutive relation to be applied on either side of the psuedo material boundary. The linkage between fractures and matrix is based on a matrix/fracture area term and another term that represents rivulet and fraction of fractures participating in flow. Neither of these terms reflects a pore-size change across a boundary, which is the essence of a capillary barrier. Hence, the behavior might mimic a capillary barrier, but the magnitude and downslope length of breakthrough are entirely incidental. The interplay of downdip (lateral) movement of water associated with a capillary barrier and matrix/fracture interaction is complicated. Hence, caution should be used when interpreting dual-permeability model results.

The ptn26 matrix to tsw31 fracture scenario has long been postulated as a possible capillary barrier that occurs at Yucca Mountain, though vapor-phase alteration may reduce its effectiveness (CRWMS M&O, 2000j). The ptn26 matrix block overlying the tsw31 fracture block cannot be modeled correctly using TOUGH2 (Pruess, 1991) from a physical process perspective in a full dual-continuum model. If the matrix-fracture interaction term is avoided, then the physical process associated with a capillary barrier for matrix overlying fractures can be adequately represented (e.g., a single continuum is used, with the properties of the matrix used for the overlying block and the properties of the fracture network used for the underlying block).

3.3.5.2 Analytical Expressions for Capillary Barriers

Analytical expressions have been developed in the published literature for downslope length at which breakthrough occurs, and maximum lateral flux rate for idealized capillary barriers. Application of the Webb (1997) downdip length estimate for breakthrough in a capillary barrier (Ross, 1990) ignores the possibility of water entering the fractures. Presumably, the modeling by Wu, et al. (2000) indicates that water does not enter the fractures as it moves laterally downdip, which implies that pressure is not being built up to the levels needed to either enter the fracture or break the capillary barrier. Hence, the single-continuum approach is reasonable for this problem. Details of changes to matric potential distributions near capillary barriers caused by interacting matrix and fracture continua do not negate the relevance of the analytical approaches. In fact, Wu, et al. (2000) presented a validation of the flux estimates using a comparison of results from analytical expressions and from TOUGH2. They used constitutive relations representing both fractures and matrix (i.e., the equivalent continuum model assumption). It should also be noted that Wu, et al. (2000) used the capillary barrier of ptn23 overlying ptn24 to validate the analytical approach using the equivalent continuum model with TOUGH2 simulations. As shown earlier, flow in the layers ptn23 overlying ptn24 is a permeability barrier, not a capillary barrier.

Using the suggestion in Webb (1997) for estimating the downdip length defined by Ross (1990), breakthrough would occur at approximately 500 m [1,700 ft] downslope for the ptn21/ptn22 matrix-only capillary barrier (Table 3-4). Capillary barriers in the fracture continuum are not considered here because they appear weaker, and the fracture parameter values are highly uncertain because they are entirely calibrated parameters.
Using percolation rates of 5 and 50 mm/yr [0.2 and 2 in/yr] to reasonably bound net infiltration rates, the sensitivity of the capillary barrier to future climatic conditions is shown in Table 3-4. For each interface slope angle at 50 mm/yr [2 in/yr], the downslope length before breakthrough is 20 percent of that for the 5-mm/yr [0.2-in/yr] case. For the 5.5-degree slope, this lateral diversion is near the smallest grid size of the three-dimensional site-scale unsaturated zone flow model; however, it is still larger than the grid size used by Wu, et al. (2000). It can be concluded from this analysis that with future climates, lateral diversion will be significantly reduced.

Beyond the breakthrough point, net downslope lateral flow should not increase. The analytical solution produces a sharp change in vertical flux at the breakthrough point. Numerical models should produce a smooth change with vertical flux beginning upslope of the analytical breakthrough length and full vertical flux occurring at some point downslope from the analytical breakthrough point.

Table 3-4. Estimates of Downslope Length for Breakthrough for the ptn21/ptn22 Capillary Barrier Using the Webb (1997) Extension of the Ross (1990) Equation

Slope Angle, degrees	Percolation Flux, mm/yr [in/yr]	Length, m [ft]
5.5	5 [0.2]	519 [1700]
10	5 [0.2]	951 [3120]
5.5	50 [2]	106 [347]
10	50 [2]	194 [636]

3.3.6 Grid Size Concerns

To accurately model capillary barriers, grid sizes should be fine enough to capture the sharp curvature near saturation in the retention relation. The air-entry pressure head of the upper fine layer in a capillary barrier scenario is thought to be important for predicting breakthrough. When the van Genuchten (1980) equations are used for unsaturated zone constitutive relations, the air-entry pressure head is often approximated as the inverse of the van Genuchten α term. The grid size perpendicular to the capillary barrier interface should be less than the inverse of the van Genuchten α term (in units of length). Wu, et al. (2000, Appendix 1) use a grid refined down to 0.1 m [0.3 ft] near the interface when validating the analytical solution for breakthrough and flux along the interface. In TOUGH2 modeling throughout the text, the maximum refinement is 1.0 m [3.3 ft] grids perpendicular to the interface.

Although a grid spacing of 1.0 m [3.3 ft] appears adequate based on the inverse of the van Genuchten α term, inspection of the retention curves for ptn21 and ptn23 suggests a smaller grid size should be used to capture adequately the sharp curvature near saturation (see Figure 3-5) and, thus, avoid underestimating flux across the boundary. While values of van Genuchten α affect the shape of the retention curve in medium saturated regions, the α has its most pronounced effect on the curvature of the retention curve near saturation. Instead of further refinement of the grid, the seepage model adjusts the node locations in blocks on the drift boundary to avoid overpredicting diversion around the drift (CRWMS M&O, 2001). The nodes are shifted to a location closer to the drift so the distance from the node to the drift boundary is not greater than the capillary fringe height. The capillary fringe is the height of the nearly fully saturated region at low matric potentials, which is often approximated as the inverse of the van Genuchten α term. For ptn21, the capillary fringe height based on visual inspection of the retention curve is less than 1 m [3.3 ft]. For ptn22, ptn24, ptn25, and ptn26, the capillary fringe height is less than 0.2 m [0.7 ft].

Another factor receiving less attention is the grid spacing in the coarse layer. Walter, et al. (2000) present data supporting the water-entry matric potential for the coarse lower layer as a controlling parameter for capillary diversion. The water-entry matric potential is based on the wetting curve for retention (Hillel and Baker, 1988) and would be less than the air-entry matric potential of the drying curve for retention. Hysteresis of constitutive relations, as defined by measurements of wetting and drying retention curves, commonly occurs in poorly sorted granular media and is suspected for nonwelded tuff at Yucca Mountain. Flint (1998) notes the discrepancy between measured drying curves for retention and measurements of sorptivity, which represent the wetting rate of a sample, is likely caused by hysteresis. Modeling by Winterle and Stothoff (1997) showed that the nonwelded tuffs exhibited a larger discrepancy between drying curves and sorptivity compared with welded tuffs.

Because capillary barriers also depend on the water-entry matric potential of the coarse layer, in addition to the air-entry pressure of the overlying fine layer, the grid scale in the coarse layer should be refined enough to capture the sharp curvature associated with the wetting curve for retention of the coarse layer. Otherwise, the flow across the capillary boundary will be underestimated. No wetting retention curves have been measured on the nonwelded tuffs at Yucca Mountain, but logic dictates that the water-entry matric potential is less than the air-entry matric potential estimated from the drying curves for the coarse layers (ptn22, ptn24, ptn25, and ptn26 in Figure 3-5).

3.4 Mechanisms for Flow Bypassing the Paintbrush Tuff

Water that does not flow through the nonwelded Paintbrush Tuff matrix would contribute to the fast pathway portion of percolation at the proposed repository horizon. Fault and fracture zones may be locations where bypassing occurs. Faults and fractures will be addressed in a later section ofthis report A location where the Paintbrush Tuff does not occur is on the west flank of Yucca Mountain.

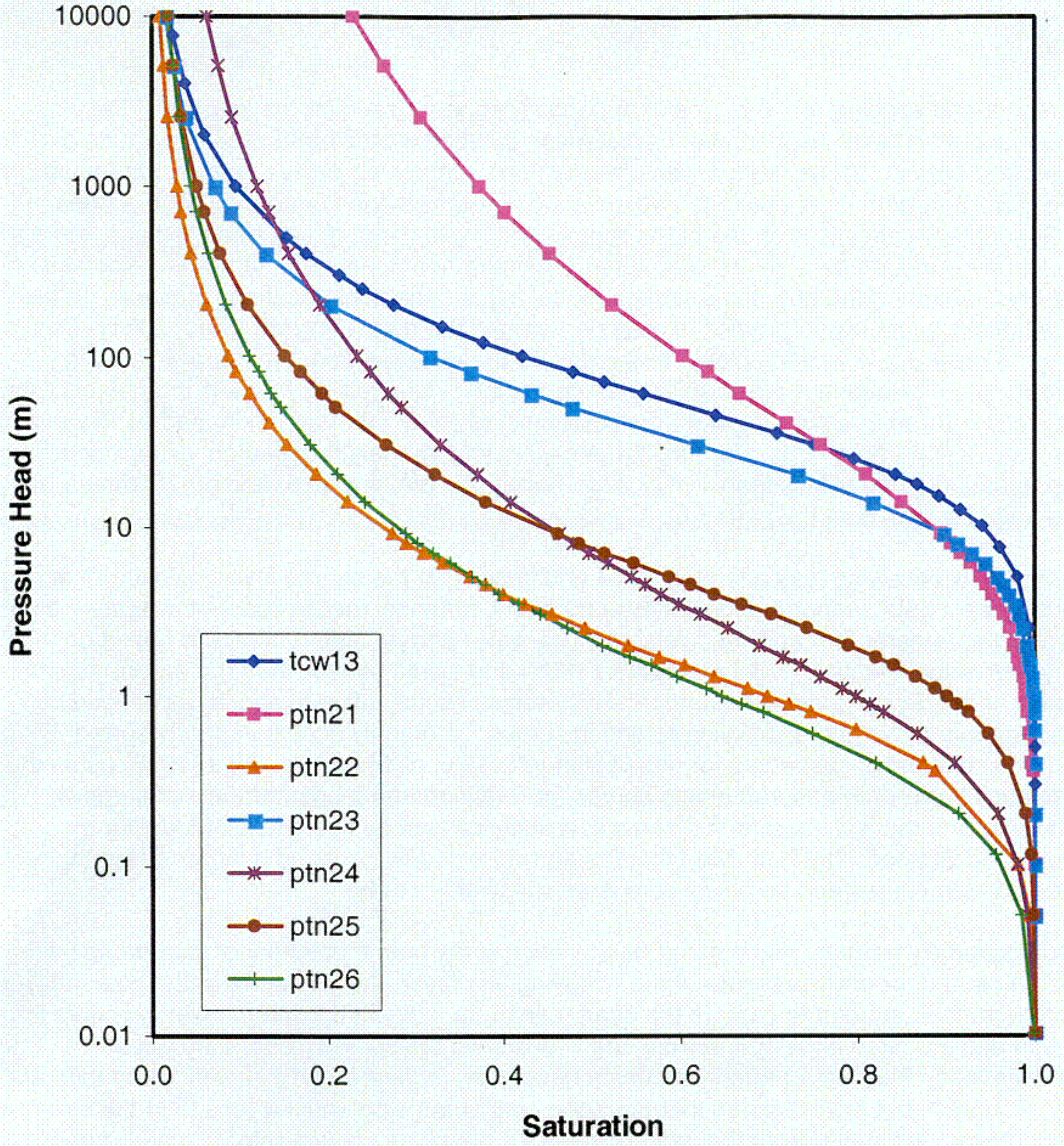

Figure 3-5. Retention Curves for All Nonwelded Paintbrush Layers Based on Parameter Values Used by Wu, et al. (2000) and CRWMS M&O (2000d) (Note: 1m = 3.2808)

C13

Precipitation directly entering the bedrock below the nonwelded Paintbrush Tuff exposure on the west flank would exhibit little dampening of episodic flow. Indications of elevated percolation near bulkhead 2 and between bulkheads 2 and 3 (Figure 3-6) of the Passive Test in the Enhanced Characterization of the Repository Block drift are consistent with the suggestion that water bypasses the Paintbrush Tuff and will affect the western edge of proposed repository drifts. Figure 3-6 shows the configuration of the Passive Test, the overlying spatial distribution of the nonwelded Paintbrush Tuff layer, and the proposed repository footprint. Wet areas in the Passive Test also suggest that subsurface lateral flow in the colluvial wedge may contribute a significant amount of percolation to the western edge of the proposed repository. Colluvial wedges are generated from the downslope movement of sediment that leads to a thickening wedge of sediment near the bases of slopes. The colluvial wedge is supplied with water at greater rates than precipitation; runoff from the west flank of Yucca Mountain likely enters the colluvial wedge as run-on surface flow and may flow laterally at the bedrock interface until the matric potential is elevated enough to cause entry of the water into the bedrock fractures of the Topopah Spring welded tuff. Run-on surface flow and subsurface lateral flow are postulated because direct infiltration into a thick colluvium or alluvium (greater than a few meters thick) rarely leads to net infiltration in the semiarid climate of Yucca Mountain. The combined zone of flow bypassing the Paintbrush Tuff and subsurface lateral flow into the colluvial wedge, and subsequent movement vertically downward, affect a small zone of the proposed repository footprint on the western side.

3.5 Effect of Fractures and Small Faults on Unsaturated Flow in Nonwelded Tuffs

The use of intralayer homogeneous hydraulic properties of the welded Tiva Canyon, nonwelded Paintbrush, and welded Topopah Spring Tuff layers in models, can lead to predictions of lateral flow along bedding planes near or in the nonwelded Paintbrush Tuff. Field observations, however, suggest the lateral downslope flow of water associated with the shallow sloping nonwelded beds is limited to tens of meters before vertical breakthrough (CRWMS M&O, 1997). No perched water has been found, nor has any evidence of modern or paleo springs been found at exposed Paintbrush Tuff bedding contacts. Numerous hypotheses have been suggested for the lack of significant lateral flow and ponding. Vertical flow through large fault zones likely occurs, but this does not explain the lack of continuity of lateral flow since mapped faults are widely spaced (hundreds to thousands of meters) in the Yucca Mountain block. Heterogeneity of matrix properties, including primary depositional textures, vapor-phase alteration, mineral alteration, and structural overprint, affects the performance of capillary and permeability barriers. The effect of heterogeneity on lateral flow of matrix properties was discussed in Section 3.3.

Secondary features, such as an overprint of deformation caused by fracturing or small-scale faulting, offer a possible explanation for the periodicity of breakthrough of flow through the nonwelded Paintbrush. The hypothesis presented here is that small faults, potentially spaced on the order of tens of meters or less, may induce local changes in matrix properties that induce vertical flow. Small faults are not generally mapped and many times are not readily visible at a macroscopic scale in cores or poorly exposed area.An important supposition needed for the lateral flow in the nonwelded Paintbrush hypothesis is that fractures and small faults do not hinder lateral flow. Dual permeability models, as used by Wu, et al. (2000), do not adequately represent the interruption of lateral flow in the matrix caused by small faults and fractures. The use of anisotropic properties (e.g., vertical permeability greater that horizontal

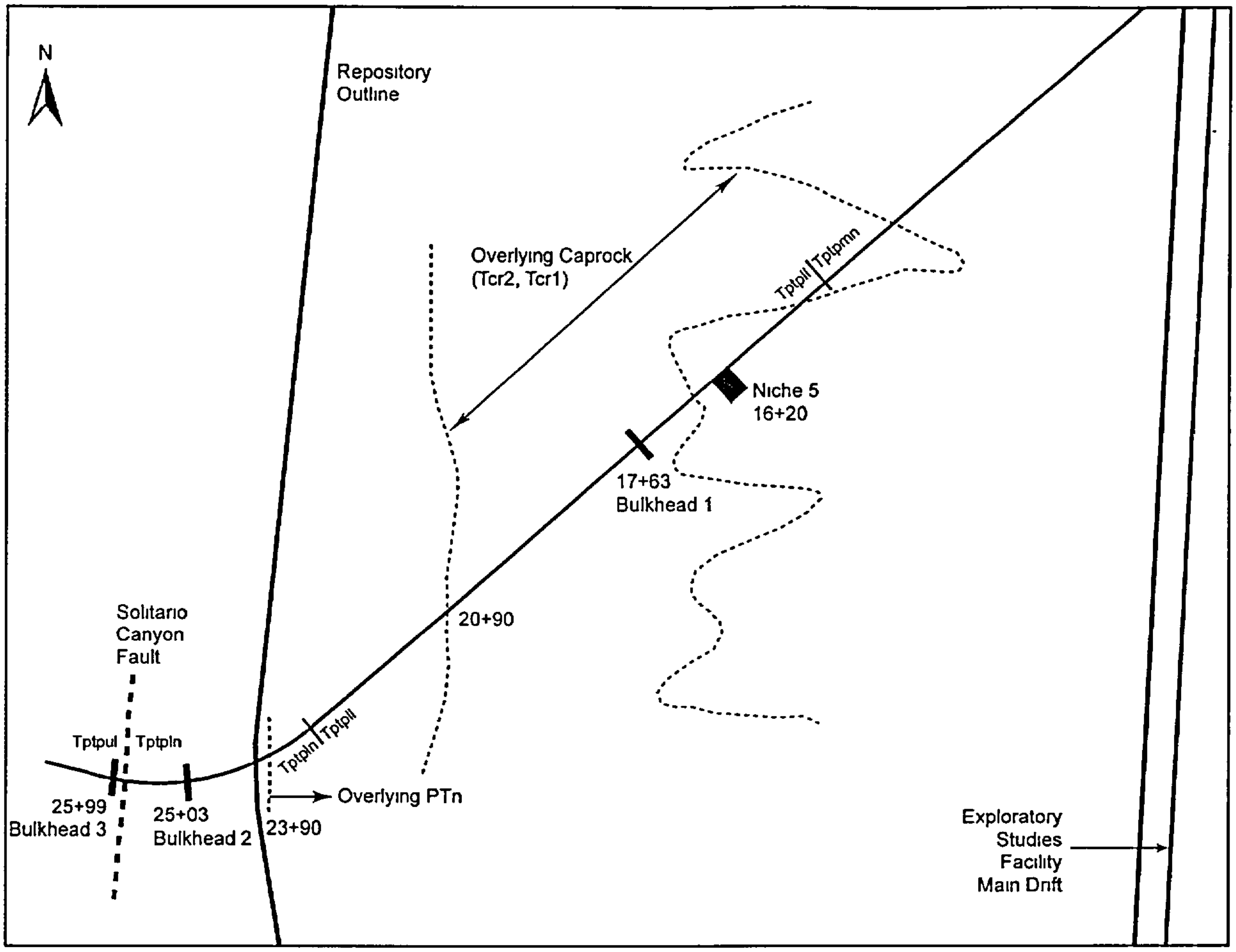

Figure 3-6. Bulkheads and Geologic Contacts in Passive Test Portion of the Enhanced Characterization of Repository Block Drift. Locations Along Drift Are in Units of Meters. (Note: 1m = 3.2808; PTn — Nonwelded Paintbrush Tuff)

permeability) can alleviate this inadequacy. At minimum, small faults and fractures cause the flow pathways to be more tortuous. The orientation of the structural plane relative to the direction of the lateral flow in the matrix plays a role in constraining lateral flow. At a maximum, small faults and fractures physically disconnect the matrix blocks on either side of the structural feature.

The effect of the structural overprint on unsaturated flow through tuffs is the focus of this section. Modeling at Yucca Mountain (Ofoegbu, et al., 2001) and work performed on the basal Bishop Tuff, a nonwelded Paintbrush analog site, suggest that small faults and fractures act to constrain lateral flow in nonwelded tuffs of the unsaturated zone.

3.5.1 Faults

Block-bounding faults and some large intrablock faults have been explicitly incorporated into the three-dimensional, site-scale unsaturated zone flow model (CRWMS M&O, 2000a) and in the supporting two-dimensional process models (Wu, et al., 2000; Bechtel SAIC Company, LLC, 2001). Other smaller faults are not directly incorporated into these models, nor are the effects of small faults on flow incorporated into their models.

Approximately 50 mapped faults of tens to hundreds of meters in length appear in the footprint of the proposed repository (Day, et al., 1997, 1998). The largest of these are the Sundance and Diabolus Ridge Faults and the splay of the Solitario Canyon Fault. The number of unmapped small faults that cut the nonwelded Paintbrush Tuff is difficult to assess. Smaller mapped faults in the Tiva Canyon Tuff exposed at the surface (Day, et al., 1997, 1998) may or may not cut the nonwelded Paintbrush at depth. Exposures of the nonwelded Paintbrush Tuff near the proposed repository are limited to the steep west flank of Yucca Mountain and a short section of the Exploratory Studies Facility. Examples of small faults exposed at both locations are shown in Figure 3-7. No systematic characterization of faults in the nonwelded Paintbrush Tuff units has been documented. Rousseau, et al. (1999) note that the minor faults, which constitute most of the discontinuities within the nonwelded Paintbrush Tuff, are generally less than 4 cm [1.6 in] wide and have thin silica or calcite fillings.

The hypothesis presented here is that small faults, potentially spaced on the order of tens of meters or less, may induce local changes in matrix properties that induce vertical flow. Changes to fracture continuum properties are not considered important for affecting flow, though matrix and fracture interaction may differ between fault and nonfault areas. Small faults are not generally mapped in poorly exposed areas. Steeply dipping small faults are severely underrepresented by vertically oriented boreholes, and the presence of small faults may not be readily discernible in cores. Secondary features, such as an overprint of deformation caused by fracturing or small-scale faulting, offer a possible explanation for the periodicity of vertical flow breakthrough within the nonwelded Paintbrush Tuff.

All faults that cut the nonwelded Paintbrush Tuff should exert a similar effect on lateral flow (i.e., constrain lateral flow and promote vertical flow for the ranges of percolation fluxes

(a)

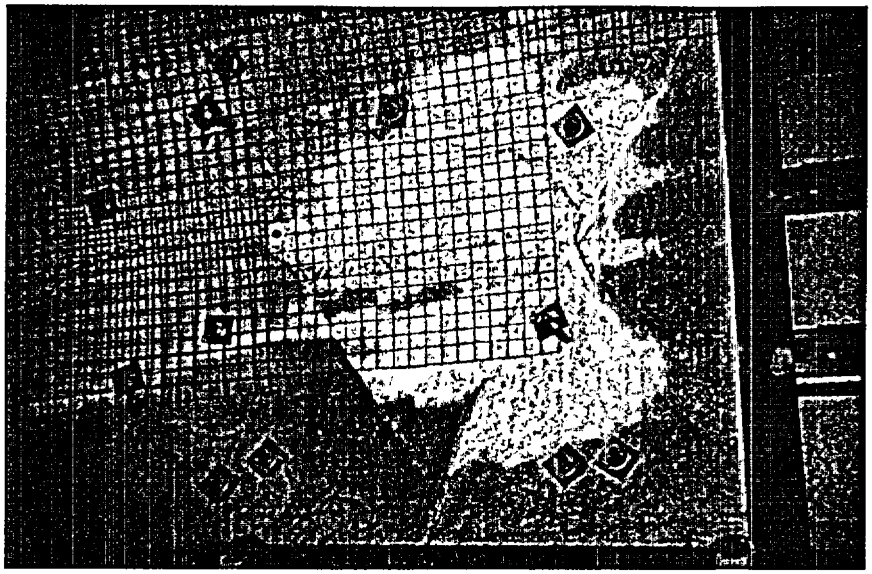

(b)

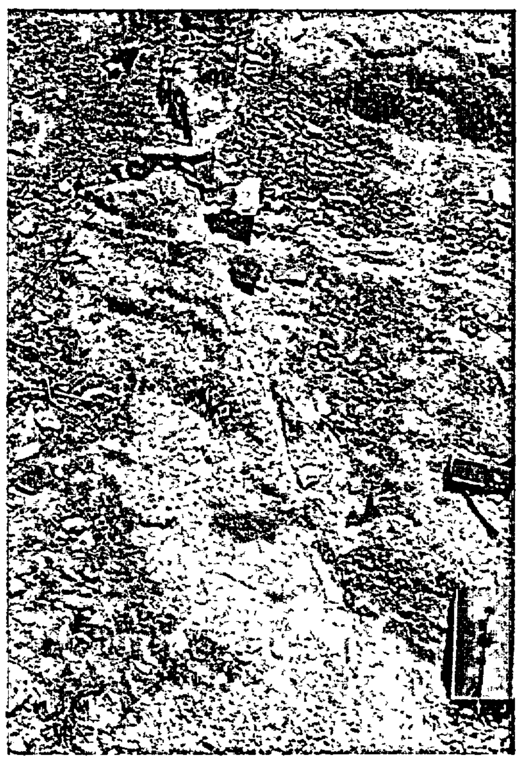

Figure 3-7. Photographs of the (a) Conjugate Normal Faulting in the Nonwelded Paintbrush Tuff Layers Exposed in the Exploratory Studies Facility (Photograph Courtesy of David Ferrill, CNWRA), and (b) a Small Fault with >15 cm [5.9 in] of Offset in the Middle Bedded Unit (Tpbt3) Exposed on the West Flank of Yucca Mountain

expected above the nonwelded Paintbrush horizons). Changes in matrix properties associated with deformation near and in faults are expected to have a more pronounced effect on constraining lateral flow than any changes to properties of the fracture continuum.

Hydrologic Properties of a Generic Minor Fault

Changes in hydrologic properties near fractures or small faults in the nonwelded tuffs at Yucca Mountain have not been directly studied. Characteristics and features of faults in poorly-lithified sediments, as described by Heynekamp, et al. (1999) and Fisher and Knipe (1999), are a good analog feature to faults in the nonwelded Paintbrush Tuff. Faults generally have a narrow core or gouge surrounded by a broad damage zone. Grain size reduction is a more prominent feature expected for large and small faults cutting the nonwelded Paintbrush Tuff.

Five types of mechanisms for grain-size reduction were noted by Fisher and Knipe (1999): (i) deformation-induced mixing of clays with framework grains, (ii) pressure solution, (iii) cataclasis, (iv) clay smear, and (v) cementation. There are no surface or borehole exposures of large faults cutting the nonwelded Paintbrush Tuff at Yucca Mountain. Moyer, et al. (1996) note there is no evidence for cementation or pressure solution modifications, though these might possibly occur at the major fault zones. For small-scale faults cutting the nonwelded Paintbrush Tuff at Yucca Mountain, textural changes in damage zones surrounding faults and in the cores of faults are likely limited to grain-size reduction, repacking and reorientation. Field observations in the nonwelded Paintbrush Tuff at Yucca Mountain and in the basal nonwelded units of the Bishop Tuff support this limited deformation (Fedors, et al., 2001).

Grain-size reduction, repacking, and reorientation will lead to reductions in porosity, permeability, and van Genuchten α parameters in the fault zone relative to the host rock. The permeability reductions caused by grain-size reduction will lead to permeability reductions perpendicular to the fault slip plane. For saturated flow, this reduction may lead to the fault becoming a barrier to flow. In the unsaturated zone, the flow behavior is more complex. The grain-size reduction may lead to a higher conductance because the finer pore size may lead to higher effective permeability at low unsaturated flux rates. At higher unsaturated flux rates, the grain-size reduction may lead to a permeability barrier. For the sloping Yucca Mountain nonwelded tuffs, the permeability barrier created by the grain-size reduction in a damage zone would cause water flowing laterally along bedding planes to flow vertically.

Fisher and Knipe (1999) note permeability reduction of three to four orders of magnitude for faults with discrete bands of differing deformation and reductions of zero to two orders of magnitude for homogeneous faults. The abundance of clays in the fault zones can be important. Heynekamp, et al. (1999) emphasized the effect of the primary clay fraction on the reduction in the interlayered sands and clay-bearing sediments. Layers with abundant clay may exhibit a repacking of grains that can lead to a permeability reduction. Smearing of clay lenses can also lead to reductions in permeability.

In sandstones at Moab, Utah, Antonellini and Aydin (1994) measured large permeability and porosity reductions in deformation bands, zones of deformation bands, and slip planes associated with faults. They note the intensity of cataclasis and the clay content of the host rock control the magnitude of permeability reduction. For deformation bands, porosity reductions of one order of magnitude and permeability reductions of three orders of magnitude relative to the host rock were measured.

At two sites in the Rio Grande Rift basin in New Mexico, Sigda, et al. (1999) measured hydraulic properties in the field and laboratory parallel and perpendicular to small faults. The small faults at one site contained no fault core or gouge zone, although the small faults at the other site contained a narrow fault gouge. At both sites in the study, the fault zone exhibited a wide range of permeability values while the undeformed areas exhibited a narrow range. Sigda, et al. (1999) note a bimodal distribution of measured permeabilities in the damaged or mixed zones. They believe the low-permeability population was associated with areas with grain-size reduction, and the high-permeability population was associated with pods of less deformed sediments. They also measured increases in clay fraction and sharp decreases in macroporosity in the fault zones.

In a modeling study by Ofoegbu, et al. (2001), the hydrologic properties (permeability, porosity, and van Genuchten α) of a column of matrix cells conceptually adjacent to a fault were modified to reflect fault-zone deformation. The Ofoegbu, et al. (2001) model consisted of a two-dimensional cross section of Yucca Mountain with sloping layers in a dual permeability representation. The focus of Ofoegbu, et al. (2001) was the elevated percolation rates seen at the proposed repository horizon caused by the fault; an increase by a factor of two to three in percolation rates was noted. In regard to the potential for extended lateral flow suggested by Wu, et al. (2000), the important result from Ofoegbu, et al. (2001) is that lateral flow was completely disrupted by the change in matrix properties from the host rock to the damage zone and core of a fault.

Injection tests at Alcove 4 in the Exploratory Studies Facility were performed to assess flow along a fracture and small fault (CRWMS M&O, 2000g). In the alcove, a small fault crosses the contact between the Pah Canyon Tuff and the lower bedded unit (Tpbt2). There is an indurated argillic layer that has low permeability near the top of the bedded tuff. Only limited details relevant to the capability of lateral flow to cross faults and fractures are presented on the Alcove 4 injection tests documented in CRWMS M&O (2000g). The focus of the presented results was to measure flow along the fault and in the matrix of the Pah Canyon Tuff. It was noted, however, that zeolitic alteration in the North Ramp of the Exploratory Studies Facility commonly follows fractures and faults that cut the Pah Canyon Tuff and the underlying bedded tuff (Tpbt2). Besides being evidence of elevated saturations, the zeolitic alteration is associated with significant reductions in permeability, which would act to constrain lateral flow across these features.

In summary, changes to matrix hydrologic properties caused by deformation associated with secondary features such as small faults have not been measured at Yucca Mountain, but may be bounded by values published for poorly lithified sediments found elsewhere. Unsaturated zone parameters have not been studied, likely because fault properties are of high interest in the oil industry and not for the near-surface unsaturated zone. The unsaturated zone parameter values used by Ofoegbu, et al. (2001) were conjectural. The use of poorly lithified sandstones as an analog may underestimate the effect of small faults because the nonwelded Paintbrush Tuff at Yucca Mountain contain abundant clays that would lead to greater reductions in permeability caused by repacking and reorientation in faults.

3.5.2 Fractures

The effect of fractures on flow through the nonwelded Paintbrush Tuffs has not been intensely studied, likely because vertical flow is thought to be predominantly through the rock matrix. Though there is little sensitivity of unsaturated flow to changes in fracture hydrologic properties, fractures play an important role in constraining lateral flow. This section discusses the fracture characterization at Yucca Mountain and then summarizes work on the basal nonwelded units of the Bishop Tuff, an analog site for the nonwelded Paintbrush Tuff of Yucca Mountain.

Fracture density generally is inversely proportional to the degree of welding, as supported by fracture mapping in the Exploratory Studies Facility (CRWMS M&O, 2000j). Fracture density in the nonwelded Paintbrush layers is much less than that in the welded units. Fracture mapping from the Exploratory Studies Facility suggests a range of fracture densities 0.5 to 1.0 m^{-1} [0.14 to 0.30 ft^{-1}] for the different hydrostratigraphic units of the nonwelded Paintbrush Tuff (CRWMS M&O 2000k). Average fracture densities calculated for the nonwelded Paintbrush Tuff in boreholes NRG–6 and NRG–7a (DTN: SNF29041993002.084) are 2.6 and 1.4 m^{-1} [0.8 and 0.4 ft^{-1}]. NRG–6 and NRG–7a are the only boreholes with fracture plane attitude (dipping angle) in the DOE Technical Data Management System. Correcting for orientation bias using the Terzaghi (1965) correction leads to fracture densities of 3.1 and 2.7 m^{-1} [0.9 and 0.8 ft^{-1}] from NRG–6 and NRG–7a. The difference between the corrected and uncorrected values illustrates the prominence of steep angled fractures. It should be noted that vertical fractures would be severely undersampled in vertical boreholes, and, hence, the uncertainty in the Terzaghi (1965) orientation bias correction correspondingly becomes larger. Dipping fractures, particularly subvertical ones oriented perpendicular to the stratigraphic dip, will have a significant effect on the extent of lateral flow in nonwelded Paintbrush subunits.

Surface exposures of the nonwelded Paintbrush Tuff at Yucca Mountain illustrate a more extensive representation of fracturing than the limited zone exposed in the Exploratory Studies Facility. Figure 3-8 illustrates the difference in fracture density between the Yucca Tuff (Tpy) and the middle bedded unit. If fractures inhibit lateral flow in the matrix, there appears to be a sufficient number of fractures to limit lateral flow to scales less than tens of meters. It should be noted that surface outcrops reflect the overprint of surficial processes that may also bias the characterization of fracture density, apertures, and filling by secondary mineralization (e.g., caliche).

The nonwelded Paintbrush Tuff at Yucca Mountain is poorly exposed. Work at an analog site for the nonwelded Paintbrush Tuff was undertaken to help understand the important flow processes in fractured nonwelded tuffs. The analog site is near Bishop, California (Figure 3-9), where the nonwelded basal units of the Bishop Tuff are exposed. The basal Bishop Tuff consists of both bedded air-fall horizons and massive ignimbrite layers that grade from nonwelded to densely welded. The Tablelands north of the town of Bishop are capped by the densely welded portion of the Bishop Tuff. Previous work on the Bishop Tuff relevant to the basal nonwelded subunits includes Bateman (1965); Hollet, et al (1991); and Wilson and Hildreth (1999).

After textural and structural observations and hydrological testing confirmed the reasonableness of the basal Bishop Tuff as an analog for the nonwelded Paintbrush Tuff (Fedors, et al., 2001), dye tracer tests were performed on fractured and unfractured nonwelded

(a)

(b)

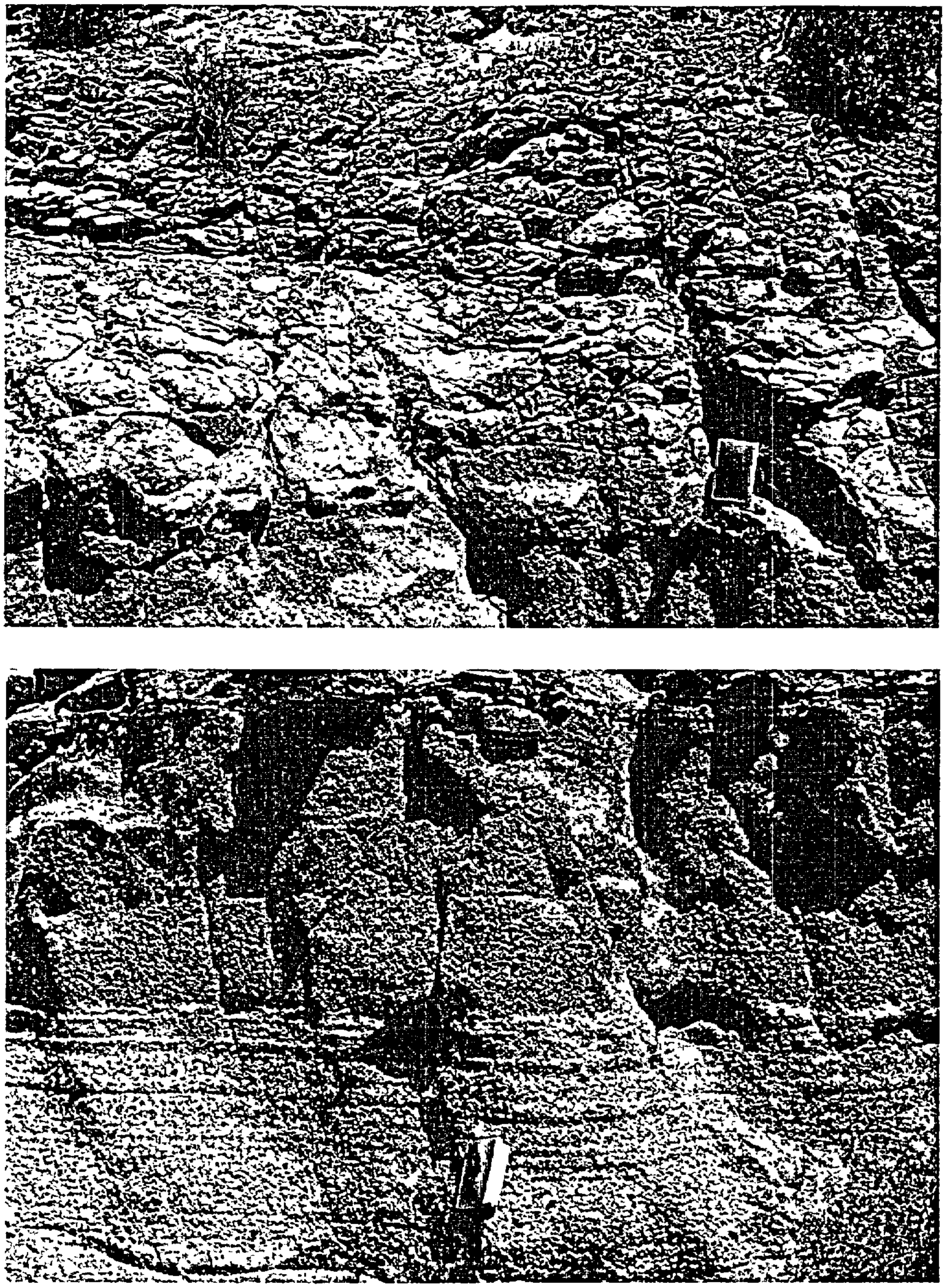

Figure 3-8. Photograph of the (a) Lower Portion of Yucca Tuff on the West Flank of Yucca Mountain Illustrating the Number of Fractures, Which Are Reflective of the Moderate Degree of Welding; the Contact with Middle Bedded Unit (Tpbt3) in Nonwelded Paintbrush Tuff Is Present in Lower Part of Photograph; and (b) Upper Portion of the Middle Bedded Unit (Tpbt3)

(a)

(b)

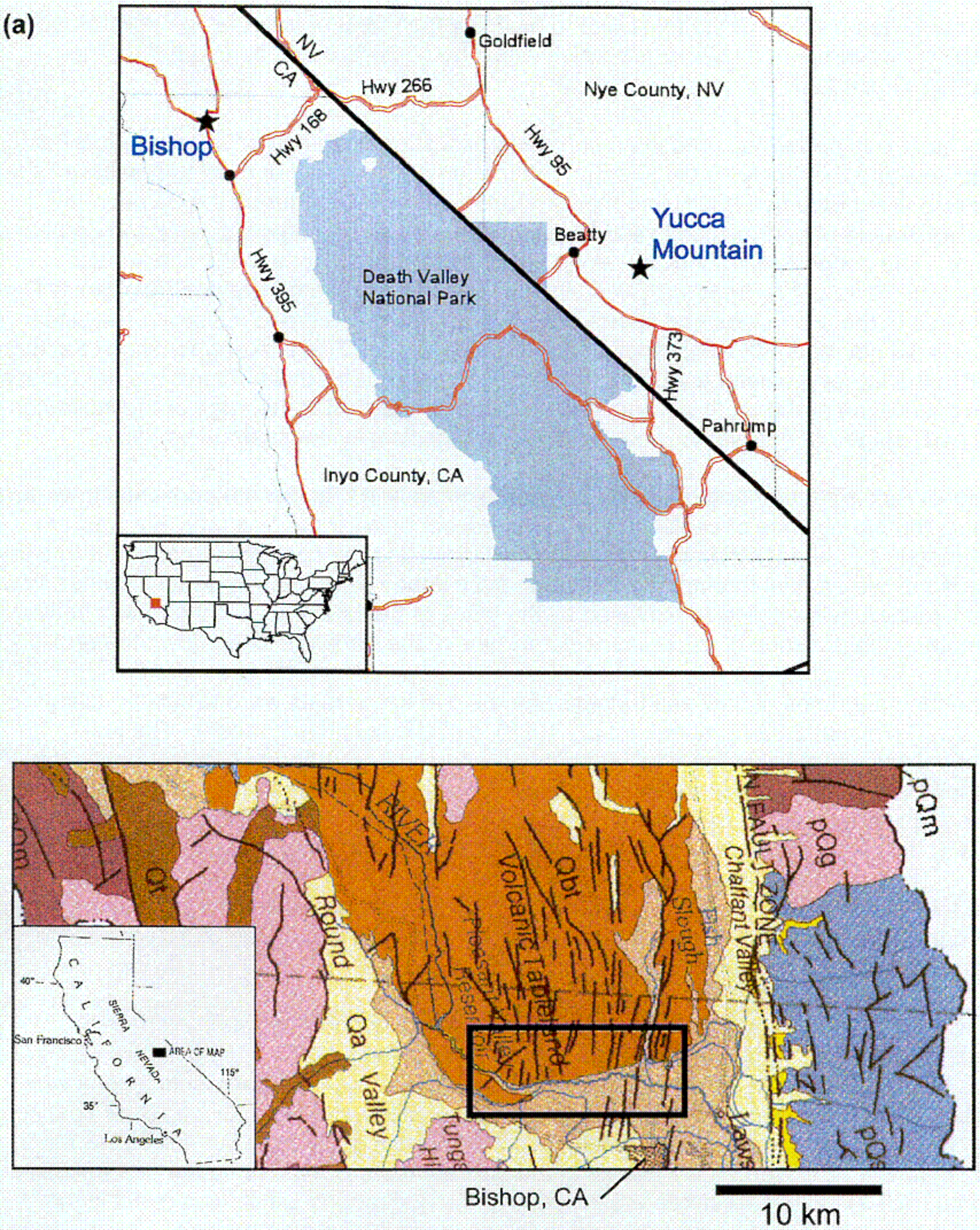

Figure 3-9. (a) The Town of Bishop, California, Is Located Northwest of Death Valley National Park and Yucca Mountain. (b) The Nonwelded Basal Bishop Tuff Crops Out at the Edge of the Volcanic Tablelands North of Bishop, California. The Inset Box in (b) Defines the Field Work Area. Figure Is Adapted from Fedors, et al. (2001). (Note: 1km = 0.6214 mi)

C14

ignimbrite. The objective of the tests was to evaluate the effect of fractures on flow through the massive portion of the nonwelded tuff, which would be considered an analog tuff for the nonwelded Yucca Tuff.

A paired test was performed, one in an unfractured location and another where vertical fracture spacing was approximately 10 cm [0.3 ft]. The fractures are coated or filled with caliche. Two pulses of Brilliant Blue dye (Flury and Fluhler, 1995) were injected during the 38 hours of ponded infiltration of approximately 473.2 liters [125 gallons], one after 0.5 hour and another at 25 hours. The ponded infiltration was along a pit, which is analogous to the line source expected for fracture flow from the Tiva Canyon Tuff overlying the nonwelded Paintbrush Tuff. The profiles of the two pulses had approximately the same aspect ratio indicating the initial conditions did not markedly affect transport of the dye (Figure 3-10). A subhorizontal fracture is evident in the tracer profile at the unfractured site (Figure 3-10b); this fracture was not exposed prior to excavation of the profiles. Subvertical fractures noted near the edge of the infiltration pit during early stages of excavation were observed to significantly constrain lateral flow.

The aspect ratio for the unfractured site was approximately 1:1, half-width horizontal to vertical, indicating the prominence of capillary drive. The aspect ratio for the fractured site was approximately 1:2, half-width horizontal to vertical, indicating the constraining effect of fractures Flow was not preferential through the fractures, even if they were open at depth. Rather, flow was constrained by fractures as exhibited by the lobes of the blue tracer in the matrix between fractures and the absence of tracer immediately next to the fractures lower down the profile.

Two conceptualizations of flow and transport for the dye tracer tests were simulated using HYDRUS2D Version 2.02 (Simúnek, et al., 1999), a single continuum model. The first conceptualization was to represent the effect of fractures by incorporating anisotropy in the permeability. The second conceptualization was to represent the fractures as discrete features. Hydrologic properties in the models were based on field and laboratory measures listed in Table 3-5. Initial conditions and permeabilities were adjusted during the calibration process.

Figure 3-11 illustrates the results of modeling using anisotropy to reflect the effect of fractures. The general shape of the dye tracer plume is readily predicted by the use of a horizontal to vertical anisotropic ratio of 1:2.

A grid with discrete cells representing fractures was developed to illustrate the effect of fractures on constraining lateral flow. Fractures are represented as 0.3-cm [0.12-in] wide cells with 0.2-cm [0.08-in] bands enveloping each fracture. The envelope represents a zone with secondary mineralization partially filling the pore space At Yucca Mountain, fracture coatings are common in most units, but were lacking in cores of the Pah Canyon Tuff (CRWMS M&O, 2000j). Figure 3-12 illustrates the results of the discrete feature representation of a fractured ignimbrite (Site 2). When fractures are included in the grid, strong similarities result in the pressure head pattern and tracer transport to the plume in the field excavation. The expanded view of the modeled plume (Figure 3-12b) exhibits the same separation of dye from the fractures as seen in the field excavation (Figure 3-12a). The fractures act to constrain lateral flow and promote additional vertical migration of the tracer and wetting front.

DOE modeling (Bechtel SAIC Company, LLC, 2001) concluded that anisotropic ratios of 10:1–100:1 could be used with the three-dimensional, site-scale unsaturated flow model to capture the effect of lateral diversion simulated in the refined two-dimensional grids of

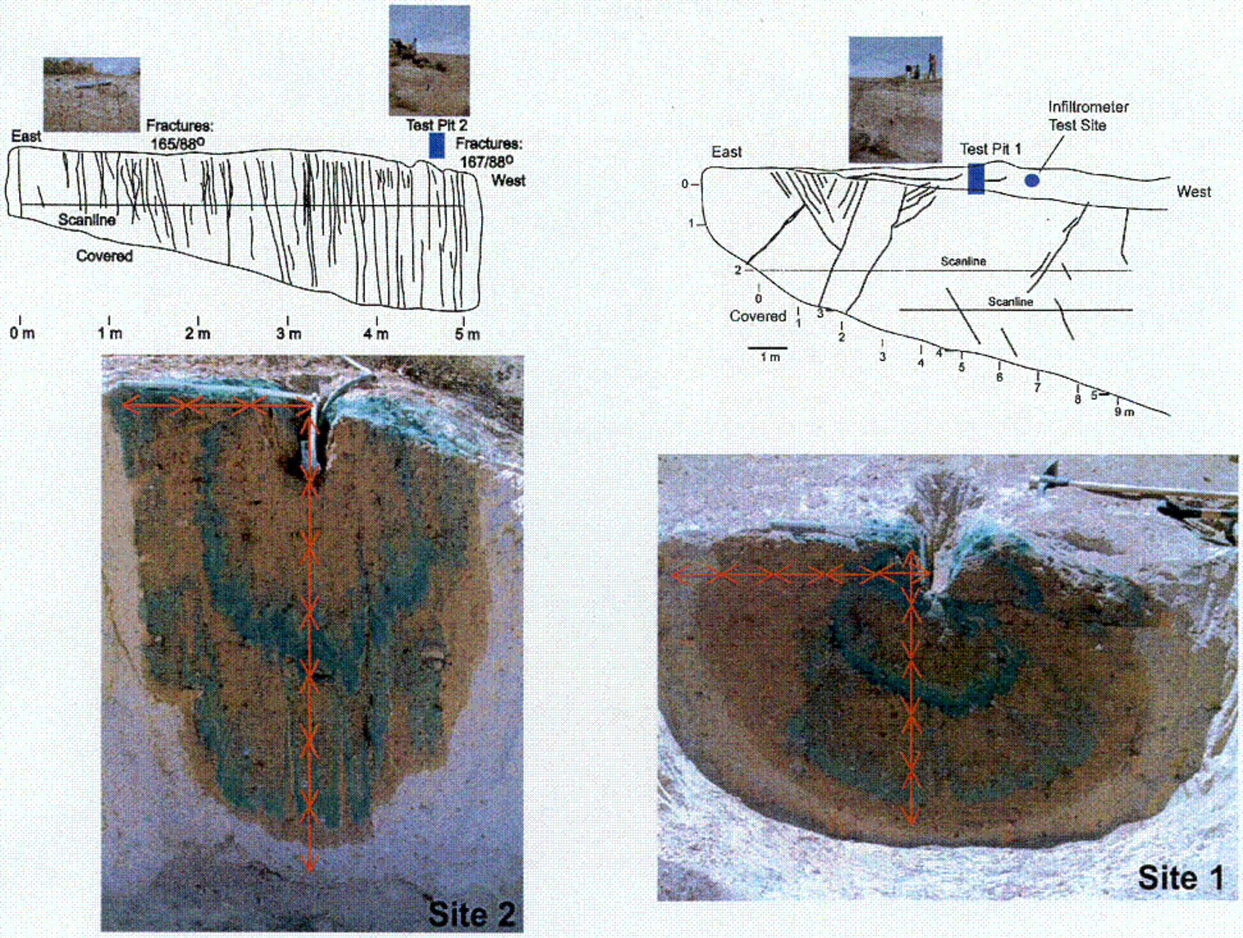

Figure 3-10. Field Dye Tracer Tests Illustrating the Constraining Effect of Fractures on Unsaturated Flow (Adapted from Fedors, et al. 2001). The Excavation Faces Are Beneath the Middle of Infiltration Pits for the (a) Fractured Site 2 and (b) Unfractured Site 1 in a Massive Ignimbrite. The Ruler Segments Are 20 cm [0.656 ft], Which Correspond to the Red Arrow Segments. (Note: 1 m = 3.2808)

C15

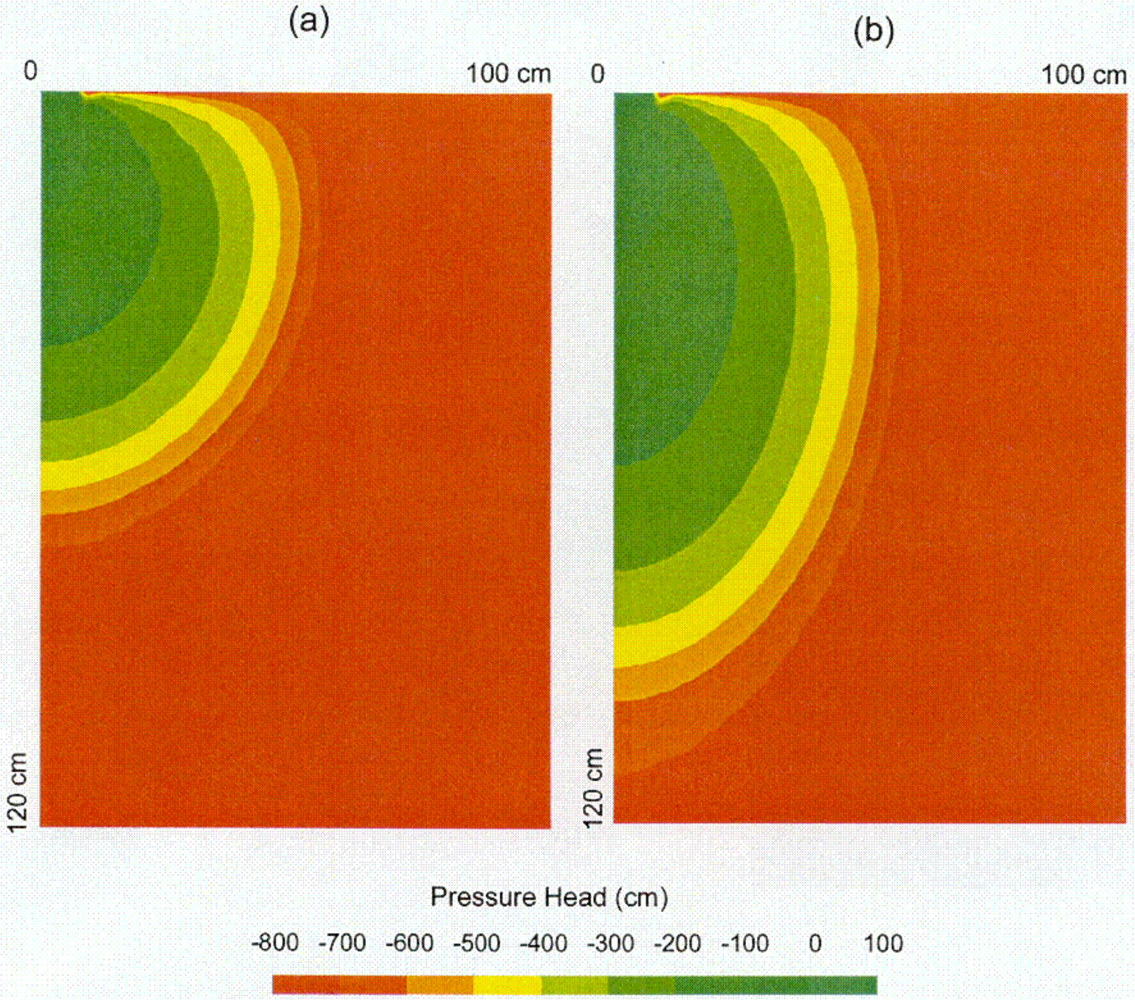

Figure 3-11. Model Results for (a) Unfractured Tuff Site and (b) Fractured Tuff Site Using Anisotopic Permeability to Reflect the Effect of Fractures on Flow (Note: 1 cm = 3.28E-02 ft)

C16

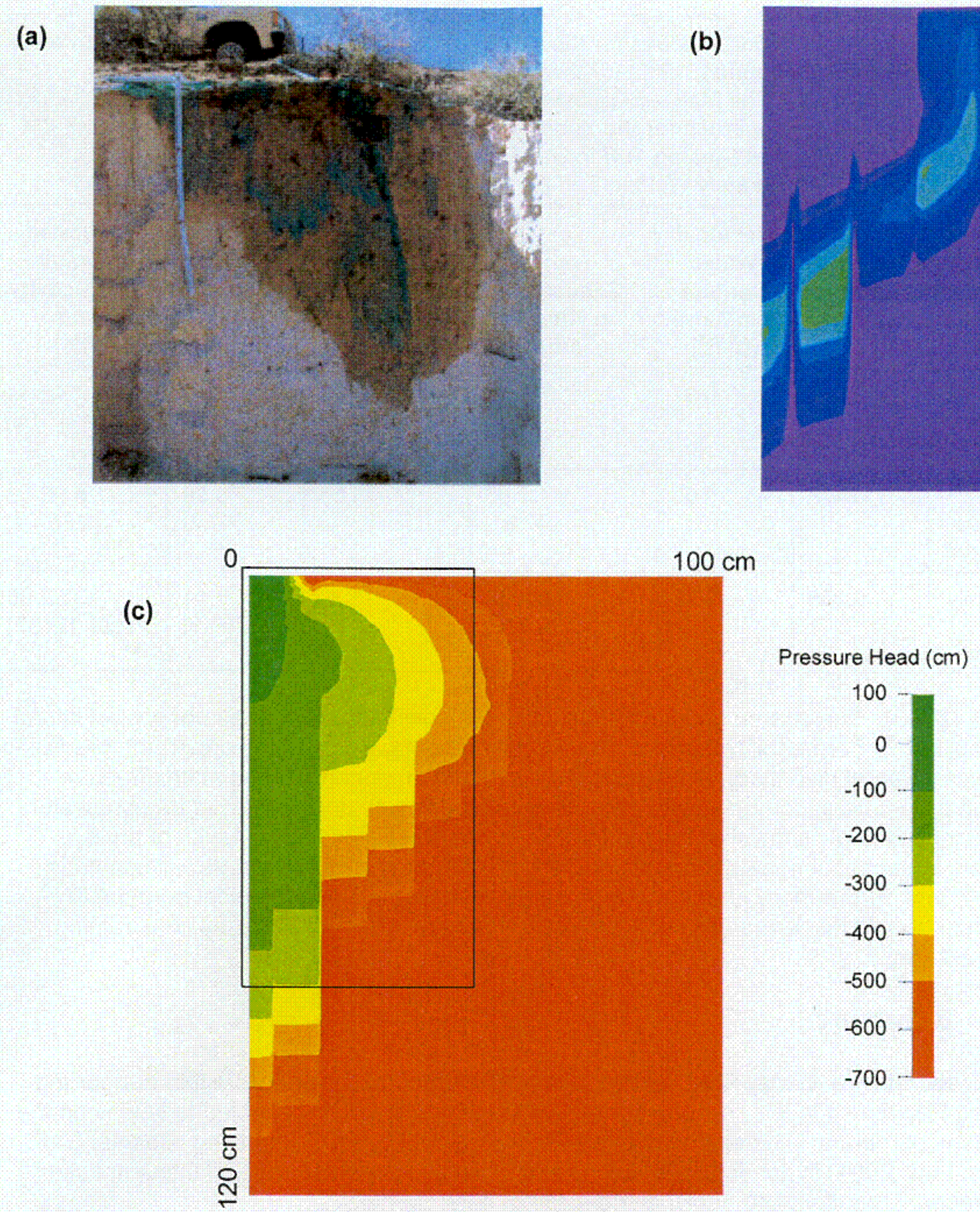

Figure 3-12. For the Discrete Feature Representation, (a) a Photograph of the Excavation Face at the Edge of the Pit, (b) an Inset of the Discrete Feature Model Results with the Plume Concentration from a Normalized Conservative Tracer, and (c) Model Results of Matric Potential for Fractured Tuff Site 2 Using Discrete Features to Reflect the Effect of Fractures on Flow. The Box in Part (c) Defines the Inset Displayed in Part (b). (Note: 1 cm = 3.28E-02 ft)

C17

Table 3-5. Hydrologic Property Values for the van Genuchten Water Characteristic Parameters (van Genuchten, 1980) for the Bishop Tuff Based on Field and Laboratory Data. The Matrix-Supported Properties Were Used in the Modeling and Are Analog Properties for the Yucca and Pah Canyon Tuffs. For Reference, the Clast-Supported (Analog Tuff for the Bedded Tuffs at Yucca Mountain) and Moderately Welded Tuff Properties Are Also Shown.

Type	Porosity (cm^3/cm^3) [ft^3/ft^3]	Residual Water Content (cm^3/cm^3) [ft^3/ft^3]	van Genuchten α (1/cm) [1/ft]	van Genuchten n (–)	Bulk Density (g/cm^3) [lb/ft^3]	Saturated Hydraulic Conductivity cm/s [ft/s]
Matrix-supported ignimbrite	0 470	0 01	0 0068 [0 21]	1 79	1.10 [68.7]	1 4E-04 [4.6E-06]
Clast-supported bedded tuff	0 478	0 00	0 03 [0 91]	1.68	0 98 [61 2]	8 6E-03 [2 8E-04]
Moderately welded ignimbrite	0.355	0.12	0 00062 [0 019]	3 33	1 44 [89 9]	3.5E-06 [1.1E-07]

Wu, et al. (2000). The coarse gridding of the three-dimensional model does not predict lateral flow at capillary or permeability barriers. Matrix chloride data are used to support the prediction of large-scale lateral diversion. Model calibrations based on unconstrained matrix/fracture interaction parameters, combined with chloride simulations with unconstrained fracture water compositions, can only show that the model is self-consistent. Modeling results of the dye tracer tests in the basal nonwelded units of Bishop Tuff suggest that fractures will constrain lateral flow and, furthermore, that anisotropic ratios reflecting elevated vertical permeability greater than horizontal permeability will capture the general effect of fractures constraining unsaturated flow.

3.6 Summary

Field and laboratory evidence indicate that localized lateral flow may occur within or near the nonwelded Paintbrush layers Strong support exists that lateral flow is limited to scales on the order of tens of meters. The extended lateral flow predicted by DOE modeling (Bechtel SAIC Company, LLC, 2001) is not supported by observations of saturation profiles, unevenness of layer surfaces, gradational contacts, and degree of heterogeneity.

Wu, et al (2000) and Bechtel SAIC Company, LLC (2001) modeling results led them to believe that lateral flow above capillary barriers could reduce percolation rates by greater than 40 percent in the proposed repository footprint. These authors contend that the ptn23/ptn24 layers constitute a prominent capillary barrier over which most of the extended lateral flow occurs. The ptn23/ptn24 layers, however, constitute a permeability barrier, not a capillary barrier This distinction in defining barriers does not eliminate the effectiveness of these layers to divert water laterally. The field contact between these layers is gradational, however, a characteristic not captured in the numerical model Thus, this layer interface is not likely to produce the degree of lateral flow suggested by the model. Furthermore, ptn23 represents the more welded internal portion of the Yucca Tuff. Moderately welded tuffs tend to have a less permeable matrix and are more fractured than nonwelded tuffs. Fracturing in that unit would also inhibit lateral flow.

The other model layer that exhibited lateral flow in the Wu, et al. (2000) model was the ptn21. The authors contend that the ptn21/ptn22 interface also constituted a capillary barrier. Analysis of the calibrated properties supports the possibility that a capillary barrier could occur. Saturation and mineral alteration data, however, support the possibility of lateral flow above the ptn21 layer, not within the layer along the ptn21/ptn22 contact surface as predicted by Wu, et al. (2000).

Simplification of the actual system by the numerical representation of Wu, et al. (2000) causes the model to miss important features of the nonwelded layers. Besides uneven and gradational contacts, small faults and fractures would act to constrain flow to vertical, thus inhibiting lateral flow. Faults and fractures are poorly characterized in the nonwelded Paintbrush layers. Using fault and deformed matrix wallrock properties from poorly lithified sandstones as analog features to fault deformation in the nonwelded Paintbrush Tuff, it was seen that vertical flow was enhanced significantly for conditions relevant to modern day conditions and percolation rates (Ofoegbu, et al., 2001). Small faults completely disrupted lateral flow in the nonwelded Paintbrush Tuff layers. There are no estimates of fault frequency in the nonwelded Paintbrush unit, however, it is reasonable to expect that fault frequency occurs on the scale of tens of meters to hundreds of meters.

The presence of faults and fractures in the nonwelded Paintbrush Tuff will act to constrain lateral flow, particularly when the fault and fracture planes are oriented perpendicular to the stratigraphic dip. Both faults and fractures would induce vertical flow in the adjoining matrix that would negate the development of lateral flow along capillary or permeability barriers associated with stratigraphic boundaries. Furthermore, the use of large horizontal to vertical anisotropic permeability ratios in the three-dimensional site-scale unsaturated flow model (Bechtel SAIC Company, LLC, 2001) is not justified.

4 CONCLUSION

DOE modeling of heterogenous flow in the Topopah Spring unit suggests that the ranges of flow-focusing factors DOE used for CRWMS M&O (2000b) are reasonably conservative. These results provide justification for DOE to rely on a single uncertainty distribution for the focusing factor in future performance assessment analyses. Improved knowledge of the correlation scale for flow-system heterogeneity is an important input for establishing appropriate values for the focusing factor and is a recommended objective for ongoing and planned field studies at Yucca Mountain.

CNWRA conducted independent stochastic simulations that showed focused flow areas in the Paintbrush unit matrix are correlated to the areas where focused fracture flow arrives from the base of the Tiva Canyon unit. The areas of focused flow are not attributable to the fracture heterogeneity within the nonwelded Paintbrush unit. Both the independent modeling and the DOE process model of heterogenous fracture networks indicate that flow exiting the base of the Paintbrush unit is quickly redistributed according to the degree of heterogeneity in the fracture continuum of the underlying Topopah Spring welded unit after traveling downward approximately three to five correlation lengths. The effects of matrix heterogeneity within the nonwelded Paintbrush Tuff unit have not been modeled. Matrix heterogeneity in the Paintbrush unit, such as zones with different degrees on mineral alteration, could lead to zones of focused flow in the Paintbrush unit that are farther apart than those simulated in this study. Widely spaced zones of focused flow may not be as readily redistributed in the Topopah Spring unit. Future modeling is recommended to evaluate matrix heterogeneity in the Paintbrush unit. Results of the independent stochastic continuum modeling also suggest the possibility that active-fracture spacing used in the DOE abstraction could result in overly optimistic radionuclide transport simulations; however, further investigation of this possibility is needed.

Wu, et al. (2000) and Bechtel SAIC Company, LLC (2001) concluded that significant lateral diversion along capillary barriers within the Paintbrush unit can divert substantial amounts of flow laterally toward faults and away from significant portions of the proposed repository area. This conclusion, however, is largely based on a layer-cake-type model that assumes homogenous layers with sharp, straight layer interfaces. Conversely, field and laboratory evidence strongly suggest lateral flow is limited to scales on the order of tens of meters. The extensive lateral flow predicted by DOE modeling (Bechtel SAIC Company, LLC, 2001) is not supported by observations of saturation profiles, unevenness of layer surfaces, gradational contacts, and degree of heterogeneity. DOE, therefore, should be cautioned against claiming credit for significant lateral diversion in the Paintbrush unit as part of a total system performance assessment to support any potential license application.

5 REFERENCES

Antonellini, M. and A. Aydin. "Effect of Faulting on Fluid Flow in Porous Sandstones: Petrophysical Properties." *American Association of Petroleum Geologists Bulletin*. Vol. 78, No. 3. pp. 355–377. 1994.

Bateman, P.C. "Geology and Tungsten Mineralization of the Bishop District, California." U.S. Geological Survey Professional Paper 470. 1965.

Bechtel SAIC Company, LLC. "FY01 Supplemental Science and Performance Analyses." Vol. 1: Scientific Bases and Analyses. TDR–MGR–MD–000007. Rev. 00 ICN 01. Las Vegas, Nevada: Bechtel SAIC Company, LLC. 2001.

Chen, G., W.A. Illman, D.L. Thompson, V.V. Vesselinov, and S.P. Neuman. "Geostatistical, Type Curve and Inverse Analyses of Pneumatic Injection Tests in Unsaturated Fractured Tuffs at the Apache Leap Research Site Near Superior, Arizona." *Dynamics of Fluids in Fractured Rocks. Geophysical Monograph 122*. Washington, DC: American Geophysical Union. pp. 73–98. 2000.

CRWMS M&O. "Seepage Calibration Model and Seepage Testing Data." MDL–NBS–HS–000004. Rev. 01. Las Vegas, Nevada: CRWMS M&O. 2001.

———. "Unsaturated Zone Flow and Transport Model Process Model Report." TDR–NBS–HS–000002. Rev. 00. Las Vegas, Nevada: CRWMS M&O. 2000a.

———. "Total System Performance Assessment (TSPA) Model for Site Recommendation." MDL–WIS–PA–000001. Rev. 00. Las Vegas, Nevada: CRWMS M&O. 2000b.

———. "Abstraction of Drift Seepage." ANL–NBS–HS–000005. Rev. 00. Las Vegas, Nevada: CRWMS M&O. 2000c.

———. "Calibrated Properties Model." ANL–NBS–HS–000003. Rev. 00. Las Vegas, Nevada: CRWMS M&O. 2000d.

———. "Simulation of Net Infiltration for Modern and Potential Future Climates." ANL–NBS–GS–000032. Rev. 00. Las Vegas, Nevada: CRWMS M&O. 2000e.

———. "Seepage Model for PA Including Drift Collapse." MDL–NBS–HS–000004. Rev. 00. Las Vegas, Nevada: CRWMS M&O. 2000f.

———. "*In-Situ* Field Testing of Processes." ANL–NBS–HS–000005. Rev. 00. Las Vegas, Nevada: CRWMS M&O. 2000g.

———. "Particle Tracking Model and Abstraction of Transport Processes." ANL–NBS–HS–000026. Rev. 00. Las Vegas, Nevada: CRWMS M&O. 2000h.

———. "Geologic Framework Model (GFM3.1) Analysis Model Report. MDL–NBS–GS–000002. Rev. 00 ICN 01. Las Vegas, Nevada: CRWMS M&O. 2000i.

———. "Yucca Mountain Site Description." TDR–CRW–GS–000001. Rev. 01. Las Vegas, Nevada: TRW Environmental Safety Systems. 2000j.

———. "Development of Numerical Grids for UZ Flow and Transport Modeling." ANL–NBS–HS–000015. Rev. 00. Las Vegas, Nevada: CRWMS M&O. 2000k.

———. "Chapter 2: Unsaturated Zone Hydrology Model. Total System Performance Assessment–Viability Assessment (TSPA-VA) Analyses Technical Basis Document." B00000000–01717–4301–00002. Rev. 00. Las Vegas, Nevada: TRW Environmental Safety Systems, Inc. 1998.

———. "Unsaturated Zone Flow Model Expert Elicitation Project." MOL.19971009.0582. Las Vegas, Nevada: CRWMS M&O. 1997.

Day, W.C., R.P. Dickerson, C.J. Potter, D.S. Sweetkind, C.A. San Juan, R.M. Drake II, and C.J. Fridrich. "Bedrock Geologic Map of the Yucca Mountain Area, Nye County, Nevada." U.S. Geological Survey Miscellaneous Investigation Series, Map I–2627. Scale 1:24,000. 1998.

Day, W.C., C.J. Potter, D. Sweetkind, R.P. Dickerson, and C.A. San Juan. "Bedrock Geologic Map of the Central Block Area, Yucca Mountain, Nye County, Nevada." U.S. Geological Survey Miscellaneous Investigation Series, Map I–2601. Scale 1:6,000. 1997.

DOE. "Viability Assessment of a Repository at Yucca Mountain. Vol. 3: Total System Performance Assessment." DOE/RW–0508/V3. Las Vegas, Nevada: DOE, Office of Civilian Radioactive Waste Management. 1998.

Fedors, R.W., J. Evans, D. Or, C. Forster, J. Heath, and K. Bradbury. "Unsaturated Flow Through Fractured and Unfractured Nonwelded Tuffs." Presentation at American Geophysical Union Fall 2001 Meeting, San Francisco, California, December 10–14, 2001. *EOS Transactions Supplement*. American Geophysical Union. Vol. 82, No. 47. p. F501. 2001.

Fisher, Q.J. and R.J. Knipe. "Fault Sealing Processes in Siliciclastic Sediments; in Faulting, Fault Sealing, and Fluid Flow in Hydrocarbon Reservoirs." G. Jones, Q.J. Fisher, and R.J.Knipe, eds. *Geological Society Special Publication*. No. 147. pp.117–135. London, England, United Kingdom: The Geological Society. 1999.

Flint, L.E. "Characterization of Hydrogeologic Units Using Matrix Properties, Yucca Mountain, Nevada." U.S. Geological Survey Water Resources Investigations Report 97-4243. 1998.

Flint, L.E., A.L. Flint, C A. Rautman, and J.D. Istok. "Physical and Hydrologic Properties of Rock Outcrop Samples at Yucca Mountain, Nevada." U.S. Geological Survey Open-File Report 95–280. 1996.

Flint, A.L., L.E. Flint, E.M. Kwicklis, G.S. Bodvarsson, and J.M. Fabryka-Martin. "Hydrology of Yucca Mountain, Nevada." *Reviews of Geophysics*. Vol. 39, No. 4. pp. 447–470. 2001

Flury, M. and H. Fluhler. "Tracer Characteristics of Brilliant Blue FCF." *Soil Science Society of America Journal.* Vol. 59. pp. 22–27. 1995.

Heynekamp, M.R., L.B. Goodwin, P.S. Mozley, and W.C. Haneberg. "Controls on Fault-Zone Architecture in Poorly Lithified Sediments, Rio Grande Rift, New Mexico: Implications for Fault-Zone Permeability and Fluid Flow." *Faults and Subsurface Fluid Flow in the Shallow Crust.* W.C. Haneberg, et al., eds. *Geophysical Monograph 113.* Washington, DC: American Geophysical Union. pp. 27–50. 1999.

Hillel, D. and R.S. Baker. "A Descriptive Theory of Fingering During Infiltration in Layered Soils." *Soil Science.* Vol. 146. pp. 51–56. 1988.

Ho, C.K. and S.W. Webb. "Capillary Barrier Performance in Heterogeneous Porous Media." *Water Resources Research.* Vol. 34, No. 4. pp. 603–609. 1998.

Hollett, K.J., W.J. Danskin, W.F. McCaffrey, and C.L. Walti. "Geology and Water Resources of Owens Valley, California." U.S. Geological Survey Water Supply Paper 2370–B. 1991.

Illman, W.A., D.L. Hughson, C. DinWiddie, and R. Fedors. "Geostatistical Analysis of Pneumatic, Hydraulic, and Thermal Properties of Unsaturated Fractured Tuffs at the Apache Leap Research Site." San Antonio, Texas: CNWRA. 2002.

Illman, W.A., D.L.Thompson, V.V. Vesselinov, and S.P. Neuman. NUREG/CR–5559, "Single-Hole and Cross-Hole Pneumatic Tests in Unsaturated Fractured Tuffs at the Apache Leap Research Site: Phenomenology, Spatial Variability, Connectivity, and Scale." Washington, DC: NRC. 1998.

LeCain, G.D., N. Lu, and M. Kurzmack. "Use of Thermal Data to Estimate Infiltration in Pageny Wash Associated with the Winter of 1997–1998 El Niño Precipitation, Yucca Mountain, Nevada." Geological Society of America Abstracts with Programs—2000 Annual Meeting, Reno, Nevada: Geological Society of America. Vol. 32, No. 7. 2000.

Lichtner, P.C., M.S. Seth, and S. Painter. "MULTIFLO User's Manual." MULTIFLO Version 1.2. Rev. 2. Two-Phase Nonisothermal Coupled Thermal-Hydrological-Chemical Flow Simulator. San Antonio, Texas: CNWRA. 2000.

Liu, H.H., C. Doughty, and G.S. Bodvarsson. "An Active Fracture Model for Unsaturated Flow and Transport in Fractured Rocks." *Water Resources Research.* Vol. 34. pp. 2,633–2,646. 1998.

Moyer, T.C., J.K. Geslin, and L.E. Flint. "Stratigraphic Relations and Hydrologic Properties of the Paintbrush Tuff Nonwelded (PTn) Hydrologic Unit, Yucca Mountain, Nevada." U.S. Geological Survey Open-File Report 95-397. 1996.

Ofoegbu, G.I., S. Painter, R. Chen, R.W. Fedors, and D.A. Ferrill. "Geomechanical and Thermal Effects on Moisture Flow at the Proposed Yucca Mountain Nuclear Waste Repository." *Nuclear Technology.* Vol. 134, No. 3. pp. 241–262. 2001.

Pruess, K. "TOUGH2—A General Purpose Numerical Simulator for Multiphase Fluid and Heat Flow." LBNL–29400. Berkeley, California: Lawrence Berkeley National Laboratory. 1991.

Rautman, C.A., L.E. Flint, and A.L. Flint. "Physical and Hydrologic Properties of Outcrop Samples from a Nonwelded to Welded Tuff Transition, Yucca Mountain, Nevada." U.S. Geological Survey Water Resources Investigations Report 95–4061. 1995.

Robin, M.J.L., A.L. Gutjahr, E.A. Sudicky, and J.L. Wilson. "Cross-Correlated Random Field Generation with the Direct Fourier Transform Method." *Water Resources Research.* Vol. 29. pp. 2,385–2,397. 1993.

Ross, B. "The Diversion Capacity of Capillary Barriers." *Water Resources Research.* Vol. 26, No. 10. pp. 2,625–2,629. 1990.

Rousseau, J.P., E.M. Kwicklis, and D.C. Gillies. "Hydrogeology of the Unsaturated Zone, North Ramp Area of the Exploratory Studies Facility, Yucca Mountain, Nevada." U.S. Geological Survey Water Resources Investigations Report 98-4050. 1999.

Sigda, J.M., L.B. Goodwin, P.S. Mozley, and J.L. Wilson. "Permeability Alteration in Small-Displacement Faults in Poorly Lithified Sediments: Rio Grande Rift, Central New Mexico." *Faults and Subsurface Fluid Flow in the Shallow Crust.* W.C. Haneberg, et al., eds. *Geophysical Monograph 113.* Washington, DC: American Geophysical Union. pp. 51–68. 1999.

Simúnek, J., M. Sejna, and M.Th. van Genuchten. "HYDRUS2D/MESHGEN-2D Simulating Water Flow and Solute Transport in Two-Dimensional Variably Saturated Media, Version 2.0." Washington, DC: U.S Salinity Laboratory, U.S. Department of Agriculture, Agricultural Research Service. 1999.

Terzaghi, R. "Source of Error in Joint Surveys." *Geotechnique.* Vol. 15. p. 287. 1965.

van Genuchten, M.T "A Closed-Form Equation for Predicting the Hydraulic Conductivity of Unsaturated Soils " *Soil Science Society of America Journal.* Vol. 44. pp. 892–898. 1980.

Vesselinov, V.V , S.P Neuman, and W.A. Illman. "Three-Dimensional Numerical Inversion of Pneumatic Cross-Hole Tests in Unsaturated Fractured Tuff 2: Equivalent Parameters, High-Resolution Stochastic Imaging and Scale Effects." *Water Resources Research.* Vol. 37. pp. 3,019–30,42. 2001.

Walter, M.T., J.-S. Kim, T.S. Steenhuis, J.-Y. Parlange, A. Heilig, R.D. Braddock, J.S. Selker, and J. Boll. "Funneled Flow Mechanisms in a Sloping Layered Soil: Laboratory Investigation." *Water Resources Research.* Vol. 36, No. 4. pp. 841–849. 2000.

Wang, J.S.Y., P.J. Cook, R.C Trautz, R. Salve, A.L. James, S. Finsterle, T.K. Tokunaga, R. Solbau, J. Clyde, A.L. Flint, and L.E. Flint. "Field Testing And Observation of Flow Paths In Niches: Phase 1 Status Report Of The Drift Seepage Test And Niche Moisture Study." Level 4 Milestone SPC314M4. Las Vegas, Nevada: Yucca Mountain Site Characterization Project. 1998.

Webb, S.W. "Generalization of Ross' Tilted Capillary Barrier Diversion Formula for Different Two-Phase Characteristic Curves." *Water Resources Research*. Vol. 33, No. 8. pp. 1,855–1,859. 1997.

Wilson, C.J.N. and W. Hildreth. "The Bishop Tuff: New Insights from Eruptive Stratigraphy." *Journal of Geology*. Vol. 105. pp. 407–439. 1999.

Winterle, J.R. and S. Stothoff. "Evaluation of Inconsistencies Between Laboratory-Derived Moisture Retention Characteristics and Matrix Sorptivity." Proceedings of the Field Testing and Associated Modeling Workshop, Lawrence Berkeley National Laboratory, December 15–16, 1997. Berkeley, California: Lawrence Berkeley National Laboratory. 1997.

Wu, Y-S., W. Zhang, L. Pan, J. Hinds, and G.S. Bodvarsson. "Capillary Barriers in Unsaturated Fractured Rocks of Yucca Mountain, Nevada." LBNL–46876. Berkeley, California: Lawrence Berkeley National Laboratory. 2000.